University of Alberta

Library Release Form

Name of Author: Yu Fu

Title of Thesis: Transmitter Precoding for Interference Mitigation in Closed-Loop MIMO OFDM Systems

Degree: Doctor of Philosophy

Year this Degree Granted: 2009

. . . . . .

Yu Fu
2nd Floor,
Electrical and Computer Engineering
Research Facility (ECERF)
University of Alberta
Edmonton, AB
Canada, T6G 2V4

Date: . . . . . .

University of Alberta

TRANSMITTER PRECODING FOR INTERFERENCE MITIGATION IN CLOSED-LOOP MIMO OFDM SYSTEMS

by

Yu Fu

A thesis submitted to the Faculty of Graduate Studies and Research in partial fulfillment of the requirements for the degree of **Doctor of Philosophy**.

Department of Electrical and Computer Engineering

Edmonton, Alberta
Fall 2009

University of Alberta
Faculty of Graduate Studies and Research

The undersigned certify that they have read, and recommend to the Faculty of Graduate Studies and Research for acceptance, a thesis entitled **Transmitter Precoding for Interference Mitigation in Closed-Loop MIMO OFDM Systems** submitted by Yu Fu in partial fulfillment of the requirements for the degree of **Doctor of Philosophy**.

. . . . . .
Dr. Tho Le-Ngoc (External Examiner)
Department of Electrical and Computer Engineering, McGill University

. . . . . .
Dr. Ehab S. Elmallah (Committee Member)
Department of Computer Science, University of Alberta

. . . . . .
Dr. Ivan Fair (Committee Member)
Department of Electrical and Computer Engineering, University of Alberta

. . . . . .
Dr. Vien Van (Committee Member)
Department of Electrical and Computer Engineering, University of Alberta

. . . . . .
Dr. Sergiy Vorobyov (Committee Member)
Department of Electrical and Computer Engineering, University of Alberta

. . . . . .
Dr. Witold A. Krzymień (Co-Supervisor)
Department of Electrical and Computer Engineering, University of Alberta

. . . . . .
Dr. Chintha Tellambura (Co-Supervisor)
Department of Electrical and Computer Engineering, University of Alberta

Date: . . . . . .

To my parents, Ryan and Chunlong, who offer me endless encouragement and support.

Acknowledgements

I would like to express my sincere thanks to my supervisors, Dr. Krzymień and Dr. Tellambura, for their invaluable guidance, encouragement, generosity, patience, advice and comments throughout my research work. I would like to appreciate all their support.

My deepest gratitude goes to my parents, my husband and my son, who have always encouraged, supported and cared for me throughout my life. They have always been the source of my power and courage.

I also wish to give my thanks to my labmates, for their helpful discussion and friendship.

Last but not the least, I would like to thank the Natural Sciences and Engineering Research Council (NSERC), Informatics Circle of Research Excellence (iCORE) and TRLabs for their financial support.

Abstract

Current trends in the development of high-data-rate wireless systems focus on the integration of orthogonal frequency-division multiplexing (OFDM), multiple-input multiple-output (MIMO) and closed-loop techniques. In closed-loop systems, transmit precoding reacts to channel conditions in order to improve the system capacity or bit error rate (BER). Closed-loop MIMO OFDM allows transmit precoding on frequency-selective channels to pre-process signals at the subcarrier level, and facilitates the utilization of capacity or performance gain. OFDM is being widely adopted in several wireless standards due to its spectrum efficiency and other advantages. Recent integration with multiple-antenna techniques promises a significant boost in performance of OFDM. However, OFDM is sensitive to frequency offset, which immediately results in intercarrier interference (ICI) and degrades the system performance. On the other hand, MIMO systems are also constrained by limited antenna spacing, which may lead to correlations among antennas. The antenna correlation always reduces the system data rate and increases the error rate. Furthermore, the original space-time techniques have poor performance if they are directly employed over antenna-correlated channels.

This thesis contributes to transmitter precoding design in MIMO OFDM systems for reducing ICI, and mitigating the degradation due to antenna correlations. Transmitter-based techniques usually require the complete channel state information at the transmitter (CSIT), which is difficult to obtain in practical applications. The complete channel information, including frequency offset and channel gains, is not readily estimated at the transmitter or feedback capability from the receiver is limited. Therefore, precoding with partial CSIT is first considered. An important property of the ICI matrix is derived and non-linear Tomlinson-Harashima precoding (THP) with only partial CSIT, not including frequency offset, is developed. To further reduce the feedback requirements, linear and non-linear limited-feedback precoders are proposed. Our results significantly reduce the BER increase due to frequency offsets in single-user and multiuser MIMO OFDM.

Precoders are developed to mitigate the impact of transmit-antenna and path correlations for MIMO OFDM systems. A pairwise error probability (PEP) optimal precoder is derived, which requires only covariance information at the transmitter. The covariance (second-order statistics)

information is primarily determined by transmitter correlation matrix, which significantly reduces feedback requirements. Furthermore, mean (first-order statistics) -feedback SNR-maximizing precoders are designed for a general transmit-antenna-correlated, frequency-selective fading MIMO channel model in an OFDM downlink system with estimation errors and feedback delay. The quality of CSIT (mean feedback) will be degraded due to estimation errors, and it is more sensitive to the channel time variations and feedback delay than covariance precoding. In contrast, covariance precoding may become less effective when mean feedback is accurate. An adaptive dual-mode precoder is thus proposed, in which either new mean-feedback precoding or covariance precoding is adaptively chosen at the receiver according to the channel conditions. The intuition is confirmed that if mean feedback is sufficiently accurate, it improves the system performance. Our proposed precoders, both the mean-feedback precoder and the dual-mode precoder, reduce the error rate. Adaptive precoding outperforms both mean-feedback precoding and covariance precoding applied individually.

Our techniques offer the flexibility of adapting original space-time multiple-antenna techniques to the antenna correlations, and require reduced feedback information at the transmitter. The proposed schemes are expected to have good performance, low feedback requirements and low complexity, which are desirable for interference reduction in the future wireless systems.

Contents

List of Figures

List of Abbreviations

Abbreviation	Definition
3G	third-generation
3GPP	third-generation partnership project
4G	fourth-generation
ADSL	asymmetric digital subscriber lines
AWGN	additive white Gaussian noise
BER	bit error rate
BS	base station
CATV	cable TV
CCI	co-channel interference
CIR	channel impulse response
CSI	channel state information
DAB	digital audio broadcasting
DFE	decision feedback equalization
DFT	discrete Fourier transform
DSL	digital subscriber line
DAB	digital audio broadcasting
DVB	digital video broadcasting
EVD	eigenvalue decomposition
FDD	frequency-division duplex
FDMA	frequency-division multiple access
FFT	fast Fourier transform
FM	frequency modulation

HDTV	high-definition television
HSDPA	high-speed downlink packet access
i.i.d	independent and identically distributed
ICI	intercarrier interference
IDFT	inverse discrete Fourier transform
IFFT	inverse fast Fourier transform
ISI	intersymbol interference
LFB-THP	limited-feedback Tomlinson-Harashima precoding
LOS	line-of-sight
MAC	medium access control
MAN	metropolitan area networks
MIMO	multiple-input multiple-output
ML	maximum likelihood
MMI	maximum mutual information
MMSE	minimum mean square error
MS	mobile station
MSI	maximum singular value
MUD	multiuser detection
MUI	multiuser interference
OFDMA	orthogonal frequency-division multiple access
OFDM	orthogonal frequency-division multiplexing
OSTBC	orthogonal space-time block coded
PAPR	peak-to-average power ratio
pdf	probability density function
PSK	phase shift keying
QAM	quadrature amplitude modulation
QoS	quality of service
RF	radio frequency
SCM	single carrier modulation
SIC	successive interference cancelation

SINR	signal-to-interference-plus-noise power ratio
SISO	single-input single-output
SNR	signal-to-noise power ratio
STBC	space-time block codes
STD	switched transmit diversity
STTC	space-time trellis codes
STTD	space-time transmit diversity
SVD	singular value decomposition
TDD	time-division duplex
TH	Tomlinson-Harashima
THP	Tomlinson-Harashima precoding
TXAA	transmit adaptive array
ULA	uniform linear array
UMTS	Universal Mobile Telecommunications System
V-BLAST	vertical-Bell laboratories layered space-time
VHDSL	very high-speed digital subscriber line
WCDMA	wideband code-division multiple access
WLAN	wireless local access network
WNG	wireless next generation
WSSUS	wide-sense stationary uncorrelated scattering
ZF	zero forcing

List of Symbols

Symbol	Definition
$\jmath$	$\sqrt{-1}$
$\mathbb{I} = \{0, \pm 1, \pm 2, \ldots\}$	set of integers
$\Re\{x\}$	real part of x
$A(m, n)$	the $\{m, n\}$ entry of **A**
$\Im\{x\}$	imaginary part of x
$\Xi(m, n)$	complex Grassmannian space
$\|\mathbf{A}\|_F$	Frobenius norm of matrix **A**
$\delta(\cdot)$	Kronecker delta
$\det(\mathbf{A})$	determinant of matrix **A**
$\gamma(\mathbf{A})$	singular values of matrix **A**
$\lceil x \rceil$	the smallest integer greater than x
$\mathfrak{C}^m$	the m-fold Cartesian product set of the ring of integers
$\mathbb{C}^{m \times n}$	the vector space of $m \times n$ complex matrices
$\mathbb{R}^m$	Euclidean m-space or Cartesian space
$\Theta(m, n)$	the set of $m \times n$ matrices with orthogonal columns
$\otimes$	Kronecker product
E	expectation operation
$\mathbf{0}_{M \times N}$	$M \times N$ all-zero matrix
$\mathbf{I}_N$	$N \times N$ identity matrix

*	element-wise conjugate
†	Moore-Penrose pseudo-inverse
^{H}	conjugate transposition
^{T}	transposition
$\mathcal{J}_0(\cdot)$	zero-order Bessel function of the first kind
$tr(\mathbf{A})$	trace of matrix $\mathbf{A}$

Chapter 1

Introduction

Wireless communications technologies have recently made great advances. Personal communication devices now enable ubiquitous communications. The spectacular growth of data communication, voice and video service over Internet, and the equally rapid expansion of mobile telephony, justify great expectations for high data rates in mobile radio communication systems. Current communication systems integrate various functions and applications, such as a mobile telephone or high-rate data in a wireless local area network (WLAN), which is expected to provide its users with over 100 Mbps information rates. Since radio spectrum is limited, supporting such high data rates and overcoming the radio channel impairments presents challengs to the design of future high-speed mobile radio communication systems. Current trends in wireless system design focus on multiple-input multiple-output (MIMO) techniques to provide capacity (data rate) gains [1, 2], closed-loop techniques to offer capacity gains or bit-error rate (BER) performance improvements [3, 4], and orthogonal frequency-division multiplexing (OFDM) to facilitate the utilization of these performance gains on frequency-selective channels [5, 6].

1.1 MIMO

MIMO antenna techniques have recently emerged as a promising performance enhancing solution for high-data-rate wireless communications. The MIMO approach employs multiple antenna arrays at both the transmitter and the receiver, effectively exploits the spatial dimension in addition

to time and frequency dimensions, and offers significant channel capacity gains [1]. These gains are available in a rich multipath scattering environment, which provides independent transmission paths from each transmit antenna to each receive antenna: specifically, the capacity of MIMO systems grows linearly as $\min(M_T, M_R)$, where M_T is the number of the transmit antennas and M_R is the number of the receive antennas. The system capacity hence scales linearly with $\min(M_T, M_R)$ relative to a single-input single-output (SISO) system [1].

MIMO systems use space-time signal processing, which exploits spatial dimension inherent in multiple spatially-distributed antenna systems. Current space-time processing techniques typically fall into two categories: spatial diversity coding and spatial multiplexing.

1.1.1 Spatial Diversity Coding

Spatial diversity codes improve power efficiency and reliability of transmission by maximizing spatial diversity gain. These codes ensure that transmit symbols are sent over multiple independently fading paths without signal power or bandwidth expansion. If the $M_T M_R$ MIMO links fade independently and the transmitted signal is constructed by suitable diversity codes, the receiver can combine the arriving signals such that the resultant signal exhibits considerably reduced amplitude variability in comparison to a SISO link and achieve the $M_T M_R$-order diversity. These techniques include delay diversity [7,8], space-time trellis coding (STTC) [9,10], and space-time block coding (STBC) [11, 12].

A space-time code is transmitted over T time slots and from M_T transmit antennas, and can generally be represented by a $T \times M_T$ transmit matrix

$$\mathbf{C} = \begin{bmatrix} c_{11} & \dots & c_{1M_T} \\ \vdots & \ddots & \vdots \\ c_{T1} & \dots & c_{TM_T} \end{bmatrix}, \tag{1.1}$$

where c_{tv} is the modulation symbol transmitted at time $t,\ t = 1, 2, \dots, T$, from the v-th transmit antenna and T is the number of time slots for transmitting the code matrix. The transmission (code) rate R_c is defined as P/T, where P represents the number of different data symbols transmitted

over the T time slots. The number of rows, T, is equal to the total number of time slots necessary to transmit P symbols. R_c is the maximum possible rate of a full-diversity code. At each time slot t, the t-th row of $\mathbf{C}$ is transmitted from all transmit antennas simultaneously. The v-th column of $\mathbf{C}$ represents the sequence of symbols transmitted from the v-th antenna.

1.1.1.1 Delay Diversity

Delay diversity, first proposed in [7] for flat-fading channels, introduces a deliberate resolvable multipath dispersion by transmitting the data bearing signal 1 and its $M_T - 1$ delayed replicas over M_T transmit antennas. The delays are unique to each antenna and are chosen to be multiples of the symbol interval. At the receiver, a maximum likelihood (ML) estimator resolves the artificial multipath in an optimal manner to obtain diversity order of M_T. For T time slots, the number of columns is M_T, thus the transmit matrix can be given as

$$\mathbf{C}_{\text{delay}} = \begin{pmatrix} c_1 & c_T & \cdots & c_{T-M_T+2} \\ c_2 & c_1 & & c_{T-M_T+3} \\ \vdots & \vdots & \cdots & \vdots \\ c_T & c_{T-1} & & c_{T-M_T+1} \end{pmatrix}, \tag{1.2}$$

where each row represents a signal c_t and its M_T delayed versions from M_T antennas.

A generalized delay diversity scheme that maximizes the diversity gains for frequency-selective fading channels was reported in [8], and applied to Global System for Mobile Communications (GSM) and Enhanced Data Rates for GSM Evolution (EDGE) in [13].

1.1.1.2 Orthogonal Space-Time Bock Coding

To minimize decoding complexity, STBC has been discovered [11, 12]. The orthogonal design of this scheme supports ML detection based only on linear processing at the receiver. In this thesis, emphasis within space-time coding is placed on block approaches, which currently dominate the literature rather than on trellis-based approaches.

STBC based on orthogonal design obtains full diversity gain with low decoding complexity,

and therefore is widely used. An OSTBC[1] matrix is composed of linear combinations of constellation symbols $c_1, c_2, \ldots, c_P$ and their conjugates, and encoding therefore only requires linear processing. The most important special case is the Alamouti code for two transmit antennas [11]. It is used to achieve space-time transmit diversity (STTD), and has been adopted in several third-generation (3G) cellular standards because it maximizes diversity gain [14, 15].

The $T \times M_T$ code matrix for OSTBC satisfies

$$\mathbf{C}^H\mathbf{C} = \left(\sum_{t=1}^{P} |c_t|^2\right) \mathbf{I}_{M_T}, \tag{1.3}$$

for all complex code symbols c_t. For example, the Alamouti code is an OSTBC with 2 transmit antennas, for which the transmit matrix is

$$\mathbf{C}^1 = \begin{pmatrix} c_1 & c_2 \\ -c_2^* & c_1^* \end{pmatrix}, \tag{1.4}$$

i.e., two symbols c_1 and c_2 and their conjugates are transmitted over two time slots [11]. In the first time slot, c_1 and c_2 are transmitted from the antenna 1 and 2, respectively; during the next symbol period, $-c_2^*$ is transmitted from the antenna 1, and c_1^* is from the antenna 2. More general OSTBC structures are discussed in [12]. For instance, code matrices for rate $1/2$ and $3/4$ code using four antennas are given by

$$\mathbf{C}^{1/2} = \begin{pmatrix} c_1 & c_2 & c_3 & c_4 \\ -c_2 & c_1 & -c_4 & c_3 \\ -c_3 & c_4 & c_1 & -c_2 \\ -c_4 & -c_3 & c_2 & c_1 \\ c_1^* & c_2^* & c_3^* & c_4^* \\ -c_2^* & c_1^* & -c_4^* & c_3^* \\ -c_3^* & c_4^* & c_1^* & -c_2^* \\ -c_4^* & -c_3^* & c_2^* & c_1^* \end{pmatrix}, \tag{1.5}$$

and

$$\mathbf{C}^{3/4} = \begin{pmatrix} c_1 & c_2 & \frac{c_3}{\sqrt{2}} & \frac{c_3}{\sqrt{2}} \\ -c_2^* & c_1^* & \frac{c_3}{\sqrt{2}} & -\frac{c_3}{\sqrt{2}} \\ \frac{c_3^*}{\sqrt{2}} & \frac{c_3^*}{\sqrt{2}} & \frac{-c_1-c_1^*+c_2-c_2^*}{2} & \frac{-c_2-c_2^*+c_1-c_1^*}{2} \\ \frac{c_3^*}{\sqrt{2}} & -\frac{c_3^*}{\sqrt{2}} & \frac{c_2+c_2^*+c_1-c_1^*}{2} & -\frac{c_1+c_1^*+c_2-c_2^*}{2} \end{pmatrix}, \tag{1.6}$$

[1]OSTBC stands for orthogonal space-time block-coded and orthogonal space-time block coding, depending on the context.

respectively.

Theoretically, the number of antenna elements through which independent symbols can be transmitted in one $T \times M_T$ code block bounds the achievable order of spatial diversity.

1.1.2 Spatial Multiplexing

Instead of maximizing spatial diversity, spatial multiplexing uses a layering approach to increase capacity. Accordingly, M_T independent symbols are transmitted per symbol period so that the transmission rate is M_T. The SM variants include vertical-Bell laboratories layered space-time (V-BLAST) [16, 17], horizontal BLAST [18], diagonal BLAST [18], and turbo BLAST [19]. Among the above spatial multiplexing techniques, V-BLAST [16] is the most promising technique due to its implementation simplicity. V-BLAST architecture uses ordered serial zero-forcing (ZF) or minimum mean square error (MMSE) nulling and successive interference cancellation (SIC). This scheme has three main steps to detect received signals:

1. Estimate the channel state information (CSI) at the receiver;

2. Determine the optimal detecting order and the nulling vectors. The nulling vector is orthogonal to the subspace spanned by the distributions to the received signal vector with the weaker signals and will detect the strongest signal.

3. Detect the received signals based on the optimal order and SIC.

    - ZF or MMSE nulling: ZF or MMSE estimation of the strongest received signal is obtained via nulling out the weaker signals.
    - Detecting: The value of the strongest signal is detected by slicing to the nearest value in the constellation.
    - SIC: The effect of the strongest signal on the other weaker signals to be detected is removed from the vector of the received signals, after which we return to the second step and continue the decoding successively.

Since the data symbols are detected consecutively in spatial (vertical) rather than temporal (horizontal) direction, this approach is called V-BLAST.

In spatial multiplexing, independent data streams are transmitted over multiple antennas to increase the data rate, but full spatial diversity is not achieved [20]. Since a spatial multiplexing detector uses some form of inverse channel matrix, a unique solution for receiver processing is only possible if the number of receive antennas is greater than or equal to that of independently transmitted signals. Performance of spatial multiplexing degrades over spatially correlated channels.

1.1.3 Diversity-Multiplexing Tradeoff

A MIMO system can provide two types of gains: spatial multiplexing gains and diversity gains. Spatial multiplexing is usually used to achieve the former and STBC is used to extract the latter. Given a MIMO channel, both gains can be simultaneously obtained. However, maximizing one type of gain trends to minimize the other. As discussed in [20], there is a fundamental tradeoff between diversity and spatial multiplexing: higher spatial multiplexing gain comes at the price of sacrificing diversity, and vice versa. The diversity-multiplexing tradeoff is essentially the tradeoff between the system error probability and the data rate. Generally speaking, to achieve high bandwidth efficiency, spatial multiplexing is a better choice. On the other hand, without coding in the time or space dimension, spatial multiplexing may have high error rates. Hence, STBC offers a lower BER.

MIMO opens the space dimension to offer the advantage of diversity and thus has been adopted in various standards and wireless networks, including broadband wireless access systems, IEEE $802.11n$ WLAN standard [21], and 3G cellular standards. MIMO can also be implemented in the high-speed downlink packet access (HSDPA) channel, which is a part of the Universal Mobile Telecommunications System (UMTS) standard [22].

1.2 OFDM

OFDM uses N orthogonal subcarriers so that a high-rate data stream is split into N lower rate substreams, which are transmitted in parallel on the subcarriers. The time duration of an OFDM symbol is therefore N times longer than that of a single-carrier symbol. Because the symbol duration increases for the lower rate parallel subcarriers, the relative amount of time dispersion caused by multipath delay spread is decreased. The concept of using parallel data transmission and frequency division multiplexing (FDM) with orthogonal spectral overlap was published in the mid 1960s [23, 24]. Some early development can be traced back in 1957, which was for bandwidth efficient transmission over telephone and high frequency (HF) radio channel [25]. The basic idea was to use parallel data and FDM with overlapping subcarriers to avoid the use of high-speed equalization and to combat impulsive noise and multipath distortion as well as to fully use the available bandwidth. The initial applications were in military communications, such as KINEPLEX [25] and KATHRYN [26] in HF military systems in the 1960s.

For a large number of subcarriers, in order to avoid the unreasonably expensive and complex sinusoid generators and coherent demodulators, the discrete Fourier transform (DFT) was implemented in the mid-1960 in military HF radios [26]. Weinstein and Ebert applied inverse and direct fast Fourier transform (IFFT/FFT) to simplify the OFDM modulation and demodulation process in the early 1970s [27]. IFFT/FFT is needed for a completely digital implementation so that the bank of subcarrier oscillators and coherent demodulators required by the original OFDM proposal [23, 24] can be eliminated. Rapid advances in very large scale integration (VLSI) technology make high-speed large size FFT chips commercially affordable. In 1985, Cimini first investigated OFDM for mobile wireless communications [28]. In 1990, Bingham has studied the performance and complexity of OFDM and concluded that the time for OFDM had come [29]. In the 1990s, OFDM has been investigated for voice-band modems such as asymmetric digital subcarrier loop (ADSL), high-bit-rate digital subscriber line (HDSL), and very high-speed digital subscriber line (VHDSL) [30]. OFDM has also been exploited for wideband data communications over mobile

radio frequency modulation (FM) channels, digital audio broadcasting (DAB) [31], digital video broadcasting (DVB) [32] and high-definition television (HDTV) [33].

A broadband wireless system with a very high data rate encounters large delay spread, and therefore, has to cope with frequency selectivity. OFDM converts a frequency-selective channel into a number of parallel frequency-flat subcarriers. The subcarriers have the minimum frequency separation required to maintain orthogonality of their corresponding time-domain waveforms yet the signal spectra associated with the different subcarriers overlap in frequency domain. The available bandwidth is hence used efficiently. If knowledge of the channel is available at the transmitter, OFDM can allocate the transmitted power on a subcarrier basis to match the channel so that the optimal BER and/or ideal water filling capacity of a frequency-selective channel can be approached [5]. Therefore, closed-loop OFDM facilitates the utilization of the capacity or BER performance gains on frequency-selective channels.

OFDM has been exploited for several wireless standards, including IEEE 802.11a LAN standard [34] and IEEE 802.16a, metropolitan area network (MAN) standard [35]. The IEEE 802.11a operates at raw data rate up to 54 Mb/s with a 20 MHz channel spacing, thus yielding a bandwidth efficiency of 2.7 b/s/Hz. The actual throughput is highly dependent on the medium access control (MAC) protocol. IEEE 802.16a operates in many modes depending on channel conditions with a data rate ranging form 4.20 to 22.91 Mb/s in a typical bandwidth of 6 MHz, the efficiency is then 0.7 to 3.82 b/s/Hz [35]. OFDM is also being considered in IEEE 802.20a, a standard in the making for maintaining high-bandwidth connections to users moving at speeds up to 100 km/h. OFDM is in addition being regarded as a potential candidate for 4G mobile wireless systems [22]. Recent integration with MIMO techniques promises a significant boost in performance of OFDM. Broadband MIMO OFDM systems with bandwidth efficiency on the order of 10 b/s/Hz are potentially feasible for LAN/MAN environments [5].

1.2.1 OFDM Systems

An OFDM system can be implemented in discrete time domain using an IDFT as a modulator and DFT as a demodulator. The transmitted data are the frequency-domain symbols and the samples at the output of the IDFT are time-domain samples of the transmitted waveform. Let $X[n]$ denote an M-ary phase shift keyed (PSK) or QAM symbol on the n-th subcarrier. The length-N input data vector can then be written as $\mathbf{X} = \big[X[0]\, X[1] \ldots X[N-1]\big]^T$. The OFDM signal may be expressed as

$$x(t) = \sum_{k=0}^{N-1} X[k] e^{\jmath 2\pi f_k t}, \;\; 0 \le t < T_s, \tag{1.7}$$

where $f_k = f_0 + k\,\Delta\tilde{f}$ is the k-th subcarrier frequency; $\Delta\tilde{f}$ is the subcarrier separation. To satisfy the orthogonal condition, $\Delta\tilde{f}\,T_s = 1$ is needed, where T_s is the OFDM symbol period. Without loss of generality, setting $f_0 = 0$, $f_k = \frac{k}{T_s}$ is obtained. With sampling rate $\frac{N}{T_s}$, the n-th sample in the discrete-time domain is

$$x(n) = \sum_{k=0}^{N-1} X[k] e^{\jmath 2\pi \frac{k}{T_s} \frac{nT_s}{N}} = \sum_{k=0}^{N-1} X[k] e^{\jmath \frac{2\pi}{N} kn}, \tag{1.8}$$

which is a form of the IDFT. Consequently, the time-domain OFDM symbol can be generated by taking an IDFT of an input data vector:

$$\mathbf{x} = \big[x(0)\, x(1) \ldots x(N-1)\big]^T = \mathcal{F}_N \mathbf{X}, \tag{1.9}$$

where $\mathcal{F}_N$ is the $N \times N$ IDFT matrix with entries $\mathcal{F}_N(m,n) = \frac{1}{N} e^{\jmath \frac{2\pi}{N} mn}$. The IDFT can be implemented efficiently by the IFFT algorithm, which reduces the number of computations drastically by exploiting the regularity of the operations in IDFT. A cyclic prefix, which is longer than the expected maximum excess delay, is customarily inserted at the beginning of each time-domain OFDM symbol to prevent inter-symbol interference (ISI).

As discussed in [36], the following key advantages make OFDM attractive in several wireless applications. OFDM is an efficient way to cope with multipath fading channels. Due to parallel transmission on different subcarriers, the deleterious effect of fading is spread over the entire symbol duration. This weakens the effects of deep fading or impulsive noise, so that only a few signals

are slightly affected instead of a number of adjacent signals completely distorted. Further improvement can be obtained with a proper coding and interleaving scheme for many practical systems, especially in a wide-band mobile environment. Spectral efficiency is another important advantage of OFDM. The spectra of subcarriers are permitted to overlap while preserving orthogonality. Another advantage lies in its easy implementation using the FFT algorithm. For a given delay spread, the implementation is much simpler than that of a single-carrier system with equalization.

However, there are two major drawbacks in OFDM. One is that OFDM is sensitive to frequency offset and phase noise, which result in intercarrier interference (ICI) and severely degrade system performance. The other is that OFDM has a relatively large peak-to-average power ratio (PAPR), which reduces the power efficiency of a radio frequency (RF) amplifier. In this thesis, approaches will be considered to reduce ICI due to frequency offset in closed-loop MIMO OFDM systems.

1.2.1.1 Impairments Due to Frequency Offset

Frequency offset due to the Doppler shift caused by the relative motion between the transmitter and receiver, or movement of other objects around transceivers destroys the orthogonality between the OFDM subcarriers. In addition, the oscillator at the receiver may not produce the exactly same carrier frequency as the transmitter's oscillator. The mismatch of oscillators also leads to frequency offset. Consequently, frequency offset exits at an OFDM receiver. Before the subcarriers are demodulated, the receiver has to estimate and correct the carrier frequency offset of the received signal to eliminate the ICI. Otherwise, the system performance will be dramatically degraded.

In the presence of frequency offset, the FFT output for each subcarrier will contain interferences from all other subcarriers [37, 38]. The lack of orthogonality results in ICI, which will be added to the desired signal and cause an error floor that increases with the Doppler shift [39]. As determined in [40], the signal-to-noise power ratio (SNR) degradation caused by a frequency offset, Δf, is approximately proportional to the square of the normalized frequency offset $\varepsilon = \Delta f T_s$. The performance degradation due to ICI thus becomes significant with increasing carrier frequency, block size and vehicle velocity [40]. The maximum normalized frequency offset should be around

1% if an SNR degradation is required to be less than 0.1 dB [40]. For example, for WLAN systems [34], with 5 GHz carrier frequency and 312.5 kHz subcarrier spacing, the oscillator accuracy needs to be ± 3 kHz or 0.6 ppm; otherwise the SNR degradation is not tolerable.

1.2.2 MIMO OFDM

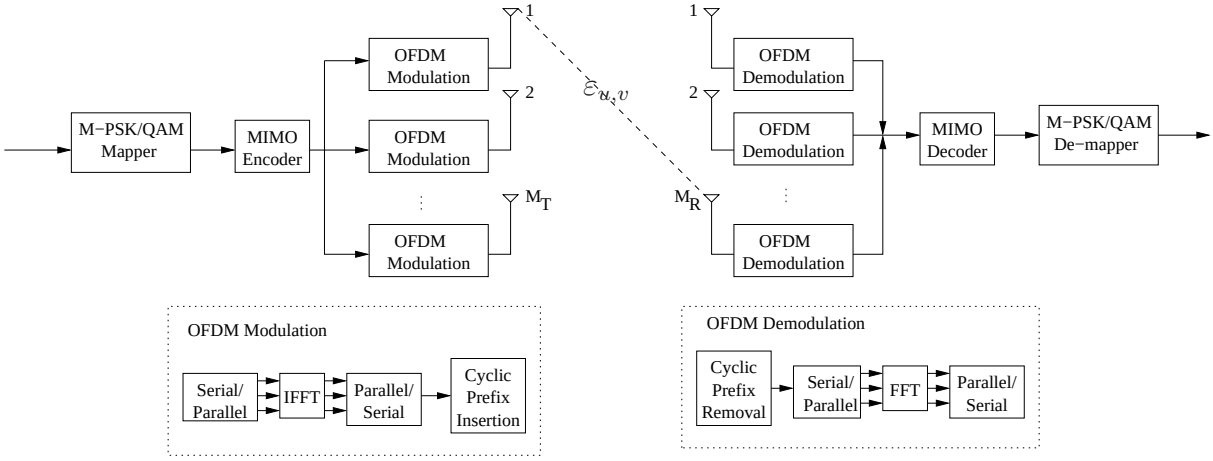

Figure 1.1: Block diagram of a MIMO OFDM link.

As the transmitted data rate (and the transmitted signal's data rate) increases, the MIMO channel can become frequency-selective. OFDM transforms a frequency-selective MIMO channel into a set of parallel frequency-flat MIMO channels, and decreases the complexity of the receiver structure. A combination of OFDM and MIMO is hence attractive for broadband wireless access schemes [5, 6].

The structure of a MIMO OFDM link is shown in Fig. 1.1. At the transmitter, the source bitstream is mapped to a modulation constellation by a signal mapper, and processed by a MIMO encoder. Each of the parallel output symbol streams corresponding to a certain transmit antenna undergoes the same transmission processing by an OFDM modulator. First, the frequency-domain symbol sequence is mapped by IFFT to a time-domain OFDM symbol sequence. A cyclic prefix is then customarily inserted to prevent ISI. Finally, the data frame is converted to an RF signal for transmission. At the receiver, the cyclic prefix is first removed from the received symbol stream

at the output of the RF front end, and the remaining OFDM symbol is then demodulated by FFT. A single-tap equalizer per antenna is usually used to compensate for distortion caused by the transmission channel.

The two space-time signal processing techniques, spatial diversity coding and spatial multiplexing, can be extended to MIMO OFDM. Let us consider, as an example, an Alamouti-coded OFDM system with 2 transmit antennas. Note that implementation of the Alamouti scheme requires that the channel remains constant over at least two consecutive symbol periods. Consider the space-frequency coding: two data symbols c_1 and c_2 to be transmitted over two consecutive OFDM subcarriers k and $k+1$. Through an Alamouti encoder, symbol c_1 and c_2 are transmitted over antenna 1 and 2, respectively, on subcarrier k, whereas $-c_2^*$ and c_1^* are transmitted over antenna 1 and 2, on subcarrier $k+1$, in the same OFDM symbol. The receiver detects the transmitted symbols from the signal received on the two subcarriers using the Alamouti combining scheme as discussed in [11]. The Alamouti scheme achieves transmit diversity of order 2 and the same diversity combining gain as maximum ratio combining (MRC). The technique can be generalized to systems with more than 2 transmit antennas using OSTBC to achieve full diversity gain.

Analogous to spatial multiplexing for frequency-flat fading MIMO channels with single-carrier systems, the objective of spatial multiplexing in conjunction with MIMO OFDM is to maximize the data rate by transmitting independent data streams over different antennas. Thus, spatial multiplexing in MIMO OFDM reduces to spatial multiplexing over each subcarrier with the choice of receiver architectures being identical to that for frequency-flat fading MIMO channels with single-carrier systems.

MIMO OFDM is also sensitive to frequency offset. Over the $\{u, v\}$-th channel, frequency offset $\varepsilon_{u,v}$ may exist. In multiuser OFDM, different users will have distinct values of frequency offsets. In the most general case, each transmit-receive antenna pair may have a different frequency offset, i.e., the maximum possible number of frequency-offset values is $M_R \times M_T$.

1.2.3 Multiuser OFDM

OFDM systems are likely deployed in environments where the base station (BS) communicates with many users simultaneously. For a multiuser system, there are two cases: the uplink, where a group of users transmits data to the same BS, and the downlink, where the BS attempts to transmit signals to multiple users. Since there is no coordination among the users, different problems arise for the uplink and downlink channels.

In the uplink case, the challenge is for the BS to separate the signals transmitted by the users, using array processing or multiuser detection (MUD). Since the users are not able to coordinate with each other, the transmitted signals are hard to optimize. If feedback is allowed from the BS back to the users, some joint process may be possible, but it may require that each user knows all other users' channels in addition to its own. Otherwise, the challenge in the uplink is mainly in the processing done by the BS to separate all the users.

In the downlink case, since the BS simultaneously transmits to a group of users, there is multiuser interference (MUI) among the users. Using MUD techniques, a given user may overcome the MUI, but such techniques are often too costly to use at the receiver. To achieve complete processing at the receiver, degree of freedom is required, i.e., the number of receive antenna of each user must be equal to or greater than the number of interferers. This may not be practical for many application cases. Alternatively, the MUI can be mitigated by intelligently designing the transmitted signals when $M_T \geq M_R$. If CSI is available at the BS, it is aware of where interference is being created for the given user by the signal transmitted to other users. The MUI can therefore be suppressed by transmitter precoding at the BS. The receiver structure is then simplified from a multiuser receiver. Moreover, correlated fading models for multiple antennas and closed-loop solutions for the same have been considered recently in 3G forums, arising when operators are constrained by considerations of space from placing antennas close to each other at the BS.

Multiuser OFDM is sensitive to frequency offsets, which lead to ICI and MUI. ICI and MUI suppression schemes will be proposed for multiuser MIMO OFDM downlink in Chapter 4 and 5.

1.2.4 OFDM Access

Orthogonal frequency-division multiple access (OFDMA), a combination of OFDM and frequency-division multiple access (FDMA), inherits OFDM's attractive features [41]. This broadband wireless access technology allows an efficient layer for multiple-user wireless applications. It allows different users to share one OFDM symbol such that separating different users using subcarrier orthogonality can avoid the MUI in a cell. Multiple subcarriers can be assigned per user to support high data rate applications. OFDMA systems can allocate power and data rate adaptively and optimally among the subcarriers to achieve high throughput. Also, compared with single-carrier multiple-access systems, OFDMA offers increased robustness to ISI and narrowband interference, allows straightforward dynamic channel assignment, and simplifies channel equalization at the receiver by performing one-tap equalization. MIMO OFDMA has been found to be capable of providing further system capacity gain by exploiting multiuser diversity in both the frequency domain and the space domain [42]. It thus becomse a strong candidate for broadband multiuser wireless communication systems, and have been considered for next-generation wireless systems such as broadband wireless multiple-access systems in the IEEE 802.16a MAN standard [35], which specifies the air interface for fixed broadband wireless access systems supporting multimedia services. OFDMA is also adopted in the Mobile WiMAX Air Interface [43] for improved multi-path performance in non-line-of-sight environments. Mobile WiMAX is a broadband wireless solution that enables convergence of mobile and fixed broadband networks through a common wide area broadband radio access technology and flexible network architecture.

In the 802.16a standard, the FFT space of OFDMA is divided into subchannels. They are used in downlink for separating the data into logical streams. Those streams employ different modulation, coding, and amplitude to address subscribers with different channel characteristics. In uplink the subchannels are used for multiple access. The subscribers are assigned on subchannels through Media Access Protocol (MAP) messages sent on the downlink. The subchannel is a subset of subcarriers out of the total set of available subcarriers. In order to mitigate the frequency selective

fading, the subcarriers of one subchannel are spread along the channel spectrum. In essence the principle of OFDMA consists of different users sharing the uplink FFT space, while each transmits over one or more subchannels. The division in subchannels is a form of FDMA. A low uplink data rate is consistent with the traffic asymmetry where the streams from each subscriber add up in a multipoint-to-point regime, while in downlink all the subchannels are transmitted together. So the OFDMA allows for fine granulation of bandwidth allocation, consistent with the needs of most subscribers, while high consumers of uplink bandwidth are allocated more than one subchannel. The subchannels in an OFDMA system are orthogonal, resulting in zero same-cell interference: the interference comes only from other cells. A variety of coding and modulation schemes are allocated selectively to each subscriber, in both upstream and downstream. There are trade-offs between throughput and robustness. The coding and modulation schemes provide efficient utilization of the spectrum, with subscribers in difficult positions taking robust schemes with low throughput. Those in better positions employ higher throughput schemes and are able to transmit the same amount of data in shorter allocations. The assignment of various modulation and coding schemes to subchannels can be used to optimize cell capacity. For urban and suburban propagation environments an OFDMA system can achieve 0.53 bit/s/Hz to 1.84 bit/s/Hz [43].

1.3 Closed-Loop Techniques

Closed-loop techniques aim to optimize SISO or MIMO systems using the CSI at the transmitter (CSIT). Closed-loop MIMO techniques can better exploit spatial diversity, help customize the transmitted waveforms to provide higher link capacity and throughput, improve system capacity by sharing the spatial channel with multiple users simultaneously, simplify multiuser receivers through interference avoidance, and enable channel-aware scheduling for multiple users [44]. Importantly, when CSI is available at the transmitter, it is easier to obtain the benefits of MIMO, while reducing the complexity of MIMO reception. Closed-loop diversity techniques, switched transmit diversity (STD) and transmit adaptive array (TXAA), have been used in the 3G standards,

including wideband code-division multiple access (WCDMA) and cdma2000 [3, 4].

The availability of CSIT is a primary requirement for closed-loop systems. This information can be estimated at the transmitter when a time-division duplex (TDD) mode is employed, when the forward and reverse links are approximately reciprocal. Alternatively, in frequency-division duplex (FDD) systems, i.e., when the forward and reverse links are independent, the CSI can be estimated at the receiver and sent back to the transmitter via a feedback link. Closed-loop systems overcome the disadvantage of open-loop systems, where the CSI is not available at the transmitter but only known at the receiver, such that open-loop techniques are one-size-fits-all approaches to achieve transmit diversity or capacity for all users. If accurate instantaneous feedback is available, closed-loop systems may offer a considerable performance gain over their open-loop counterparts. Closed-loop techniques, such as transmitter precoding, can be desired to react to the current or average channel conditions, and significantly improve system capacity or BER performance.

In closed-loop MIMO OFDM, if complete CSI, including both the frequency offset and channel response, is available at the transmitter, precoding is possible on frequency-selective channels to pre-process signals at the subcarrier level, and facilitates the utilization of the capacity or performance gain. Feedback requirements increase as the number of transmit and receive antennas, delay spread and the number of users grow, while the feedback capacity is usually limited. Imperfect feedback additionally results in CSI transmitter mismatch, i.e., the CSI which is available at the transmitter differs from the actual CSI at the time of transmission, which significantly degrades the system BER due to residual interference. Consequently, reduction of feedback requirements is an essential issue for precoding design in closed-loop MIMO OFDM systems.

It has been shown that additional performance can be extracted from multiple antennas in the presence of CSIT through, e.g., waterfilling [45]. It should be noted that although waterfilling may be optimal from an information theoretic point of view, it is not necessarily the best scheme using CSIT in practice [1]. This is because the performance of real-world MIMO links are sensitive to BER performance rather than mutual information performance. Schemes that exploit

CSIT to directly minimize BER-related metrics are therefore of interest, examples of which are found in [46–52]. In this thesis, the objective is to design transmitter precoding that could mitigate interference and save feedback capacity in closed-loop OFDM over uncorrelated and spatially-correlated MIMO channels. Linear precoding and non-linear Tomlinson-Harashima precoding (THP) are considered. The proposed precoders are expected to have good performance, relatively low complexity and low feedback requirements, which are disable features for interference mitigation schemes in closed-loop MIMO OFDM systems.

1.4 Organization and Contributions

In this thesis, several precoding schemes with only partial CSIT are proposed for ICI reduction in closed-loop MIMO OFDM systems. Precoders are also developed to reduce BER for OFDM over spatially correlated MIMO channels. The rest of the thesis is organized as follows.

Chapter 2 reviews pre-processing and post-equalization schemes, and compares their performance. It shows advantages of non-linear THP over linear precoding and successive interference cancellation (SIC) for MIMO transmission. The concept and matrix design of THP in MIMO systems are introduced. It is clarified that the non-linear TH precoder offers a significant BER gain over its linear counterpart and the SIC scheme, which is used in V-BLAST.

In Chapter 3, a TH precoder for closed-loop MIMO OFDM system with frequency offsets is introduced when only partial CSI (no knowledge of frequency offsets) is available at the transmitter. Firstly it is shown that the ICI coefficient matrix is approximately unitary. An immediate consequence is that the proposed precoder at the transmitter does not need to know the frequency offset. This avoids feedback in a TDD system, where frequency offsets may not be readily estimated at the transmitter. In FDD systems, this leads to savings of feedback capacity since a system with M_T transmit and M_R receive antennas may have $M_T \times M_R$ different frequency offsets. Frequency-offset mismatch due to imperfect feedback is also avoided. The proposed precoded OFDM significantly suppresses the BER degradation due to frequency offsets. Furthermore, for

spatially-correlated MIMO channels, proposed THP performs with negligible BER-performance loss.

Chapter 4 presents a novel two-stage technique for ICI and MUI suppression in closed-loop multiuser spatially-multiplexed (SM) OFDM downlink. The first stage applies non-linear THP at the BS transmitter to mitigate the MUI and the second stage employs an iterative MMSE equalizer at each user's receiver to suppress the ICI due to the frequency offset. The spatial channel gain matrix $\mathbf{H}$ is available at the BS in a typical closed-loop system. Since the precoder only needs $\mathbf{H}$ at the BS, the feedback load is reduced. The MMSE equalizer at each user's receiver has low complexity due to the unitary property of the ICI matrix. Our scheme significantly reduces the BER increase due to frequency offsets. When the feedback link is perfect, the proposed technique almost completely cancels the ICI and MUI, and experiences the same BER as in the case when only full-CSI (channel gains and frequency offset) precoding is used at the BS. Hence, sending frequency offset information to the BS does not offer additional BER improvement. When the feedback is inaccurate, our technique outperforms the case of full-CSI feedback since it avoids the possible frequency-offset mismatch.

In Chapter 5, both linear precoding and non-linear limited-feedback THP (LFB-THP) are developed for closed-loop multiuser MIMO OFDM systems with frequency offsets. SM MIMO OFDM with a linear receiver and OSTBC MIMO OFDM with an ML receiver are considered. Frequency offsets are shown to have no impact on precoding, and hence precoding on per-subcarrier basis is possible. Exploiting this property, the codebook design criterion previously used for flat-fading MIMO systems [53–56] is generalized to OFDM systems with frequency offsets. A pre-designed codebook of precoding matrices, available at both the transmitter and the receiver, is proposed. The receiver selects optimal matrices at the subcarrier level according to a certain criterion and sends only their indexes to the transmitter. The explicit values of CSI are hence not needed at the transmitter. Three precoding matrix selection criteria are analyzed. To further reduce the number of feedback bits, grouping with interpolation schemes is also introduced. In our pre-

coders, the feedback load is reduced to only a limited number of bits, which reduces feedback bit rate, and the non-linear property reduces power efficiency loss inherent in linear precoding, which makes non-linear precoding outperform linear precoding. Our precoders also display significant BER improvement for OFDM with frequency offsets over spatially correlated MIMO channels.

Chapter 6 considers covariance-based linear and non-linear precoding for MIMO OFDM systems. The main objective is to design precoders to mitigate the impact of transmit-antenna and path correlations. First, the impact of path correlations on the pairwise error probability (PEP) is analyzed, and closed-form, waterfilling-based linear and non-linear precoders are derived to minimize the worst-case PEP in OSTBC OFDM. Second, an adaptive transmission strategy is also developed for switching between precoded SM OFDM and precoded OSTBC OFDM. The system is designed to achieve a low BER with a target fixed transmission rate. The switching criterion is the minimum Euclidean distance of the received codebook. A lower complexity switching criterion is also developed. The switching decision sent to the transmitter requires one feedback bit per subcarrier. To reduce the number of feedback bits, the switching decision can be made for groups of neighboring subcarriers. The proposed precoders considerably reduce the error rate in antenna and path-correlated channels. The adaptive strategy outperforms either SM or OSTBC individually in terms of the BER.

In Chapter 7, precoding is investigated to effectively exploit mean and covariance feedback for error-rate improvement in OSTBC OFDM downlink. A general system model is considered in which the receiver imperfectly estimates CSI and sends the inaccurate estimates back to the BS via a feedback channel which introduces delay. The conditional mean and covariance of the channel matrix are derived. Mean-feedback precoding is proposed to achieve the maximum possible SNR in the general OSTBC OFDM system model. Our precoding takes into account the estimation errors and channel time variations over feedback delay and offers the optimal power allocation. The long-term channel statistics, including the variance of the estimation error and feedback delay, are assumed to be available at the transmitter. An adaptive dual-mode precoding

which switches between new mean-feedback precoding and covariance precoding is developed. Our adaptive precoding significantly reduces the required capacity of the feedback link since only covariance feedback is used when the channel conditions become severe, and individually outperforms either mean-feedback or covariance precoding.

Chapter 8 concludes this thesis by summarizing the major contributions and suggesting the future work.

Chapter 2

Transmitter Precoding for Closed-Loop MIMO Systems

This chapter reviews transmitter pre-processing schemes in MIMO channels. It shows advantages of non-linear THP over linear precoding and successive interference cancellation (SIC) for MIMO transmission. The concept and matrix design of THP in MIMO systems are introduced. Simulation results clarify that the non-linear TH precoder offers a significant BER gain over its linear counterpart and the SIC scheme, which is used in V-BLAST.

2.1 Introduction

In an $M_R \times M_T$ MIMO system, different data streams are transmitted simultaneously from the M_T transmit antennas to the M_R receive antennas. The general system model can be described by the basic relation $\mathbf{y} = \mathbf{H}\mathbf{x} + \mathbf{w}$ (2.1). The transmitted data vector $\mathbf{x}$ comprises the transmitted symbols of M_T parallel data streams. These streams can be formed by parallelizing of a high-rate data signal, or they can belong to different and independent users. The parallel transmission of independent streams ensures a high data rate, but results in severe inter-stream (inter-layer) interference at each receive antenna.

The main challenge in MIMO detection is the separation of the layered data streams. To recover the components of the transmitted data vector $\mathbf{x}$ which interfere at the receiver, interference cancellation algorithms at the receiver or precoding at the transmitter need to be applied. The

simplest strategy for separating the data streams is linear ZF schemes at the receiver, where the decision vector is generated by $\hat{\mathbf{x}} = \mathbf{H}^{\dagger}\mathbf{y}$, where $\dagger$ stands for Moore-Penrose pseudo-inverse operation. Both ZF and MMSE linear layer separation schemes suffer from noise enhancement and hence have poor BER performance. This disadvantage can be overcome by SIC or V-BLAST [16]. V-BLAST is a non-linear approach, but error propagation may occur.

The above methods are signal detection algorithms, which need CSI only at the receiver. Most practical systems will require some CSI available at the transmitter, in addition to the usual assumption of CSI known at the receiver. It is necessary since practical MIMO channels show highly varying transmission characteristics, which have to be accounted for in order to reach acceptable average performance. Complete CSIT enables the received data to be separated by means of pre-processing at the transmitter, which reduces the complexity of MIMO receivers. With perfect CSIT, interference at the receiver can be completely avoided by a multiplication of the data vector $\mathbf{A}$ with the right (pseudo) inverse $\mathbf{H}^{\dagger}$ of the channel matrix at the transmitter under the ZF criterion. Instead of transmitting the original data symbols $\mathbf{A}$, the pre-distorted symbols $\mathbf{x} = \mathbf{H}^{\dagger}\mathbf{A}$ are transmitted through the channel. However, linear precoding increases the transmit power such that it has the same loss in power efficiency as the linear separation scheme at the receiver. Another popular method for channel pre-processing in MIMO systems is to use the singular value decomposition (SVD) of the channel matrix $\mathbf{H}$ as in (2.3). Since the SVD-based precoding matrix is unitary, transmit power increase is avoided. However, the performance of SVD-based precoding is mainly determined by the smallest singular value of the channel. It thus approaches linear precoding at high SNR.

If CSI is available at the transmitter, the SIC at the receiver can be moved to the transmitter, leading to a TH precoder [57–61]. It is a transmitter-based pre-processing technique, which was originally proposed for temporal equalization of dispersive channels [57–59], and has been extended to flat-fading MIMO systems in [60,61] to combat the interference between different spatial transmission layers. Generally, each pre-processing strategy at the transmitter has its counterpart

of signal detection algorithm at the receiver [62]. Non-linear THP avoids the error propagation typical of DFE or SIC (its signal-detection counterparts) since the feedback filter is shifted to the transmitter, and eliminates the transmit power increase (noise enhancement) typical of linear precoding (its linear counterpart). This chapter studies linear and non-linear precoders, which require CSIT and reduce complexity of the receiver. The SIC signal detection algorithm is also investigated for performance comparison. THP is shown to outperform its linear precoding counterpart, SVD-based precoding and its signal-detection counterpart SIC.

The remainder of this chapter is organized as follows. Section 2.2 describes a general MIMO system model. Linear precoding schemes and V-BLAST are then briefly reviewed. Section 2.3 introduces the background and basic concept of TH precoder, and gives the matrix design of the THP with the ZF criterion. The simulation results are provided in Section 2.4 to illustrate the advantages of TH precoder. Section 2.5 concludes this chapter.

2.2 Layer Separation in MIMO Channels

This section first gives a general flat-fading MIMO system model. It then briefly introduces linear ZF/MMSE precoding, SVD-based precoding and V-BLAST techniques. Different scheme requires different system configurations. Degree of freedom is needed to perform the inverse format of the channel matrix. Generally speaking, complete transmitter pre-processing needs the number of transmit antennas is equal to or greater than the number o of receive antennas, $M_T \geq M_R$. Post-processing schemes require $M_R \geq M_T$.

The general model of transmission over a Rayleigh flat-fading MIMO channel can be considered as

$$\mathbf{y} = \mathbf{H}\mathbf{x} + \mathbf{w}, \tag{2.1}$$

where $\mathbf{x} = \begin{bmatrix} x_1 \ \dots \ x_{M_T} \end{bmatrix}^T$ is the vector of the transmitted symbols; x_v, $v = 1, \dots, M_T$ is the symbol sent by the v-th antenna. The $M_R \times M_T$ $\mathbf{H} = \begin{bmatrix} h_{u,v} \end{bmatrix}$ denotes the channel matrix of complex channel gains. The u-th additive white Gaussian noise (AWGN) sample in the M_R-dimensional

vector $\mathbf{w}$ has zero mean and variance σ_w^2, and $\mathbf{y} = \begin{bmatrix} y_1 & \dots & y_{M_R} \end{bmatrix}^T$ is the complex-valued vector of received signals. The data symbols transmitted in parallel experience inter-layer interference at the receiver. This interference caused by the MIMO channel has to be eliminated, i.e., an end-to-end transfer matrix $\mathbf{I}_{M_T}$ is desired such that M_T parallel, independent channels are generated.

2.2.1 Linear Precoding

For simplicity, linear precoding considers the number of transmit antennas is equal to or greater than the number o of receive antennas, i.e., $M_T \geq M_R$. When complete CSI is available at the transmitter, an $M_T \times M_R$ linear transformation matrix $\mathbf{L}$ can be used to pre-process transmitted symbols so that $\mathbf{x} = \mathbf{LA}$ instead of $\mathbf{A}$ is transmitted. With the ZF criterion, the end-to-end transfer matrix needs to be $\mathbf{HL}_{\text{ZF}} = \mathbf{I}$, such that $\mathbf{L}_{\text{ZF}} = \mathbf{H}^{\dagger}$. The inter-layer interference is thus eliminated. However, the channel inverse $\mathbf{H}^{\dagger}$ may increase the average transmit power, which will vary from symbol to symbol. In practical implementation, the average transmit power should be constant and large fluctuations are undesirable. Moreover, if the channel transfer function has zeros outside the unit circle, the pseudo inverse of the channel matrix will be unbounded. To alleviate these problems, one can design a linear precoder subject to a power constraint. Under the average transmit power constraint E_L and the MMSE criterion, the precoding structure is

$$\mathbf{L}_{\text{MMSE}} = \sqrt{\frac{E_L}{M_R}}\mathbf{H}^H \left(\mathbf{H}\mathbf{H}^H + \frac{M_R}{E_L}\mathbf{R}_{ww} \right)^{-1}, \tag{2.2}$$

where $\mathbf{R}_{ww} = \text{E}\left[\mathbf{w}\mathbf{w}^H\right]$. MMSE precoding outperforms ZF precoding at low SNR and approaches the latter at high SNR due to noise enhancement.

2.2.2 Singular Value Decomposition

Given the channel matrix $\mathbf{H}$ at both the transmitter and the receiver, an SVD of $\mathbf{H}$ generates

$$\mathbf{H} = \mathbf{U}\boldsymbol{\Gamma}\mathbf{V}^H, \tag{2.3}$$

where $\mathbf{U}$ is $M_R \times M_T$ and $\mathbf{U}^H\mathbf{U} = \mathbf{I}_{M_T}$; $\mathbf{V}$ is an $M_T \times M_T$ unitary matrix. $\boldsymbol{\Gamma}$ is the singular value matrix of $\mathbf{H}$; it is an $M_T \times M_T$ diagonal matrix with real, non-negative entries γ_n, $n = 1, \dots, M_T$,

in descending order $\gamma_1 \geq \gamma_2 \geq \cdots \geq \gamma_{M_T} \geq 0$. The SVD-based transmission scheme is to apply $\mathbf{V}$ as the transmitter precoding matrix and $\mathbf{U}^H$ at the receiver such that M_T independent parallel channels are generated. Since $\mathbf{U}$ and $\mathbf{V}$ are unitary matrices, in contrast to linear precoding, the noise enhancement is avoided. SVD-based precoding enables waterfilling power allocation, which increases capacity of the MIMO link. However, SVD-based precoding may suffer from highly unequal distribution of the singular values. The worst channel (the smallest singular value) dominates the error rate. Therefore, at high SNR the performance of the SVD-based scheme approaches that of linear precoding.

2.2.3 V-BLAST

The noise enhancement of linear precoding can be overcome by V-BLAST, which involves successive cancellation of inter-layer interference. V-BLAST is the most popular spatial multiplexing technique, the details of which have been described in Chapter 1. The architecture uses an ordered serial ZF or MMSE nulling and SIC scheme [16]. V-BLAST needs perfect CSI only at the receiver, and $M_R \geq M_T$. Since there is no precoding at the transmitter, the channel symbols x_u are equal to the data carrying symbols, i.e., $x_v = a_v$, $v = 1, \ldots, M'$. The key idea in V-BLAST is layer peeling where the individual data streams are successively decoded and stripped away layer by layer. Under the ZF or MMSE criterion, V-BLAST finds optimal order of processing the receive signals such that the most reliable decisions are taken initially to reduce the probability of error propagation. It thus selects the stream with highest signal-to-interference-plus-noise power ratio (SINR) at each decoding stage. Upon detection of the chosen symbol, its contribution from the received signal vector is subtracted and the procedure is repeated until all the symbols are detected.

In the absence of error propagation V-BLAST converts the MIMO channel into a set of parallel SISO channels with increasing diversity order at each successive stage. However, in practice, error propagation may be encountered. One possible solution to come close to the performance of an error-free SIC is to move the feedback filter of SIC to the transmitter, which leads to the TH

precoder.

2.3 Tomlinson-Harashima Precoding

THP was invented independently by Tomlinson [57], and Harashima and Miyakawa [58] for equalization of dispersive SISO channels. It is a very efficient strategy to remove ISI in single-carrier systems. It enables the application of coded modulation in a seamless fashion and is able to come close to the channel capacity of the underlying channel [59]. Spatial separation in MIMO systems is tightly related to temporal equalization for SISO transmission over ISI channels. The TH precoder is then extended to MIMO channels to combat the interference between different spatial transmission layers [60, 61]. This section first briefly reviews the THP structure and matrix calculation, and then describes the concepts of THP. For convenience of signal detection, $M_R \geq M_T$ and the zero-forcing criterion is assumed.

2.3.1 THP Structure and Matrix Calculation

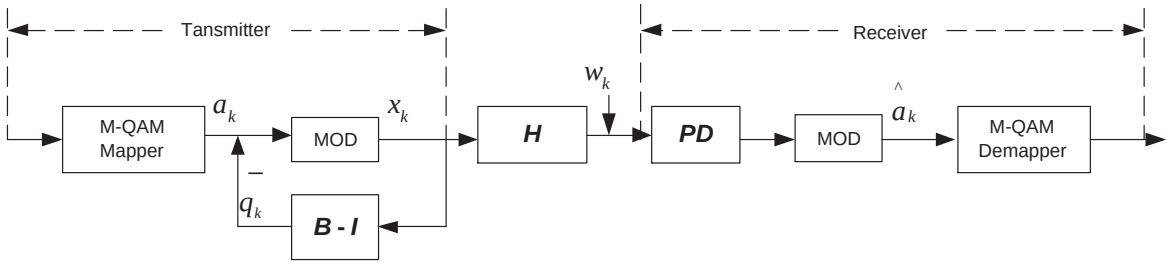

Figure 2.1: The block diagram of THP in MIMO links.

The structure of the TH precoder is shown in Fig. 2.1. The transmitter includes a modulo arithmetic device and an $M_T \times M_T$ feedback filter $\mathbf{B} - \mathbf{I}$, and the receiver consists of an $M_T \times M_T$ scaling matrix $\mathbf{P}$, an $M_R \times M_T$ feedforward filter $\mathbf{D}$, and a modulo arithmetic device. As discussed in [61], the feedback matrix must be strictly upper triangular to allow data precoding in a recursive fashion.

To explain the rationale behind the THP transmit structure, we temporarily neglect the non-linear operator in Fig. 2.1. The precoded symbols are recursively computed from the feedback structure as follows:

$$x_k = a_k - \sum_{i=k}^{M_T} (B(k,i) - 1) x_i. \tag{2.4}$$

Eq. (2.4) can be re-written in a matrix format as

$$\mathbf{x} = \mathbf{B}^{-1}\mathbf{a}, \tag{2.5}$$

where the $M_T \times M_T$ feedback filter $\mathbf{B}$ needs to be unit diagonal so that the average transmit power is constant. For the ZF criterion, the cascade of $\mathbf{PDHB}^{-1}$ must be an identical matrix such that the interfering parallel channels are transformed into non-interfering ones. Therefore, the feedback matrix and feedforward matrix need to satisfy

$$\mathbf{H} = (\mathbf{PD})^{\dagger}\mathbf{B}. \tag{2.6}$$

Therefore, the calculation of the filters in THP can be considered as performing a QR decomposition of the channel matrix:

$$\mathbf{H} = \mathbf{D}^H\mathbf{T}, \tag{2.7}$$

where $\mathbf{T} = \left[T(u,v)\right]$ is an $M_T \times M_T$ upper triangular matrix and $\mathbf{D}$ is an $M_T \times M_R$ matrix and $\mathbf{DD}^H = \mathbf{I}_{M_T}$. The matrices $\mathbf{P}$ and $\mathbf{B}$ can be obtained by:

$$\begin{aligned} \mathbf{B} &= \mathbf{PT}; \\ \mathbf{P} &= \text{diag}\left[T^{-1}(1,1) \ \ldots \ T^{-1}(M_T, M_T)\right], \end{aligned} \tag{2.8}$$

The scaling matrix $\mathbf{P}$ is to keep the average transmit power constant. Since $\mathbf{DD}^H = \mathbf{I}_{M_T}$ and $\mathbf{P}$ is a diagonal matrix, no matrix inversion is needed. The receiver structure is thus simplified. At the receiver, the cascade of the matrix is

$$\mathbf{PDHB}^{-1} = \mathbf{PDD}^H\mathbf{TT}^{-1}\mathbf{P}^{-1} = \mathbf{I}. \tag{2.9}$$

The inter-layer interference are therefore eliminated. The filtered noise then has the variance matrix $\mathbf{R}_{w'w'} = \mathbf{P}^2\sigma_w^2$. Discarding the congruent signals, the data symbols a_k are corrupted by an additive

noise as $Y_k = a_k + w'_k$, where w'_k is the k-th entry of filtered noise vector $\mathbf{w}'$. The extension from ZF to MMSE design is straightforward. The general case is discussed in [61].

2.3.2 Basic Concepts

By passing through the feedback structure, the transmitted symbols x_k are successively calculated for the data symbols a_k drawn from the initial M-ary QAM square signal constellation

$$\mathcal{A} = \left\{ a_{\mathrm{I}} + \jmath a_{\mathrm{Q}} \mid a_{\mathrm{I}},\ a_{\mathrm{Q}} \ \in \ \pm 1, \pm 3, \ldots, \pm(\sqrt{M} - 1) \right\}. \tag{2.10}$$

Inspection of (2.4) reveals that the dynamic range of the precoded sequence depends on $\mathbf{B}$ and may become large in the presence of deep fades. To overcome transmit power boosting, THP adopts a non-linear modulo-$2\sqrt{M}$ device, which acts independently over the real and imaginary parts of its input. The modulo operation generates a unique precoding sequence q_k, $q_k \in \mathcal{Q} = \left\{ 2\sqrt{M}(q_{\mathrm{I}} + \jmath q_{\mathrm{Q}}) \right\}$, where $q_{\mathrm{I}}, q_{\mathrm{Q}} \in \mathbf{I}$ and $\mathbf{I}$ is the set of integers. From the set $\mathcal{J} = \{a + q | a \in \mathcal{A},\ q \in \mathcal{Q}\}$, the effective data symbols $a_k + q_k$, instead of data symbols a_k, are passed into the modulo arithmetic feedback structure. Mathematically, integer multiples of $2\sqrt{M}$ are added to the real and imaginary part of x_k. The transmitted symbols after the modulo-$2\sqrt{M}$ operation can be written as

$$x_k = \mathrm{MOD}_{2\sqrt{M}} \left\{ a_k - \sum_{i=k}^{M_T} B(k,i) x_i \right\} = a_k + q_k - \sum_{i=k}^{M_T} B(k,i) x_i. \tag{2.11}$$

The modulo device periodically limits the expansion due to the inversion of $\mathbf{B}$ to a set $\mathcal{J}$. From $\mathcal{J}$ the current effective data symbol is selected, which minimizes the magnitude of the corresponding transmitted channel symbol x_k. The real and imaginary parts of q_k are chosen symbol-by-symbol by the memoryless modulo-$2\sqrt{M}$ operation, such that the transmitted channel symbols $\Re\{x_k\} \in \left(-\sqrt{M}, \sqrt{M}\right]$ and $\Im\{x_k\} \in \left(-\sqrt{M}, \sqrt{M}\right]$. Hence, the transmitted channel symbols x_k are restricted in the boundary region of $\mathcal{A}$, resulting in a transmit signal with smaller power. At the receiver, a slicer produces estimates $\hat{a}_k + \hat{q}_k$ of the effective data symbols, from which the unique estimated data symbols are generated by the same modulo operation.

The extension to a non-square constellation is straightforward if the boundary region $\mathcal{A}$ is rotated by 45°. For M-ary QAM, when $\log_2(M)$ is odd, the length of a side of $\mathcal{A}$ is $2\sqrt{M}$ and q_k comes from $\sqrt{2M}\mathbf{O}\mathbb{I}$, where $\mathbf{O} = \begin{pmatrix} 1 & -1 \\ 1 & 1 \end{pmatrix}$ is the rotation operator.

THP generates a nearly independent and identically distributed (i.i.d) transmit sequence x_k, uniformly distributed over the initial signal constellation $\mathcal{A}$. The approximation of i.i.d transmit sequence becomes accurate as M goes to infinity. The average transmit power of THP is thus by $\mathrm{E}\left[|x_k|^2\right] = 2M/3$ for the M-ary square constellation [61]. For an M-ary constellation the average power $\mathrm{E}\left[|a_k|^2\right] = 2(M-1)/3$; the precoding loss can thus be obtained by

$$\vartheta = \frac{\mathrm{E}\left[|x_k|^2\right]}{\mathrm{E}\left[|a_k|^2\right]} = \frac{M}{M-1}. \tag{2.12}$$

As M increases, the precoding loss becomes negligible. Moreover, x_k can be assumed mutually uncorrelated with variance $E_s = \mathrm{E}\left[|x_k|^2\right]$, $\forall\, k$. In MIMO systems, each symbol interval is processed separately. The precoding loss of spatial THP is lower than (2.12) because the channel symbols take on more discrete levels when going from component x_1 to x_{M_T} [61].

The non-linear property of THP eliminates transmit power increase in linear precoding or, in the case of spectral zero, linear precoding even does not exist. In addition, THP avoids error propagation, the main shortcoming of V-BLAST, since the feedback filter is moved to transmitter. Consequently, THP can provide better performance than linear precoding and V-BLAST.

2.4 Simulation Results

Fig. 2.2 compares BERs of linear precoding, SVD-based precoding, V-BLAST (SIC) and THP. The ZF criterion is used. A 4×4 16-QAM MIMO system is considered. The fading gains are i.i.d Gaussian random variables with unit variance. The 4×4 channel matrix $\mathbf{H}$ is assumed to change independently from symbol to symbol, and the receive antennas are already sorted in optimal order. Obviously, THP can achieve considerable performance gains over its linear precoding counterparts and the SVD-based scheme. SVD-based precoding outperforms linear precoding at a low SNR region since it avoids noise enhancement, however, it approaches linear precoding for high SNRs

because the BER of linear precoding is also dominated by the smallest singular value of the channel matrix. Since THP can avoid the error propagation, it has a clear advantage over SIC. Hence, like in SISO transmission, the same advantages of THP over its linear precoding counterparts and SIC (DFE for a SISO link) are achievable.

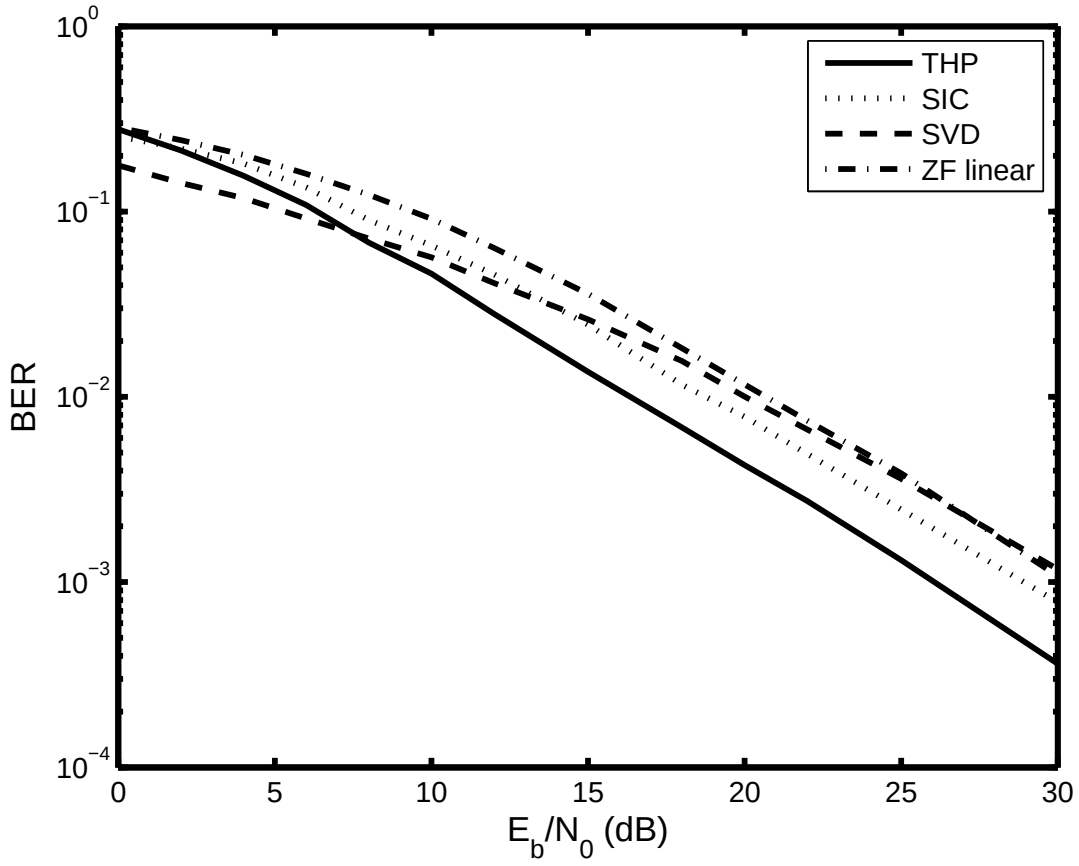

Figure 2.2: BERs for THP, SIC, SVD-based precoding and linear precoding with the ZF criterion in a 4×4 16-QAM system.

2.5 Summary

This chapter has introduced linear pre-equalization schemes and SIC, which is used in V-BLAST technique. The basic concept of a non-linear TH precoder has also been reviewed and the application of THP to the transmission over multiple-antenna communication links has been described. TH precoder outperforms the linear pre-equalization schemes and V-BLAST because it avoids noise enhancement and error propagation.

Chapter 3

ICI Reduction for Closed-Loop MIMO OFDM

As discussed in Chapter 1, MIMO OFDM is sensitive to frequency offset. ICI reduction schemes thus need to be applied. In a typical closed-loop system, the channel gains can be readily obtained at the transmitter, while the frequency offset may not be. In a TDD system, the frequency offset may be difficult to be estimated at the transmitter. In an FDD system, the frequency offset has to be estimated at the receiver and fed back to the transmitter. Therefore, a conventional closed-loop scheme may not be used for ICI suppression since the complete CSI, including both channel gains and frequency offsets, is needed at the transmitter. The feedback link is needed to convey the frequency offset in a TDD mode and the complete CSI in FDD systems. This chapter thus investigates the possibility to use precoding for ICI mitigation in closed-loop MIMO OFDM when only partial CSI (no knowledge of frequency offsets) is available at the transmitter.

We first show that the ICI coefficient matrix is approximately unitary. An immediate consequence is that the proposed precoder at the transmitter does not need to know the frequency offset. This avoids feedback in a TDD system. In FDD systems, this leads to significant savings of feedback capacity since a system with M_T transmit and M_R receive antennas may have $M_T \times M_R$ different frequency offsets. Frequency-offset mismatch due to imperfect feedback is also avoided. The proposed precoder includes two parts: the feedback filter at the transmitter and the feedforward filter at the receiver. It takes advantage of the property of the ICI matrix and the receiver

structure is effectively designed for ICI reduction. The presented precoded MIMO OFDM system significantly suppresses the impact due to frequency offsets. Furthermore, for spatially-correlated MIMO channels, proposed THP performs with negligible BER-performance loss.

Previous work on ICI reduction has focused on open-loop SISO and MIMO OFDM. For SISO systems, an optimum time-domain Nyquist windowing function has been derived in [63], which mitigates the joint effect of AWGN and ICI. Selected mapping and partial transmit sequence approaches have been developed in [64] to reduce ICI. In [65] MMSE receivers based on a finite power series expansion for the time-varying frequency response have been proposed. A two-stage ICI-suppressing equalizer is presented in [66], which applies a linear preprocessing at the transmitter and an iterative MMSE estimation at the receiver. Self-cancellation schemes involving mapping of each input symbol to a group of subcarriers have been investigated in [67, 68], at the price of halving the bandwidth efficiency. For open-loop MIMO OFDM, a bank of time-domain ICI cancellation filters is proposed to maximize ratio of signal energy to ICI-plus-noise energy [69].

The remainder of this chapter is organized as follows. Section 3.1 describes a MIMO OFDM system model in the presence of frequency offsets. In Section 3.2, the ICI coefficient matrix is proven to be unitary and a TH precoder is proposed based on this property. Two cases of channel mismatch are analyzed. Section 3.3 analyzes the proposed THP in spatial correlated channels. Simulation results in Section 3.4 show how the proposed TH precoder reduces ICI. Section 3.5 concludes this section.

3.1 System Model

This section will introduce the MIMO OFDM system model with frequency offsets. This model can also be simplified to SISO OFDM systems.

Consider an OFDM system with M_T transmit antennas and M_R receive antennas (Fig. 1.1). Let $X_v[n]$ denote an M-ary QAM symbol on the n-th subcarrier sent by the v-th transmit antenna. The length-N input data vector can then be written as $\mathbf{X}_v = \left[X_v[0]\, X_v[1]\, \ldots\, X_v[N-1]\right]^T$. In MIMO

OFDM transmission, each of the M_T time-domain transmitted vectors is generated by taking an IDFT of an information vector:

$$\mathbf{x}_v = \left[x_v(0)\, x_v(1) \ldots\, x_v(N-1)\right]^T = \mathcal{F}_N \mathbf{X}_v. \tag{3.1}$$

Considering a wideband frequency-selective fading channel with L resolvable paths between the v-th transmit antenna and u-th receive antenna, the discrete-time domain received signal can be represented as

$$y_{u,v}(k) = e^{\jmath \frac{2\pi}{N} \varepsilon_{u,v} k} \sum_{l=0}^{L-1} h_{u,v}(l) x_v(k-l) + w_{u,v}(k) \tag{3.2}$$

where $\varepsilon_{u,v} = \Delta f_{u,v} T_s$ is the normalized frequency offset between the u-th ($u = 1, \ldots, M_R$) receive and v-th ($v = 1, \ldots, M_T$) transmit antenna. The complex channel gain $h_{u,v}(l), l = 0, 1, \ldots, L-1$ refers to the l-th path. Each path gain is a zero-mean complex Gaussian random variable (Rayleigh fading) with variance σ_l^2 (see the simulation section for details). The channel gains are assumed to remain constant over several OFDM symbol intervals.

Discarding the cyclic prefix and performing DFT on the received samples, the signal received at the u-th receive antenna for the k-th subcarrier is given by

$$Y_u[k] = \underbrace{\sum_{v=1}^{M_T} S_{u,v}[0] H_{u,v}[k] X_v[k]}_{\text{desired signal}} + \underbrace{\sum_{v=1}^{M_T} \sum_{n=0, n\neq k}^{N-1} S_{u,v}[n-k] H_{u,v}[n] X_v[n]}_{\text{ICI component}} + \sum_{v=1}^{M_T} W_{u,v}[k] \tag{3.3}$$

for $k = 0, 1, \cdots, N-1$, where $W_{u,v}[k]$ is an AWGN sample with zero mean and variance σ_W^2, and $W_{u,v}[k], \forall\, k$, are assumed i.i.d. The channel gain on the k-th subcarrier is

$$H_{u,v}[k] = \sum_{l=0}^{N-1} h_{u,v}(l) e^{-\jmath \frac{2\pi}{N} lk}, \tag{3.4}$$

$H_{u,v}[k]$ are i.i.d. complex Gaussian random variables with zero mean and variance normalized to unity. $S_{u,v}[n-k]$ is an ICI coefficient given by [67, 70]

$$S_{u,v}[m] = \frac{\sin \pi(\varepsilon_{u,v} + m)}{N \sin \frac{\pi}{N}(\varepsilon_{u,v} + m)} e^{\jmath \pi (1 - \frac{1}{N})(\varepsilon_{u,v} + m)}, \quad m = 0, 1, \ldots, N-1. \tag{3.5}$$

All received signals can thus be represented in matrix form as

$$\mathbf{Y} = \mathbf{SHX} + \mathbf{W} = \mathbf{GX} + \mathbf{W} \tag{3.6}$$

where the NM_R-dimensional vector $\mathbf{Y} = \left[Y_1[0] \ \ldots \ Y_1[N-1] \ \ldots \ Y_{M_R}[N-1]\right]^T$; the $NM_T \times 1$ transmitted vector $\mathbf{X} = \left[\mathbf{X}_1^T \ldots \mathbf{X}_{M_T}^T\right]^T$; the noise vector $\mathbf{W}$ with the $\{(u-1)N+k\}$th entry $W_u[k] = \sum_{v=1}^{M_T} W_{u,v}[k]$, $\forall\, k, u$. The $NM_R \times NM_T$ overall channel matrix is $\mathbf{G} = \mathbf{SH}$, where $\mathbf{S}$ is an $NM_R \times NM_R M_T$ ICI matrix

$$\mathbf{S} = \text{diag}\left[\mathbf{S}_1 \quad \ldots \quad \mathbf{S}_{M_R}\right] \tag{3.7}$$

with $\mathbf{S}_u = \left[\mathbf{S}_{u,1} \quad \ldots \quad \mathbf{S}_{u,M_T}\right]$; the $\{u,v\}$th element is the ICI coefficient matrix between the u-th receive and v-th transmit antenna

$$\mathbf{S}_{u,v} = \begin{bmatrix} S_{u,v}[0] & S_{u,v}[1] & \ldots & S_{u,v}[N-1] \\ S_{u,v}[-1] & S_{u,v}[0] & \ldots & S_{u,v}[N-2] \\ \vdots & & \ddots & \vdots \\ S_{u,v}[-(N-1)] & S_{u,v}[-(N-2)] & \ldots & S_{u,v}[0] \end{bmatrix}. \tag{3.8}$$

And $\mathbf{H}$ is an $NM_RM_T \times NM_T$ channel gain matrix, which is given by

$$\mathbf{H} = \left[\mathbf{H}_1 \quad \ldots \quad \mathbf{H}_{M_R}\right]^T = \begin{bmatrix} \mathbf{H}_{1,1} & \ldots & \mathbf{0} & \ldots & \mathbf{H}_{M_R,1} & \ldots & \mathbf{0} \\ \vdots & \ddots & \vdots & & \vdots & \ddots & \vdots \\ \mathbf{0} & \ldots & \mathbf{H}_{1,M_T} & \ldots & \mathbf{0} & \ldots & \mathbf{H}_{M_R,M_T} \end{bmatrix}^T, \tag{3.9}$$

where $\mathbf{H}_u = \text{diag}\left[\mathbf{H}_{u,1} \quad \ldots \quad \mathbf{H}_{u,M_T}\right]$ with elements being the $\{u,v\}$th channel gain matrix $\mathbf{H}_{u,v}$ at the N orthogonal subcarriers,

$$\mathbf{H}_{u,v} = \text{diag}\left[H_{u,v}[0] \quad H_{u,v}[1] \quad \ldots \quad H_{u,v}[N-1]\right]. \tag{3.10}$$

When $M_T = 1$ and $M_R = 1$, (3.6) reduces to the system model of a SISO OFDM system.

3.2 ICI Reduction in MIMO OFDM

To eliminate the interference from the overall channel matrix (including both $\mathbf{S}$ and $\mathbf{H}$), transmitter pre-processing or receiver post-processing needs to be applied. For a system with conventional

precoding, the full CSI information is required at the transmitter. As discussed in Chapter 2, the ZF-THP requires $\mathbf{B} = \mathbf{PDH}$. The feedforward matrix of THP is thus designed at the receiver by using a QR decomposition of the overall channel matrix

$$\mathbf{G} = \mathbf{D}^H \mathbf{T}, \tag{3.11}$$

where $\mathbf{DD}^H = \mathbf{I}$ and $\mathbf{T} = \left[T(i,j)\right]$ is an upper triangular matrix [71]. The feedback matrix $\mathbf{B}$ and the scaling matrix $\mathbf{P}$ can be constructed as in Chapter 2.

This conventional precoding design requires complete CSI at the transmitter. The provision of frequency-offset estimates at the transmitter is difficult, and hence is undesirable. A precoder for MIMO OFDM with only partial CSIT is therefore of interest. The ICI coefficient matrix between the v-th transmit and the u-th receive antenna $\mathbf{S}_{u,v}$ is first proven to be unitary. Consequently, the frequency offsets do not need to be fed back to the transmitter. The proposed THP can thus take advantage of the frequency offset at the receiver and reduces ICI in its feedforward filter.

3.2.1 Unitary Property of ICI Coefficient Matrix

The following unitary property related to the ICI coefficient matrix on the $\{u, v\}$th channel (3.8) can be derived using (3.5):
The ICI coefficient matrix can be approximated as a unitary matrix, i.e., $\mathbf{S}_{u,v}\mathbf{S}_{u,v}^H = \mathbf{S}_{u,v}^H\mathbf{S}_{u,v} = \mathbf{I}_N$. Therefore, the inverse of the matrix can be easily calculated by taking the conjugate transpose since $\mathbf{S}_{u,v}^{-1} = \mathbf{S}_{u,v}^H$. A proof of this property is in the appendix. The property is used in the design of the proposed precoder.

3.2.2 THP for MIMO OFDM

For convenience of signal detection, the number of receive antennas is assumed greater than or equal to that of the transmit antennas, i.e., $M_R \geq M_T$. Considered the case of M_R different frequency offsets is , i.e., for the u-th receive antenna, $\varepsilon_{u,1} = \varepsilon_{u,2} = \cdots = \varepsilon_{u,M_T} = \varepsilon_u$, and $\varepsilon_u \neq \varepsilon_{u'}, \forall\, u \neq u'$.

Since the frequency offset $\varepsilon_{u,v}$, $\forall v$, is identical to ε_u, $\mathbf{S}_{u,1} = \cdots = \mathbf{S}_{u,M_T} = \mathcal{S}_u$; and $\mathcal{S}_u$ is an $N \times N$ unitary matrix. The overall channel matrix $\mathbf{G}$ can be re-written as

$$\mathbf{G} = \mathcal{S}\mathcal{H}, \tag{3.12}$$

where the $NM_R \times NM_T$ channel gain matrix is

$$\mathcal{H} = \begin{bmatrix} \mathbf{H}_{1,1} & \cdots & \mathbf{H}_{1,M_T} \\ \vdots & \ddots & \vdots \\ \mathbf{H}_{M_R,1} & \cdots & \mathbf{H}_{M_R,M_T} \end{bmatrix}, \tag{3.13}$$

and the $NM_R \times NM_R$ ICI matrix is

$$\mathcal{S} = \text{diag}\begin{bmatrix} \mathcal{S}_1 & \cdots & \mathcal{S}_{M_R} \end{bmatrix}. \tag{3.14}$$

Since $\mathcal{S}_u$ is unitary, $\mathcal{S}$ is also a unitary matrix.

Instead of factorization of the overall channel matrix $\mathbf{G}$, the filters of THP are designed by QR decoposition of the channel gain matrix $\mathcal{H}$

$$\mathcal{H} = \mathbf{F}^H\mathbf{T} \tag{3.15}$$

with an $NM_T \times NM_R$ matrix $\mathbf{F}$ satisfying $\mathbf{F}\mathbf{F}^H = \mathbf{I}_{NM_T}$, and an $NM_T \times NM_T$ upper triangular matrix $\mathbf{T}$. The feedforward matrix needs to satisfy $\mathbf{D}\mathbf{D}^H = \mathbf{I}_{NM_T}$. Since $\mathcal{S}$ is unitary, the feedforward matrix is designed as $\mathbf{D} = \mathbf{F}\mathcal{S}^H$ so that $\mathbf{G} = \mathbf{D}^H\mathbf{T} = \mathcal{S}\mathbf{F}^H\mathbf{T} = \mathcal{S}\mathcal{H}$, which meets the basic relationship of ZF THP in (2.6).

The feedback filter is set as an $NM_T \times NM_T$ matrix $\mathbf{B} = \mathbf{P}\mathbf{T}$, where the $NM_T \times NM_T$ diagonal matrix $\mathbf{P}$ satisfies $\text{E}\left[\mathbf{T}^H\mathbf{P}^H\mathbf{P}\mathbf{T}\right] = \mathbf{I}$. The received signals at the output of the slicer can be given as

$$\hat{\mathbf{A}} = \mathbf{P}\mathbf{D}\mathbf{G}\mathbf{B}^{-1}\mathbf{A} + \mathbf{P}\mathbf{D}\mathbf{W} = \mathbf{\Psi}\mathbf{A} + \mathbf{W}', \tag{3.16}$$

where $\mathbf{\Psi} = \mathbf{P}\mathbf{D}\mathbf{G}\mathbf{B}^{-1} = \mathbf{P}\mathbf{D}\mathbf{D}^H\mathbf{P}^{-1}$ is an $NM_T \times NM_T$ identity matrix, if the channel gain matrix $\mathcal{H}$ is perfectly known at the transmitter. The feedforward matrix in the proposed precoder consists of the inverse (Hermitian) ICI matrix, and eliminates ICI. Because the ICI matrix is unitary, no inversion operation is needed and the receiver structure is simple.

With the property of the ICI matrix, the proposed precoder takes advantage of the CSIR (frequency offset at the receiver), and intelligently reduce ICI in the feedforward structure. No additional ICI reduction schemes [63–67, 69] are needed. The proposed THP for MIMO OFDM systems, which does not require the knowledge of frequency offsets at the transmitter, reduces information load in the feedback channel and avoids the possible frequency-offset transmitter mismatch due to feedback errors and delay in practical implementation. With perfect information of channel gains at the transmitter and knowledge of frequency offset at the receiver, proposed THP outperforms linear precoding. Furthermore, because the feedback filter is moved to the transmitter in the TH precoder, the error propagation, which inevitably degrades BER in SIC, is avoided. Therefore, lower BER can be expected for THP.

3.2.3 The Effect of Mismatch on Precoding Performance

If ideal feedback and precise channel estimates exist, closed-loop systems offer a substantial advantage over their open-loop counterparts. However, erroneous estimates and/or imperfect feedback results in transmitter channel mismatch, i.e., the channel information which is available at the transmitter differs from the actual channel at the time of transmission due to imperfect estimation, feedback delay and errors. Two cases of channel mismatch are considered. In the first case, the receiver knows $\mathbf{H}$ perfectly, but the transmitter has imperfect channel matrix $\hat{\mathbf{H}}$ because of feedback delay or noise. In the second case, the receiver has the imperfect channel estimate $\mathbf{H}_R$, while the transmitter has $\mathbf{H}_T$, which is a noise-corrupted version of $\mathbf{H}_R$ because of imperfect feedback. $\mathbf{H}_T$ is unknown at the receiver. Since frequency offsets do not need to be sent back to the transmitter, the frequency-offset transmitter mismatch is not considered here. The impact of frequency-offset mismatch in conventional THP is shown in the simulation section.

3.2.3.1 First Case

In the first case, the receiver has perfect knowledge of the channel $\mathbf{H}$, but the transmitter has an incorrect estimate $\hat{\mathbf{H}}$ because of errors or delay in the feedback link. The received signals are

$$\hat{\mathbf{A}} = \mathbf{PDG}\hat{\mathbf{B}}^{-1}\mathbf{A} + \mathbf{W}' = \hat{\mathbf{\Psi}}\mathbf{A} + \mathbf{W}', \tag{3.17}$$

where $\hat{\mathbf{\Psi}} = \mathbf{PT}\hat{\mathbf{B}}^{-1} = \mathbf{B}\hat{\mathbf{B}}^{-1}$. Obviously, $\hat{\mathbf{\Psi}}$ is not a diagonal matrix as $\mathbf{\Psi}$ in (3.16). Generally, $\mathbf{B}\hat{\mathbf{B}}^{-1}$ is an upper triangular matrix and introduces residual ICI.

3.2.3.2 Second Case

In the second case of channel information mismatch, the receiver has an imperfect frequency offset estimate $\hat{\mathbf{S}}$ and the incorrect channel gain estimate $\mathbf{H}_R$, while the transmitter has $\mathbf{H}_T$, which is the noise-corrupted version of $\mathbf{H}_R$. The $\mathbf{H}_T$ is unknown at the receiver, and $\mathbf{H}_T \neq \mathbf{H}_R \neq \mathbf{H}$. At the transmitter $\hat{\mathbf{B}}$ is constructed from $\mathbf{H}_T$, and at the receiver $\hat{\mathbf{D}}$ from $\mathbf{H}_R$ and $\hat{\mathbf{S}}$. This leads to a non-identity matrix $\hat{\mathbf{\Psi}} = \hat{\mathbf{P}}\hat{\mathbf{D}}\mathbf{G}\hat{\mathbf{B}}^{-1}$.

With the proposed THP in 2×2 OFDM, the received signals become

$$\hat{\mathbf{A}} = \hat{\mathbf{\Psi}}\mathbf{A} + \mathbf{W}' = \begin{bmatrix} \hat{\mathbf{\Psi}}_1 & \hat{\mathbf{\Psi}}_2 \\ \hat{\mathbf{\Psi}}_3 & \hat{\mathbf{\Psi}}_4 \end{bmatrix} \mathbf{A} + \mathbf{W}', \tag{3.18}$$

where the $N \times N$ matrix $\hat{\mathbf{\Psi}}_1$ and $\hat{\mathbf{\Psi}}_4$ are not approximately identity, and $\hat{\mathbf{\Psi}}_2$ and $\hat{\mathbf{\Psi}}_3$ are not zero matrices. Clearly, co-channel interference (CCI) and residual ICI are introduced to the combined signals. In SISO systems, no CCI occurs, however, since $\hat{\mathbf{D}}\mathbf{D}^H \neq \mathbf{I}_N$ and $\mathbf{T}\hat{\mathbf{T}}^{-1} \neq \mathbf{I}_N$, residual ICI is still introduced.

3.3 Correlated Spatial Channels

The MIMO channel with spatial correlations of its gains is studied in this section. The correlated channel model builds on previous work reported in [72]. For the sake of simplicity, a uniform linear array (ULA) is assumed at the transmitter and receiver with identical antenna elements. The

channel matrix $\tilde{\mathbf{H}}$ is assumed to be zero-mean circularly symmetric complex Gaussian (Rayleigh fading) distributed with a separable spatial correlation function.

For a frequency-selective channel with M_T transmit and M_R receive antennas, the l-th tap gain can be represented by an $M_R \times M_T$ matrix $\mathbf{h}(l)$, $\forall\, l$. According to the model in [72], the spatial gain correlation matrix can be represented by

$$\mathbf{R} = \mathbf{R}_P \otimes \mathbf{R}_T^T \otimes \mathbf{R}_R, \tag{3.19}$$

where $\mathbf{R}_P$ is the $L \times L$ path correlation matrix; if the paths between each transmit-receive antenna pair are uncorrelated, $\mathbf{R}_P = \text{diag}\left[\sigma_0^2 \ldots \sigma_{L-1}^2\right]$ is only determined by the power delay profiles. $\mathbf{R}_T$ and $\mathbf{R}_R$ are the transmit and receive antenna correlation matrices with entries [72]

$$\begin{aligned} R_T(m,n) &= \mathcal{J}_0\left(2\pi|m-n|\zeta_T\right) \\ R_R(m,n) &= \mathcal{J}_0\left(2\pi|m-n|\zeta_R\right), \end{aligned} \tag{3.20}$$

where $\mathcal{J}_0$ is zero-order Bessel function of the first kind. $\zeta_T = \Delta\frac{d_T}{\lambda_c}$ and $\zeta_R = \frac{d_R}{\lambda_c}$; $\lambda_c = c/f_c$ is the wavelength at the carrier frequency f_c, Δ is the angle of arrival spread. The transmit and receive antennas are respectively spaced by d_T and d_R. The tap gain vector therefore can be obtained as

$$\text{vec}\left(\mathbf{h}(l)\right) = \left[\mathbf{R}_T^T \otimes \mathbf{R}_R\right]^{1/2} \text{vec}\left(\mathbf{h}_w(l)\right), \tag{3.21}$$

where $\text{vec}\left(\mathbf{h}_w(l)\right)$ is an $M_R M_T$-dimensional vector of i.i.d zero mean complex Gaussian random variables with variance σ_l^2.

Using $\mathbf{h}(l)$ in (3.21), $\forall\, l$, the channel gain matrix with spatial correlations $\tilde{\mathbf{H}}$ can be constructed having the same structure as $\mathbf{H}$ (3.9) or $\mathcal{H}$ (3.13). The proposed non-linear TH precoder can be also used in MIMO OFDM when the spatial channels are correlated. With known fading correlations at the transmitter, QR factorization of $\tilde{\mathbf{H}}$ is performed instead of $\mathcal{H}$ or $\mathbf{H}$. The design of feedback and feedforward filters is the same as that described in the Section 3.2.

3.4 Simulation Results

In this section, simulation results show how proposed THP suppresses ICI in OFDM. The vehicular B channel specified by ITU-R M. 1225 [73], is used where the channel taps are zero-mean complex Gaussian random processes with variances of -4.9 dB, -2.4 dB, -15.2 dB, -12.4 dB, -27.6 dB, and -18.4 dB relative to the total power normalized to unity. The excess delays of the channel taps are 0, 300 ns, 8900 ns, 12900 ns, 17100 ns, and 20000 ns, respectively. For many wireless systems, the multipath channels fade slowly. Thus the fading gains are assumed constant over several OFDM symbol intervals.

3.4.1 SISO OFDM

Fig. 3.1 gives the BER as a function of SNR for different values of the normalized frequency offset in SISO OFDM with perfect channel knowledge at both the transmitter and the receiver. The performance of OFDM without precoding is shown as a reference. The proposed THP-OFDM reduces ICI significantly. For instance, with a normalized frequency offset of 10%, THP-OFDM has almost the same BER as an OFDM system in the absence of frequency offset, i.e., the ICI has been cancelled almost completely.

Fig. 3.2 presents BER of THP-OFDM when the receiver has perfect knowledge of channel gain matrix $\mathbf{H}$, while the transmitter has an imperfect channel $\hat{\mathbf{H}}$ due to the feedback channel noise. Since the feedback channel bandwidth is usually much smaller than the downlink traffic channel capacity, the noise variance of the feedback link is assumed to be $\sigma_F^2 = \sigma_W^2/100$. The frequency offset is perfectly estimated at the receiver. The BER of OFDM with conventional THP is also shown as a reference in the Fig. 3.2. In that reference case, conventional THP uses a noise-corrupted frequency offset at the transmitter, which leads to serious ICI residuals. The proposed precoder minimizes the BER degradation by avoiding such frequency-offset mismatch.

In Fig. 3.3, the channel gain matrix estimate $\mathbf{H}_R$ is assumed imperfect at the receiver, while the transmitter uses a channel gain matrix estimate corrupted further by feedback errors. The frequency

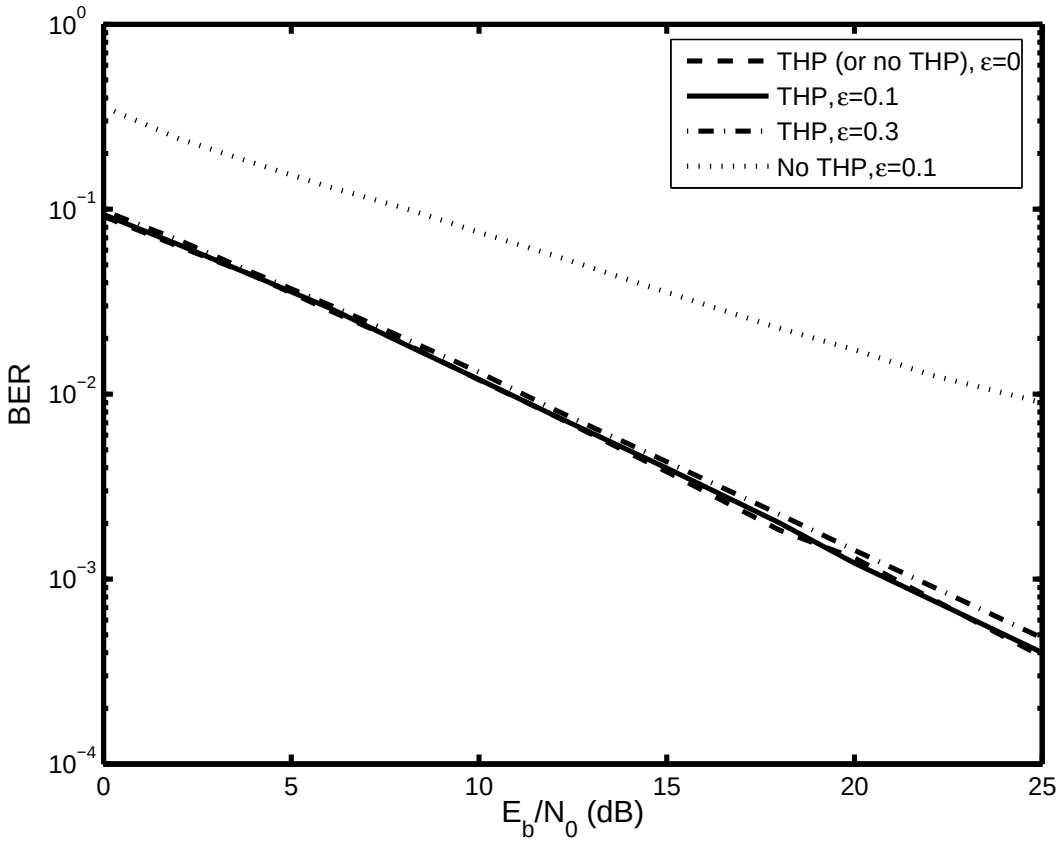

Figure 3.1: BER with THP as a function of the SNR for different values of the normalized frequency offset for closed-loop SISO 4-QAM 64-subcarrier OFDM, with perfect channel gain matrix at both the transmitter and the receiver.

offset is also estimated at the receiver with reasonable quality. The estimation schemes used are described in [5] and the references therein. The channel gain matrix $\mathbf{H}$ does not change within two consecutive OFDM symbol periods. At SNR=20 dB, with the frequency offset estimation algorithm described in [5], the average normalized MSE of the frequency offset estimate is 1.44×10^{-3} for 10% normalized frequency offset, and 6.30×10^{-3} for 30% normalized frequency offset. With the estimated frequency offset assumed constant over at least one OFDM symbol, the channel gains are estimated using pilot symbols as in [74], where pilot symbols are multiplexed with the OFDM blocks in the time domain to enable channel estimation. In order to guarantee reasonable performance of the channel estimator, every OFDM symbol is followed by a pilot block of length

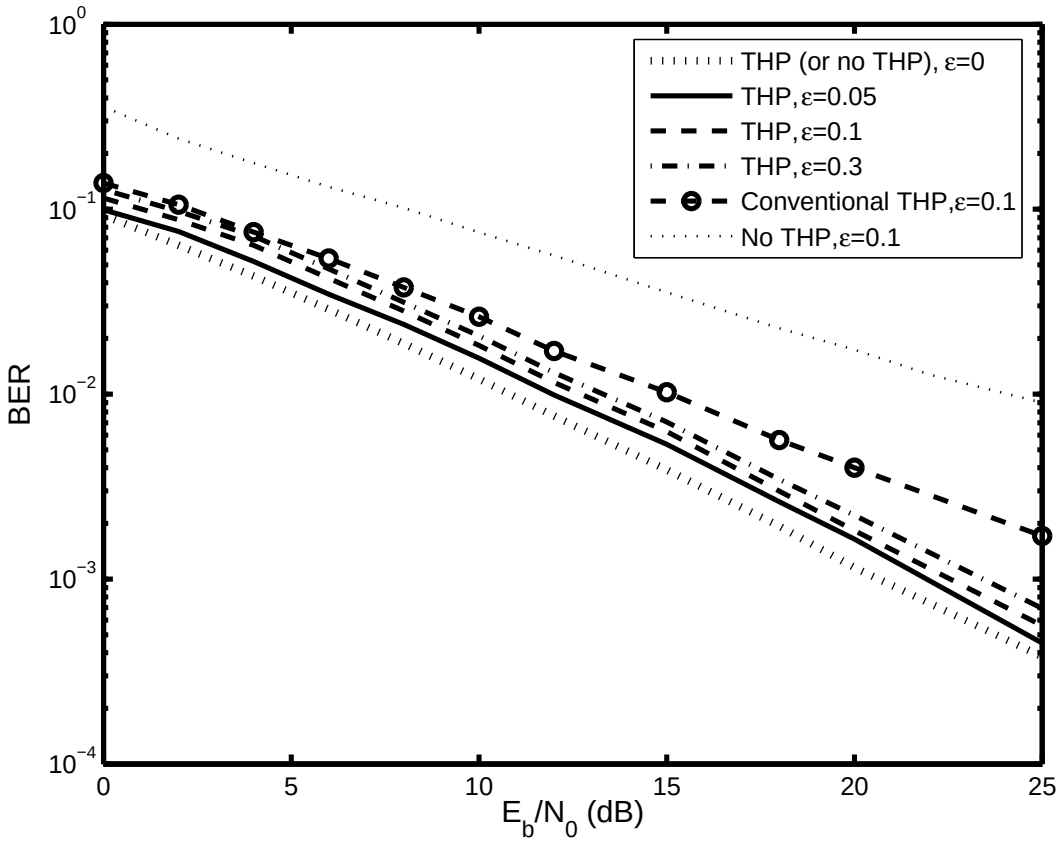

Figure 3.2: BER with THP as a function of the SNR for different values of the normalized frequency offset for closed-loop SISO 4-QAM 64-subcarrier OFDM, with perfect channel gain matrix at the receiver, and inaccurate channel gain matrix at the transmitter.

$2N_{CP}$, where N_{CP} is the length of cyclic prefix. In the simulation, $N = 64$ and $N_{CP} = 16$. The throughput loss incurred due to the pilot blocks is $2N_{CP}/(N + N_{CP})$. For a given data rate, it is possible that $N \gg N_{CP}$ if the number of subcarriers is large. In this case, the throughput loss will be small. With the estimation algorithm used, at SNR=20 dB, the average normalized MSE of the channel gain estimates is around 0.036 with a normalized frequency offset of 10%, and 0.047 with a normalized frequency offset of 30%. The value of MSE decreases as SNR increases. The channel gain estimates are conveyed to the transmitter via a noisy feedback link with noise variance $\sigma_F^2 = \sigma_W^2/100$. In OFDM with conventional THP, the estimated frequency offset has to be sent back, which introduces further mismatch due to errors in frequency offset information available at

the transmitter and results in severe performance loss. In proposed THP, however, frequency offset information is not needed at the transmitter, and the errors in channel estimates only lead to slight BER degradations.

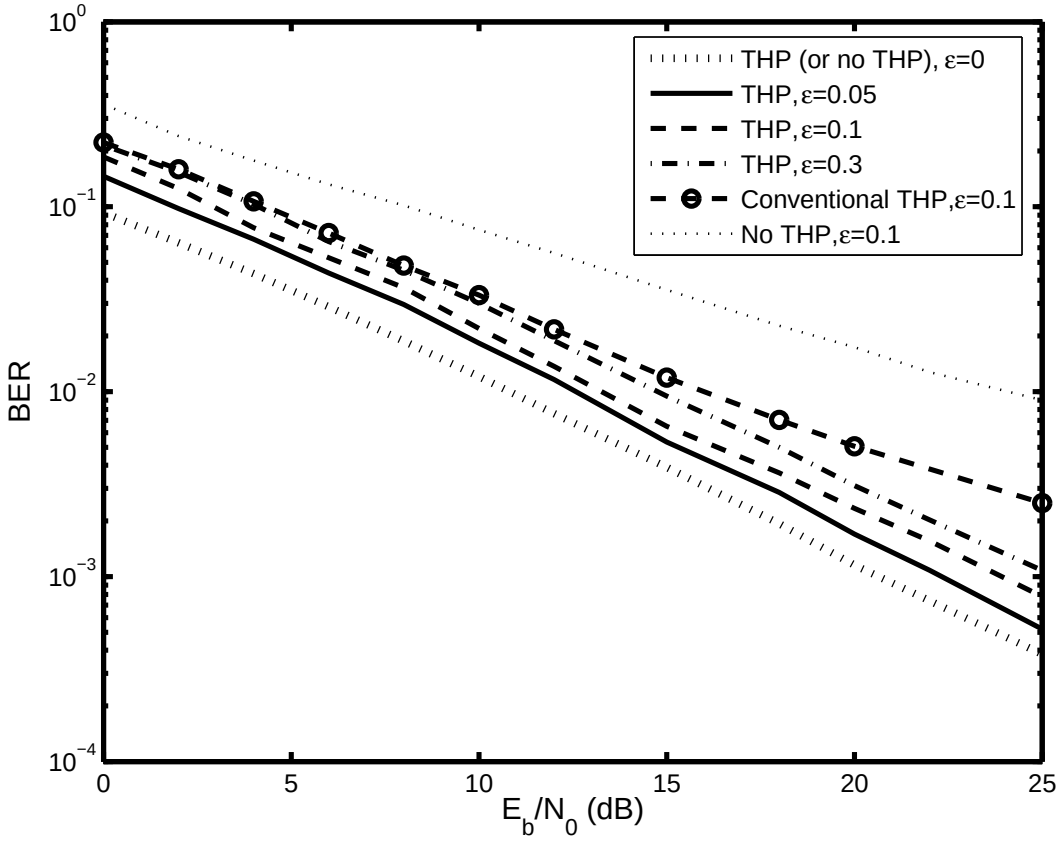

Figure 3.3: BER with THP as a function of the SNR for different values of the normalized frequency offset for SISO 4-QAM 64-subcarrier OFDM with inaccurate channel gain matrices used at both transmitter and receiver.

3.4.2 MIMO OFDM

The performance of MIMO OFDM with THP is shown in this subsection. For simplicity, both the transmitter and the receiver are assumed to have the perfect channel gain matrix $\mathbf{H}$, and the receiver has the perfect knowledge of frequency offsets. A general case is considered where there are M_R different frequency offsets. The values of normalized frequency offsets are assumed to be

uniformly distributed in two intervals $\mathcal{I} = (0, 0.1]$ and $\mathcal{II} = (0.1, 0.3]$.

In Fig. 3.4, the spatial channels between different transmit and receive antenna pairs are uncorrelated. This figure shows the BER performance of 2×2 and 2×4 spatially-multiplexed OFDM with THP in the presence of M_R different frequency offsets. The BER of 2×2 OFDM without THP when $\varepsilon_v \in \mathcal{I}$ is provided as a reference. Just as previous results, the proposed THP-OFDM reduces ICI significantly in this case. When the normalized frequency offsets $\varepsilon_u \in \mathcal{I}$, the ICI can be cancelled almost completely.

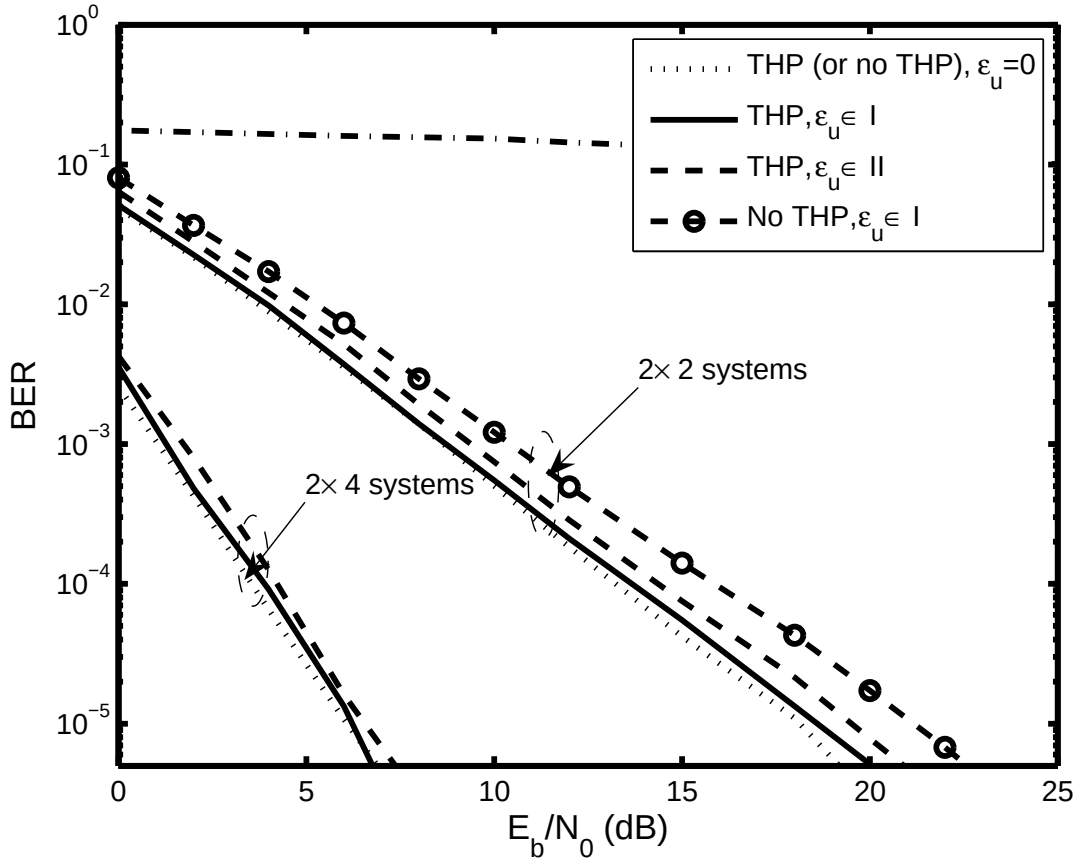

Figure 3.4: The BER as a function of the SNR for different values of the normalized frequency offset for 2×2 and 2×4 4-QAM 64-subcarrier OFDM with THP; perfect channel estimates and uncorrelated spatial channels.

Fig. 3.5 considers 2×2 OFDM with M_R different frequency offsets. The angle spread Δ in (3.20) is set to 0.1. Antenna spacing is assumed to be less than $\lambda/2$, which causes sufficient fading

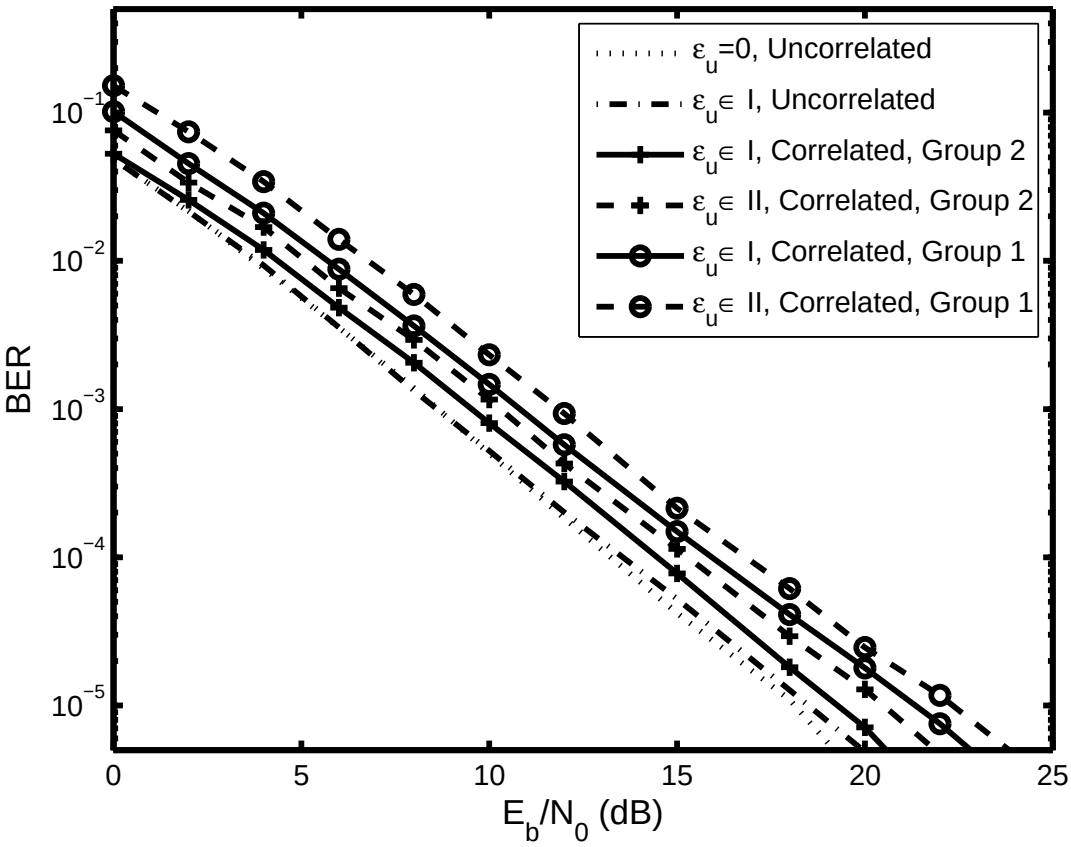

Figure 3.5: The BER as a function of the SNR for different values of the normalized frequency offset for 2×2 4-QAM 64-subcarrier OFDM with THP and correlated spatial channels. The fading correlations are unknown and $\rho = 0.3$ in Group 1. The fading correlations are known at the transmitter and $\rho = 0.7$ in Group 2.

correlations. The correlation coefficient ρ is defined as $\rho = \max \left[\frac{r(m,n)}{\sqrt{r(m,m)r(n,n)}} \right], \forall\, m \neq n$, where $r(m,n)$ is the $\{m,n\}$th entry of $\left[\mathbf{R}_T^T \otimes \mathbf{R}_R\right]^{1/2}$ in (3.21).

Fig. 3.5 shows two groups of BER curves for two cases of correlations. In the first group, $\rho = 0.3$ and the fading correlations are unknown at the transmitter. In the second group, $\rho = 0.7$ and the fading correlations are known at the transmitter. With the known fading correlations at the transmitter, we QR factorize $\tilde{\mathbf{H}}$ instead of $\mathcal{H}$. The BERs of 2×2 OFDM with zero frequency offset and THP-OFDM with $\varepsilon_v \in \mathcal{I}$ in uncorrelated spatial fading channels are given as references. The fading correlations degrade the MIMO OFDM performance. However, THP reduces the effect of

fading correlations and the BER loss is marginal when the fading correlations are known at the transmitter.

3.5 Summary

This section has derived a non-linear TH precoder for in closed-loop MIMO OFDM with frequency offsets. It has been shown that the ICI coefficient matrix is approximately unitary. With this property the designed precoder only needs partial CSI available at the transmitter, not including the knowledge of frequency offsets. Since frequency offsets are not necessary to be fed back to the transmitter, the proposed approach reduces the feedback load in closed-loop MIMO OFDM systems and avoids detrimental effect of frequency-offset mismatch due to imperfect feedback. The degradation due to frequency offset can be significantly reduced in the proposed THP-OFDM systems. For spatially-correlated channels, the proposed system performs with negligible BER-performance loss.

Chapter 4

MUI and ICI Suppression in Multiuser Multiple-Antenna OFDM Downlink

This chapter considers the multiuser spatially-multiplexed OFDM downlink. Multiuser MIMO OFDM inherits the attractive features of OFDM but also sensitive to frequency offset. Frequency offset estimation and ICI suppression schemes [75–78] have been reported to address the ICI and MUI problem in for the uplink case. However, the ICI and MUI still remain to be mitigated in the broadcast (downlink) case because of the difficulty of MUI mitigation and signal detection caused by lack of coordination among the independent mobile users. In the downlink case, each mobile station (MS) knows the frequency offset and channel gains affecting its receiver only, but not those of other users. If only post-processing techniques are used at each user's receiver to reduce MUI due to spatial multiplexing, the number of receive antennas at each user terminal must be greater than or equal to the number of transmit antennas, which may not be practical for many applications. The processing at the user level can hence be quite complex or even impossible. On the other hand, since the users are decentralized, it may be difficult to know at the BS the frequency offsets of all users. Hence, the application of only transmitter precoding for ICI and MUI mitigation, which requires full CSI including both $\mathbf{H}$ and $\mathbf{S}$ at the BS, is problematic.

A novel two-stage technique for ICI and MUI suppression is thus proposed, in which the first stage applies non-linear THP at the BS transmitter to mitigate the MUI and the second stage employs an iterative MMSE equalizer at each user's receiver to suppress the ICI due to the frequency

offset. The overall channel matrix can be divided into two parts: the spatial channel gain matrix **H** which is determined by the channel gains, and the ICI matrix **S** which depends on frequency offsets. In a typical closed-loop system **H** is available at the BS. Since the precoder only needs **H** at the BS, the feedback load is reduced. The MMSE equalizer at each user's receiver has low complexity due to the unitary property of the ICI matrix demonstrated in Chapter 3. Our scheme significantly reduces the BER increase due to frequency offsets in closed-loop multiuser spatially-multiplexed OFDM downlink. When the feedback link is perfect, the proposed technique almost completely cancels the ICI and MUI, and experiences the same BER as in the case when only full-CSI (channel gains and frequency offset) precoding is used at the BS. Hence, sending frequency offset information to the BS does not offer additional BER improvement. When the feedback is inaccurate, our technique outperforms the case of full-CSI feedback since it avoids the possible frequency-offset mismatch.

The remainder of this chapter is organized as follows. In Section 4.1 briefly describes the system model of a multiple-antenna downlink multiuser OFDM system with frequency offsets. Section 4.2 proposes a two-stage equalizer with a non-linear TH precoder at the BS and an iterative MMSE symbol estimation at the receiver for ICI and MUI suppression. The simulation results of downlink multiuser OFDM are given in Section 4.3. Section 4.4 concludes this chapter.

4.1 System Model

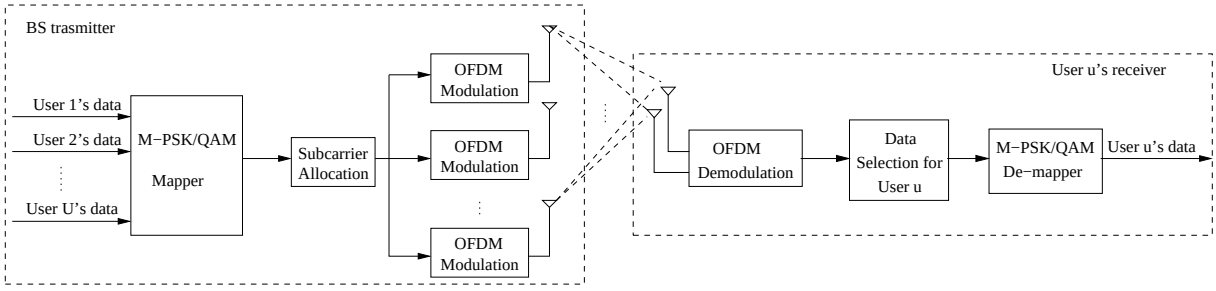

Figure 4.1: Block diagram of a multiuser MIMO OFDM downlink.

This section introduces a model for the downlink of multiuser multiple-antenna OFDM systems with frequency offset.

Consider a multiuser OFDM system employing N subcarriers with M_T transmit antennas and U simultaneously active users. Each user has a single receive antenna and the u-th user is assigned a subset $\mathbb{K}_u$ containing $N_u \leq N$ subcarriers. The same subcarriers can be used for transmission to different users (spatial multiplexing). The transmitter and the u-th user's receiver are shown in Fig. 4.1. At the BS, a subcarrier allocation algorithm maps the user data to the corresponding subcarriers, and this algorithm is known at both the BS and the user side.

A wideband frequency-selective fading channel with L resolvable paths is considered, and it remains constant during at least one OFDM symbol interval T_s. The received signal for the k-th subcarrier of the u-th user can be expressed as

$$\begin{aligned} Y_u[k] = & \underbrace{\sum_{v=1}^{M_T} S_u[0] H_{u,v}[k] X_v[k]}_{\text{desired signal}} + \underbrace{\sum_{v=1}^{M_T} \sum_{\substack{n \neq k, \\ n=n_1}}^{n_{Q_u}} S_u[n-k] H_{u,v}[n] X_v[n]}_{\text{ICI}} \\ & + \underbrace{\sum_{v=1}^{M_T} \sum_{\substack{n \neq k, \\ n=j_1}}^{j_J} S_u[n-k] H_{u,v}[n] X_v[n]}_{\text{MUI}} + \sum_{v=1}^{M_T} W_{u,v}[k], \end{aligned} \tag{4.1}$$

where $k = 0, \ldots, N-1$, $v = 1, \ldots, M_T$ and $u = 1, \ldots, U$; n_q is the index of the subcarriers assigned only to the u-th user, belonging to the subset $\mathbb{Q}_u = \{n_q,\, q = 1,\, \ldots,\, Q_u,\, Q_u \leq N_u\} \subset \mathbb{K}_u$; $j_p \in \overline{\mathbb{Q}}_u$ is the index of subcarriers assigned to other users; $\overline{\mathbb{Q}}_u$ is the complementary set of $\mathbb{Q}_u$. $H_{u,v}[k] = \sum_{l=0}^{L-1} h_{u,v}[l] e^{-\jmath \frac{2\pi}{N} lk}$, and the interference coefficient $S_u[n-k]$ is as in (3.5) with the normalized frequency offset $\varepsilon_u = \varepsilon_{u,v} = \varepsilon_{u,v'}$ of the u-th user. Since different users experience different fading channels and may move at different speeds, their offsets are different $\varepsilon_u \neq \varepsilon_{u'}$, $\forall$ $u \neq u'$.

The matrix format of the received signal can therefore be expressed as

$$\mathbf{Y}_u = \sum_{v=1}^{M_T} \mathbf{S}_u \mathbf{H}_{u,v} \mathbf{X}_v + \mathbf{W}_{u,v} = \mathbf{S}_u \mathbf{H}_u \mathbf{X} + \mathbf{W}_u, \tag{4.2}$$

where the N-dimensional receive vector is $\mathbf{Y}_u = \left[Y_u[0] \ ... \ Y_u[N-1]\right]^T$; the $N \times NM_T$ channel gain matrix of the u-th user is

$$\mathbf{H}_u = \begin{bmatrix} \mathbf{H}_{u,1} & \mathbf{H}_{u,2} & ... & \mathbf{H}_{u,M_T} \end{bmatrix}, \tag{4.3}$$

where $\mathbf{H}_{u,v}$ is an $N \times N$ diagonal matrix as in (3.10). The $N \times N$ interference matrix of the u-th user can be given as

$$\mathbf{S}_u = \begin{bmatrix} S_u[0] & S_u[1] & ... & S_u[N-1] \\ S_u[-1] & S_u[0] & ... & S_u[N-2] \\ \vdots & & \ddots & \vdots \\ S_u[-(N-1)] & S_u[-(N-2)] & ... & S_u[0] \end{bmatrix}, \tag{4.4}$$

where the $\{m,k\}$th entry is an MUI coefficient if $k \in \overline{\mathbb{Q}}_u$; otherwise it is an ICI coefficient. The $\mathbf{S}_u$ has the same structure as the $\mathbf{S}_{m,n}$ in (3.8), therefore it is unitary as shown in Appendix. The received signals of all users can hence be expressed as

$$\begin{bmatrix} \mathbf{Y}_1 \\ \mathbf{Y}_2 \\ \vdots \\ \mathbf{Y}_U \end{bmatrix} = \mathbf{SHX} + \mathbf{W} = \begin{bmatrix} \mathbf{S}_1\mathbf{H}_{1,1} & ... & \mathbf{S}_1\mathbf{H}_{1,M_T} \\ \mathbf{S}_2\mathbf{H}_{2,1} & ... & \mathbf{S}_2\mathbf{H}_{2,M_T} \\ \vdots & \ddots & \vdots \\ \mathbf{S}_U\mathbf{H}_{U,1} & ... & \mathbf{S}_U\mathbf{H}_{U,M_T} \end{bmatrix} \begin{bmatrix} \mathbf{X}_1 \\ \mathbf{X}_2 \\ \vdots \\ \mathbf{X}_{M_T} \end{bmatrix} + \begin{bmatrix} \mathbf{W}_1 \\ \mathbf{W}_2 \\ \vdots \\ \mathbf{W}_U \end{bmatrix} \tag{4.5}$$

where $\mathbf{S} = \text{diag}\left[\mathbf{S}_1 \ ... \ \mathbf{S}_U\right]$, and $\mathbf{H}$ is the $NU \times NM_T$ spatial channel gain matrix, which is given by

$$\mathbf{H} = \begin{bmatrix} \mathbf{H}_1 & \mathbf{H}_2 & ... & \mathbf{H}_U \end{bmatrix}^T. \tag{4.6}$$

4.2 MUI and ICI Reduction

From the observation of $\mathbf{Y}_u$ in (4.2), each user attempts to detect the transmitted symbols $\mathbf{X}$. A non-linear TH precoder at the BS is proposed to mitigate the impact on ICI and MUI due to the spatial channel gain matrix $\mathbf{H}$, and a linear equalizer at each user's receiver to suppress the remaining ICI and MUI due to frequency offset. With proper design, the transmitted data symbols can be directly detected from the equalized samples.

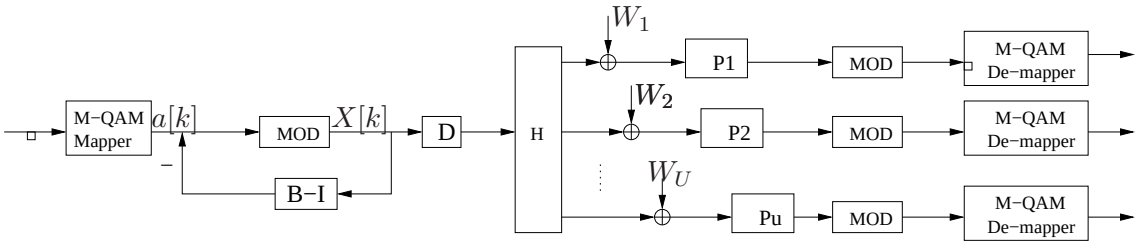

Figure 4.2: Block diagram of THP in multiuser MIMO OFDM for decentralized receivers.

4.2.1 Non-Linear Tomlinson-Harashima Precoding

Non-linear THP is proposed as the first stage to mitigate the impact of the spatial channel gain matrix $\mathbf{H}$ (4.2) at the BS. For detection convenience, wthe number of transmit antennas is assumed greater than or equal to the number of users, i.e., $M_T \geq U$.

The structure of the TH precoder in multiuser OFDM downlink is shown in Fig. 2. Because the users are distributed, the received symbols $Y_u[k]$, $\forall\ u$, cannot be processed jointly by the feedforward receiver filter. The feedforward matrix $\mathbf{D}$ is thus moved to the transmitter side as in [60]. Similar to Chapter 2, the linear pre-distortion via $\mathbf{B}^{-1}$ equalizes the cascade $\mathbf{PHD}$. The feedforward matrix can be obtained by

$$\mathbf{H} = \mathbf{T}\mathbf{D}^{H}, \tag{4.7}$$

where $\mathbf{T}$ is an $NU \times NU$ lower triangular matrix with the $\{m, n\}$th entry $T(m, n)$; $\mathbf{D}$ is an $NM_T \times NU$ matrix and $\mathbf{D}^H\mathbf{D} = \mathbf{I}_{NU}$. The calculations of $\mathbf{B}$ and $\mathbf{P}$ are similar to Section 2.3. The feedback matrix $\mathbf{B} = \mathbf{PT}$, and the $NU \times NU$ scaling matrix is $\mathbf{P} = \text{diag}\left[1/T(1,1)\ \ldots\ 1/T(NU, NU)\right]$. For each user, $\mathbf{P}_u$ is an $N \times N$ diagonal matrix with the main-diagonal entry $P_u[k] = T^{-1}(N(u-1)+k, N(u-1)+k)$.

The proposed TH precoder in multiuser OFDM completely suppresses the interference due to $\mathbf{H}$. Because only $\mathbf{H}$ is needed at the BS, the feedback capacity requirement is reduced.

4.2.2 Iterative ICI and MUI Equalization

Iterative linear MMSE equalization is introduced to suppress the remaining MUI and ICI due to frequency offset at the individual receiver level. The u-th user is assumed to know its frequency offset, ε_u, and its channel gains $h_{u,v}(l)$, $\forall\, l$.

After modulo reduction at the users' receivers, as shown in Fig. 4.2, the received signals become:

$$\begin{aligned}\begin{bmatrix}\mathbf{Y}_1 & \dots & \mathbf{Y}_U\end{bmatrix}^T &= \mathbf{PSHDB}^{-1}\mathbf{A} + \mathbf{PW} \\ &= \mathbf{PSTD}^H\mathbf{DT}^{-1}\mathbf{P}^{-1}\mathbf{A} + \mathbf{PW} = \mathbf{PSP}^{-1}\mathbf{A} + \mathbf{PW}.\end{aligned} \tag{4.8}$$

Clearly, the spatial channel gain matrix $\mathbf{H}$ becomes a diagonal matrix, i.e., the spatial channel has been converted into NU parallel, independent sub-channels. Since $\mathbf{S} = \text{diag}\begin{bmatrix}\mathbf{S}_1 & \dots & \mathbf{S}_U\end{bmatrix}$ and $\mathbf{P}$ is a diagonal matrix, the received signal vector of the u-th user in (4.2) is reduced to the single transmit-antenna case with the interference due to frequency offsets only, which is

$$\mathbf{Y}_u = \mathbf{P}_u\mathbf{S}_u\mathbf{P}_u^{-1}\mathbf{A} + \mathbf{W}'_u, \tag{4.9}$$

where $\mathbf{W}'_u = \mathbf{P}_u\mathbf{W}_u$. Here the index of the transmit antenna in $\mathbf{A}$ is omitted for simplicity. The MMSE linear estimator of $a[k]$ given $\mathbf{Y}_u$ is [79, page 382]

$$\hat{a}[k] = \text{E}\left(a[k]\right) + \mathbf{Cov}\left(a[k], \mathbf{Y}_u\right)\mathbf{Cov}\left(\mathbf{Y}_u, \mathbf{Y}_u\right)^{-1}\left(\mathbf{Y}_u - \text{E}(\mathbf{Y}_u)\right). \tag{4.10}$$

If $\text{E}\left[\mathbf{W}_u\right] = \mathbf{0}$, $\text{E}\left[\mathbf{W}'_u\mathbf{W}'^H_u\right] = \sigma_W^2\mathbf{P}_u\mathbf{P}_u^H$, $\text{E}\left[\mathbf{A}\mathbf{W}_u^H\right] = \mathbf{0}$ and independence among $a[k]$ with $\text{E}\left[a[k]\right] = \bar{a}[k]$, $\bar{a}[k] \in \bar{\mathbf{A}} = \text{E}\left[\mathbf{A}\right]$ are assumed, the statistical properties are

$$\begin{aligned}\text{E}\left[\mathbf{Y}_u\right] &= \mathbf{P}_u\mathbf{S}_u\mathbf{P}_u^{-1}\bar{\mathbf{A}}, \\ \mathbf{Cov}\left(a[k], \mathbf{Y}_u\right) &= C_a[k]P_u^{-1}[k]\mathbf{S}_u^H[k]\mathbf{P}_u^H, \\ \mathbf{Cov}\left(\mathbf{Y}_u,\, \mathbf{Y}_u\right) &= \sigma_W^2\mathbf{P}_u\mathbf{P}_u^H + \mathbf{P}_u\mathbf{S}_u\mathbf{P}_u^{-1}\mathbf{C}_a\mathbf{P}_u^{-H}\mathbf{S}_u^H\mathbf{P}_u^H,\end{aligned} \tag{4.11}$$

where $\mathbf{C}_a = \text{diag}\begin{bmatrix}C_a[0] & \dots & C_a[N-1]\end{bmatrix} = E_s\mathbf{I}_N$ with entries $C_a[k] = E[|a[k]|^2] = E_s$, and $\mathbf{S}_u[k] = \begin{bmatrix}S_u[k] & S_u[k-1] & \dots & S_u[k-(N-1)]\end{bmatrix}^T$ is the k-th column in $\mathbf{S}_u$. The linear iterative MMSE estimate of $a[k]$ is

$$\hat{a}[k] = \bar{a}[k] + \mathbf{\Delta}_u[k]\left(\mathbf{Y}_u - \mathbf{P}_u\mathbf{S}_u\mathbf{P}_u^{-1}\bar{\mathbf{A}}\right), \tag{4.12}$$

where $\mathbf{\Delta}_u[k] = E_s P_u^{-1}[k]\mathbf{S}_u^H[k]\mathbf{P}_u^H \left(\mathbf{Cov}\left(\mathbf{Y}_u,\, \mathbf{Y}_u\right)\right)^{-1}$.

With the first-stage precoding at the BS, the design for second-stage equalization at each user's receiver is simplified to process a single-input OFDM system. The complexity of the receiver's MMSE equalization is hence primarily determined by the operation of the inversion of $\mathbf{Cov}\left(\mathbf{Y}_u,\, \mathbf{Y}_u\right)$ in (4.12). Since $\mathbf{S}_u$ is unitary, the covariance is given by

$$\begin{aligned}\mathbf{Cov}\left(\mathbf{Y}_u,\, \mathbf{Y}_u\right) &= \sigma_W^2 \mathbf{P}_u\mathbf{P}_u^H + \mathbf{P}_u\mathbf{S}_u\mathbf{P}_u^{-1}\mathbf{C}_a\mathbf{P}_u^{-H}\mathbf{S}_u^H\mathbf{P}_u^H \\ &= \mathbf{P}_u\mathbf{S}_u\left[\sigma_W^2\mathbf{I}_N + E_s\mathbf{P}_u^{-1}\mathbf{P}_u^{-H}\right]\mathbf{S}_u^H\mathbf{P}_u^H = \mathbf{P}_u\mathbf{S}_u\mathbf{\Psi}_u\mathbf{S}_u^H\mathbf{P}_u^H.\end{aligned} \tag{4.13}$$

Since $\mathbf{P}_u$ is a diagonal matrix constant for all $k = 0, \ldots, N-1$ over at least one OFDM symbol interval, $\mathbf{\Psi}_u$ is a diagonal matrix as well. Therefore, one can easily obtain

$$\left(\mathbf{Cov}\left(\mathbf{Y}_u,\, \mathbf{Y}_u\right)\right)^{-1} = \mathbf{P}_u^{-H}\mathbf{S}_u\mathbf{\Psi}_u^{-1}\mathbf{S}_u^H\mathbf{P}_u^{-1}. \tag{4.14}$$

The inversion in (4.12) only requires simple operations, while a typical MMSE estimator needs at least $\mathcal{O}(N^2)$ operations [80]. Complexity of calculations in (4.12) is significantly reduced.

The iterative algorithm is initialized with $\bar{a}[k] = 0$ and $C_a[k] = 1$. $\hat{a}[0]$ is calculated via (4.12) and updated the initial values $\bar{a}[0]_{\text{new}} = \hat{a}[0]$. $\hat{a}[1]$ is next calculated and then immediately update $\bar{a}[1]_{\text{new}} = \hat{a}[1]$. This calculation continues until $\hat{a}[N-1]$ is computed, and then repeats again starting from $\hat{a}[0]$. $\bar{a}[k]_{\text{new}}$ is used for next calculation instead of the initial $\bar{a}[k]$. The algorithm terminates when the estimate of $a[k]$ converges or a specified number of iterations elapses. After the algorithm terminates, the u-th user selects the $\hat{a}[k],\ k \in \mathbb{K}_u$, which are the data symbols transmitted on the k-th subcarrier assigned to the u-th user, and discards the other $\hat{a}[k]$.

4.3 Simulation Results

The simulation results show how the proposed two-stage precoder/equalizer suppresses ICI and MUI in multiuser multiple-antenna OFDM. A multiuser MIMO OFDM system with 64 4-QAM subcarriers and 4 or 8 transmit antennas over a 6-tap Rayleigh fading channel is considered. The channel model is vehicular B as defined in ITU R-M1225 [73]. Each user exactly estimates the

frequency offset and channel gains affecting its receiver, and the channel gains are sent back to the BS. Two intervals are considered for the normalized frequency offsets, $\mathcal{I} = [-0.1, 0.1]$, and $\mathcal{II} = [-0.3, -0.1) \cup (0.1, 0.3]$, and the frequency offset values are assumed to be uniformly distributed in these intervals. The maximum possible number of distinct frequency offset values is U.

Two benchmark systems are provided for reference. In the first system (System 1), the BS employs non-linear THP with perfect or imperfect full knowledge of CSI, i.e., both $\mathbf{S}$ and $\mathbf{H}$ are available at the transmitter. Full-CSI THP pre-equalizes both $\mathbf{S}$ and $\mathbf{H}$, and no individual equalization at each user's receiver is applied. Since the feedback channel bandwidth is usually much smaller than the downlink traffic channel capacity,the noise variance of the feedback link is assumed to be $\sigma_F^2 = \sigma_W^2/100$. In the second system (System 2), THP or linear precoding is used at the BS to pre-equalize $\mathbf{H}$; time-domain compensation (phase-rotation in (3.2)) for frequency offset is used at users' terminals.

Fig. 4.3 gives the BERs of our technique and System 1 (zero-forcing full-CSI THP only) with perfect or imperfect feedback; four transmit antennas and four users are considered. The performance of 4-user MIMO OFDM without any precoder/equalizer and with zero-frequency offset are also shown for reference. With perfect feedback, our technique exhibits practically the same BER as System 1 when full-CSI THP only is used, and almost completely cancels the ICI and MUI, even for normalized frequency offsets as high as in the interval $\mathbb{II}$. Hence, System 1, in which all users' frequency offsets are sent back to the BS, does not offer any BER improvement over our scheme. Therefore, frequency offsets do not need to be fed back, which reduces feedback bandwidth requirements. When the feedback link is noisy, our scheme has a noise-corrupted $\mathbf{H}$ at the BS and accurate frequency offset at each user's receiver, while both $\mathbf{S}$ and $\mathbf{H}$ are inaccurate at the BS in System 1. Hence, the proposed scheme outperforms System 1 since it avoids the frequency-offset mismatch at the BS. It is also easier to implement, because for System 1 the BS needs to know the frequency offset of each user, which may be difficult to achieve.

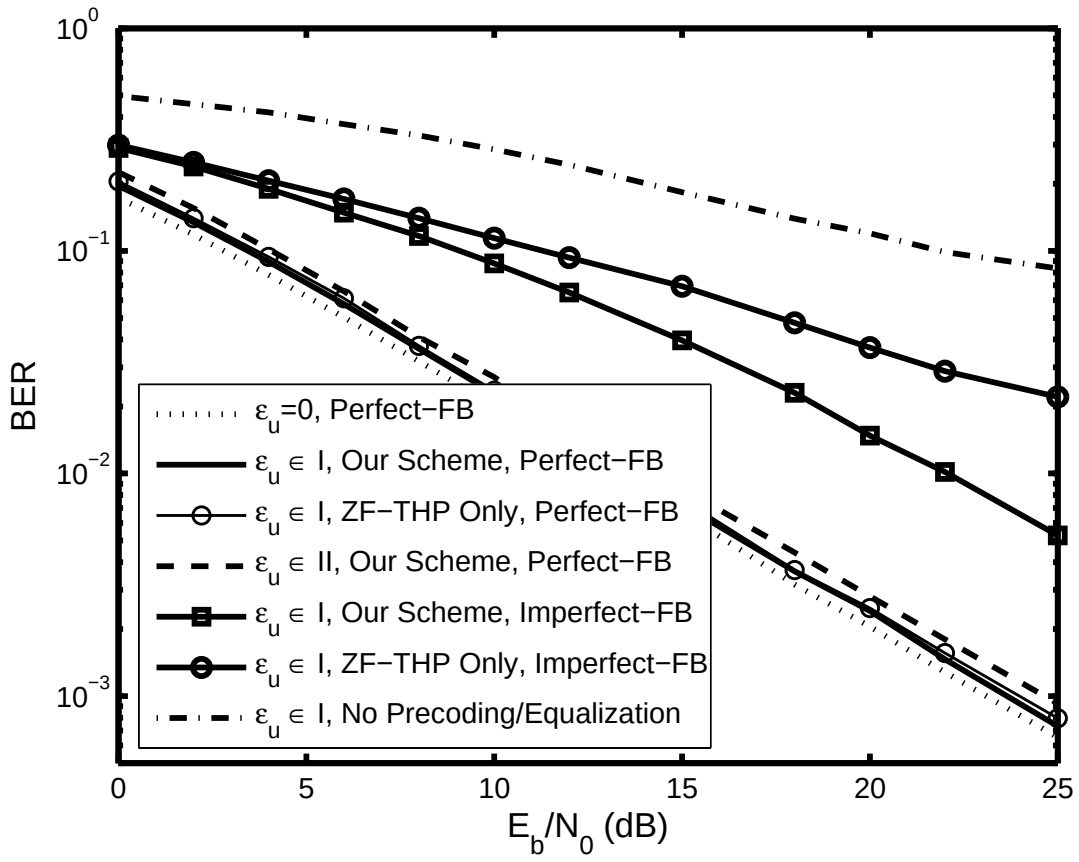

Figure 4.3: BER of the proposed precoder/equalizer and full-CSIT THP as a function of the SNR for different values of the normalized frequency offset for 64-subcarrier 4-QAM 4-user MIMO OFDM with perfect and imperfect feedback; $M_T = 4, U = 4$.

Fig. 4.4 shows the BERs of our technique and for both reference systems for multiuser MIMO OFDM with four transmit antennas, wousers, and eight transmit antennas, 4 users; $\varepsilon \in \mathcal{I}$. Zero-forcing linear precoding (LP) and ZF-THP are considered. For simplicity, perfect feedback is assumed. THP with full perfect CSI (System 1) and THP/frequency-offset-compensation (System 2) do not offer BER gain over our scheme. Furthermore, in System 2, THP/FO-compensation outperforms LP/FO-compensation, i.e., lower BER can be expected if non-linear precoding is used at the BS.

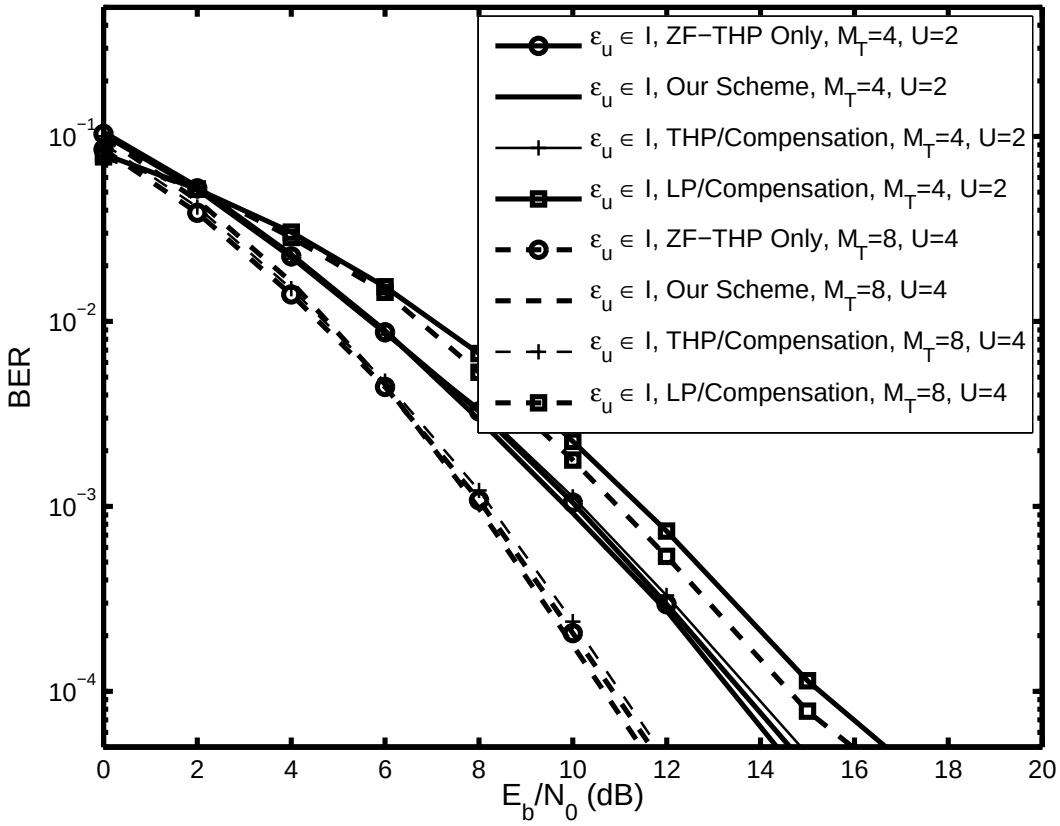

Figure 4.4: BER of the proposed precoder/equalizer, full-CSIT THP, THP/frequency-offset-compensation and LP/frequency-offset-compensation as a function of the SNR for different values of the normalized frequency offset for 64-subcarrier multiuser 4-QAM MIMO OFDM with perfect feedback; $M_T = 4, U = 2$ and $M_T = 8, U = 4$.

4.4 Summary

Two-stage transmitter/receiver processing has been developed to reduce ICI and MUI in downlink multiuser OFDM with multiple transmit antennas. The first stage employs a TH precoder at the BS to mitigate multiuser interference in a spatial MIMO channel. The second stage applies a low-complexity linear equalizer to suppress ICI and MUI due to frequency offset at each user's receiver. Our proposed precoder/equalizer significantly reduces the BER increase due to frequency offset.

Chapter 5

Limited-Feedback Precoding for Multiuser MIMO OFDM Systems with Frequency Offsets

In an open-loop spatially-multiplexed (SM) system, the number of receive antennas must be equal to or greater than the number of transmit antennas. In closed-loop systems, transmitter precoding can overcome ill-conditioning of the channel matrix and improve the system performance. In Chapter 3 and 4, non-linear THP has been proposed to suppress ICI, using only partial CSI, not including the knowledge of frequency offsets, at the transmitter. Perfect channel gains at the transmitter may require a high-rate feedback link. Thus, limited-feedback signal design and linear precoders have been explored for flat-fading MIMO channels for feedback volume reduction [44, 53–55, 81, 82]. The basic idea of this approach is to choose the precoding matrix at the receiver (rather than at the transmitter) using full CSI such that only the index of the selected matrix needs to be sent back to the transmitter. Limited-feedback precoding not only can reduce the number of feedback bits, but also can minimize the system error rate and maximize capacity. Nevertheless, this approach so far has only been considered for single-user systems over flat-fading channels, and is suitable for an ideal OFDM case without frequency offset, in which the overall channel gain matrix is a block-diagonal matrix. With frequency offsets, the overall channel gain matrix is not a block-diagonal matrix any more. The original limited-feedback design in [53–55, 81, 82] cannot hence be applied to a more practical OFDM system with frequency

offsets.

This chapter develops both linear precoding and non-linear limited-feedback THP (LFB-THP) for closed-loop multiuser MIMO OFDM systems with frequency offsets. SM MIMO OFDM with a linear receiver and OSTBC MIMO OFDM with an ML receiver are considered. Frequency offsets are shown to have no impact on precoding, and hence precoding on per-subcarrier basis is possible. Exploiting this property, the codebook design criterion previously used for flat-fading MIMO systems [53–56] is generalized to multiuser OFDM systems with frequency offsets. The use of a pre-designed codebook of precoding matrices, available at both the transmitter and the receiver, is proposed. The receiver selects optimal matrices at the subcarrier level according to a certain criterion and sends only their indexes to the transmitter. The explicit CSI is hence not needed at the transmitter. Three precoding matrix selection criteria, MMSE, maximum singular value (MSV) and maximum mutual information (MMI) are analyzed. To further reduce the number of feedback bits, grouping and interpolation schemes are also introduced. In our precoders, the feedback load is reduced to only a limited number of bits, which reduces feedback bit rate, and the non-linear property reduces power efficiency loss inherent in linear precoding, which makes non-linear precoding outperform linear precoding. Our precoders also significantly improve BER for OFDM with frequency offsets over spatially correlated MIMO channels.

This chapter is organized as follows. Section 5.1 proposes linear and non-linear precoding for both SM and OSTBC multiuser MIMO OFDM in the presence of frequency offset along with the matrix selection criteria. The impact of the ICI matrix on the optimal precoding matrix and develop the codebook design scheme is studied. Section 5.2 considers spatially correlated MIMO channels, and analyze the effect of fading correlations on the feedback matrix design. The simulation results for SM MIMO OFDM, OSTBC MIMO OFDM and OFDM in spatially correlated channels are given in Section 5.3. Section 5.4 concludes this chapter.

5.1 Limited-Feedback Precoding for MIMO OFDM with Frequency Offsets

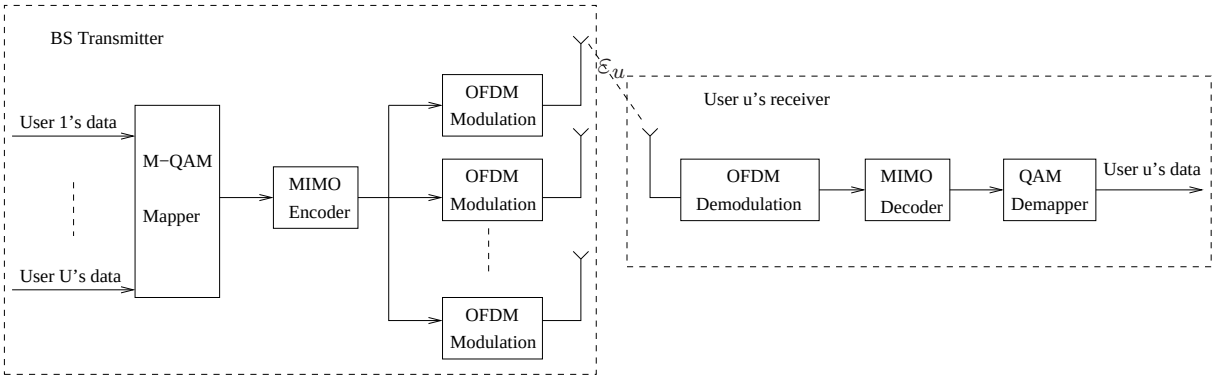

Figure 5.1: Block diagram of a multiuser OFDM downlink.

This chapter considers the system model of an N-subcarrier multiuser OFDM downlink system with M_T transmit antennas and U simultaneously active users in the presence of frequency offsets. The u-th user has M_u receive antennas, $M_u < M_T$, and the total number of receive antennas is $M_R = \sum_{u=1}^{U} M_u$. The structure of a MIMO OFDM link is shown in Fig. 5.1.

M_R different frequency offsets are assumed, i.e., for the u-th receive antenna, $\varepsilon_{u,1} = \cdots = \varepsilon_{u,M_T} = \varepsilon_u$, and $\varepsilon_u \neq \varepsilon_{u'}, \forall\, u \neq u'$. For the u-th user, the $NM_u \times NM_T$ channel matrix is

$$\mathbf{G}_u = \mathbf{S}_u \mathbf{H}_u, \tag{5.1}$$

where the $NM_u \times NM_T$ channel gain matrix is

$$\mathbf{H}_u = \begin{bmatrix} \mathbf{H}_{1,1} & \cdots & \mathbf{H}_{1,M_T} \\ \vdots & \ddots & \vdots \\ \mathbf{H}_{M_u,1} & \cdots & \mathbf{H}_{M_u,M_T} \end{bmatrix}, \tag{5.2}$$

with elements being the $\{u_m, v\}$th channel gain matrix $\mathbf{H}_{u_m,v}$ for the N orthogonal subchannels,

$$\mathbf{H}_{u_m,v} = \text{diag}\left[H_{u_m,v}[0] \quad H_{u_m,v}[1] \quad \ldots \quad H_{u_m,v}[N-1]\right]. \tag{5.3}$$

And the $NM_u \times NM_u$ ICI matrix is

$$\mathbf{S}_u = \text{diag}\left[\mathbf{S}_1 \quad \cdots \quad \mathbf{S}_{M_u}\right] \tag{5.4}$$

with the unitary $\mathbf{S}_{u_m}$ as in (3.8). Stacking all the users, the $NM_R \times NM_T$ overall channel matrix $\mathbf{G}$ as (3.12) is,

$$\mathbf{G} = \mathbf{SH}, \tag{5.5}$$

where the $NM_R \times NM_T$ channel gain matrix is

$$\mathbf{H} = \begin{bmatrix} \mathbf{H}_1 \\ \vdots \\ \mathbf{H}_U \end{bmatrix}, \tag{5.6}$$

and the $NM_R \times NM_R$ ICI matrix is

$$\mathbf{S} = \text{diag}\begin{bmatrix} \mathbf{S}_1 & \cdots & \mathbf{S}_U \end{bmatrix}. \tag{5.7}$$

Similar to $\mathbf{S}_u$, $\mathbf{S}$ is a unitary matrix.

Previous limited-feedback precoding work focused on the ideal case of MIMO OFDM without frequency offsets [81, 82]. In this case, the $NM_R \times NM_T$ overall channel matrix $\mathbf{G}$ (5.5) is only determined by channel gains and becomes

$$\mathbf{G}' = \text{diag}\begin{bmatrix} \mathbf{H}[0] & \ldots & \mathbf{H}[N-1] \end{bmatrix}. \tag{5.8}$$

The $M_R \times M_T$ sub-matrix $\mathbf{H}[k]$ is the channel matrix on the subcarrier k with i.i.d. $\mathcal{CN}(0,1)$ entries. Precoding can thus be designed on a subcarrier basis using the limited-feedback approach for flat-fading MIMO systems [54, 55]. However, in the presence of frequency offsets, the overall channel matrix is dependent on both frequency offset and channel gains. The limited-feedback precoding design in [54, 55, 81, 82] cannot be directly applied.

Before developing a limited-feedback precoder for both SM and OSTBC MIMO OFDM systems with frequency offset, the relationship between $\mathbf{G}$ in (5.5) and $\mathbf{G}'$ in (5.8) is first analyzed. The channel gain matrix $\mathbf{H}$ can be permuted into $\mathbf{G}'$:

$$\mathbf{H} = \mathbf{Q}_1 \mathbf{G}' \mathbf{Q}_2, \tag{5.9}$$

where $\mathbf{Q}_1$ is an $NM_R \times NM_R$ unitary permutation matrix and $\mathbf{Q}_2$ is an $NM_T \times NM_T$ unitary permutation matrix. The SVD of $\mathbf{G}'$ is given by

$$\mathbf{G}' = \mathbf{U}' \mathbf{\Gamma}' \mathbf{V}'^H, \tag{5.10}$$

where $\mathbf{U}'$ is an $NM_R \times NM_T$ matrix and $\mathbf{U}'^H\mathbf{U} = \mathbf{I}_{NM_T}$; $\mathbf{V}'$ is an $NM_T \times NM_T$ unitary matrix. Since $\mathbf{G}'$ is a block-diagonal matrix, $\mathbf{V}'$ can be constructed by $\mathbf{V}'[k]$, which is generated from the SVD of $\mathbf{H}[k]$ in (5.8). Therefore, $\mathbf{V}'$ is also a block-diagonal matrix. The singular value matrix $\mathbf{\Gamma}'$ is an $NM_T \times NM_T$ diagonal matrix with real, positive entries γ_n, $n = 1, \ldots, NM_T$, in descending order $\gamma'_1 \geq \gamma'_2 \geq \cdots \geq \gamma'_{NM_T} > 0$. The SVD of the overall channel matrix becomes

$$\mathbf{G} = \mathbf{SH} = \mathbf{SQ}_1\mathbf{G}'\mathbf{Q}_2 = \mathbf{SQ}_1\mathbf{U}'\mathbf{\Gamma}'\mathbf{V}'^H\mathbf{Q}_2 = \mathbf{U}\mathbf{\Gamma}\mathbf{V}^H. \tag{5.11}$$

Since $\mathbf{Q}_1$ and $\mathbf{Q}_2$ are unitary matrices, we have $\mathbf{U} = \mathbf{SQ}_1\mathbf{U}'$, $\mathbf{\Gamma} = \mathbf{\Gamma}'$ and $\mathbf{V} = \mathbf{Q}_2^H\mathbf{V}'$. Similarly, for the u-th user, the SVD of the channel matrix is

$$\mathbf{G}_u = \mathbf{S}_u\mathbf{Q}_1\mathbf{G}'_u\mathbf{Q}_2 = \mathbf{U}_u\mathbf{\Gamma}_u\mathbf{V}_u^H, \tag{5.12}$$

where $\mathbf{U}_u = \mathbf{S}_u\mathbf{Q}_1\mathbf{U}'_u$, $\mathbf{\Gamma}_u = \mathbf{\Gamma}'_u$ and $\mathbf{V}_u = \mathbf{Q}_2^H\mathbf{V}'_u$.

For each user, the precoding matrix is an $NM_T \times NM_C$ matrix, i.e., on each subcarrier the incoming data streams are multiplexed into M_C streams and sent over M_T transmit antennas, $M_T \geq M_C$. For convenience of detection, we need $M_u \geq M_C$. In the single-user case, we assume $M_R \geq M_C$. We construct a finite codebook of matrices and choose the precoding matrix from the codebook at the receiver. The codebook is known at both the transmitter and the receiver such that only the index of the selected matrix needs to be sent back to the transmitter. We analyze the matrix selection criteria, and propose the codebook design algorithms.

5.1.1 Precoding Matrix Selection Criteria for Linear Receivers

The matrix selection criteria are analyzed for SM MIMO OFDM with a ZF receiver. The precoding matrix of the user u $\breve{\mathbf{B}}_u = \mathcal{P}(\mathbf{G}_u)$ is assumed, where $\mathcal{P}(\mathbf{G}_u)$ is a mapping from the channel matrix $\mathbf{G}_u$ to the codebook $\mathcal{B} = \{\breve{\mathbf{B}}_1, \ldots, \breve{\mathbf{B}}_K\}$, optimizing the precoding matrix based on some performance criterion; K is the size of the codebook. All users share the same codebook. Once the optimal $\breve{\mathbf{B}}_{\text{u,opt}}$ is chosen, the ZF receiver applies a $NM_C \times NM_u$ matrix $\mathbf{D}_u = \left[\mathbf{G}_u\breve{\mathbf{B}}_{\text{u,opt}}\right]^\dagger$. For simplicity, in the following analysis, the user index u is omitted.

5.1.1.1 Minimum Mean Squared Error (MMSE) Criterion

The MSE for precoding matrix $\breve{\mathbf{B}}$ can be expressed as [46, 54]

$$\begin{aligned}\overline{\text{MSE}}(\breve{\mathbf{B}}) &= E_s \left(\mathbf{I}_{NM_C} + E_s \breve{\mathbf{B}}^H \mathbf{G}^H \mathbf{R}_{WW}^{-1} \mathbf{G} \breve{\mathbf{B}}\right)^{-1} \\ &= E_s \left(\mathbf{I}_{NM_C} + \frac{E_s}{\sigma_W^2} \breve{\mathbf{B}}^H \mathbf{Q}_2^H \mathbf{G}'^H \mathbf{G}' \mathbf{Q}_2 \breve{\mathbf{B}}\right)^{-1},\end{aligned} \tag{5.13}$$

where $\mathbf{R}_{WW} = \text{E}\left[\mathbf{W}\mathbf{W}^H\right]$ is the noise covariance matrix; E_s is the average power of the transmitted symbols. Eq. (5.13) is used to select $\breve{\mathbf{B}}$ from $\mathcal{B}$ according to minimize the MSE

$$\mathcal{P}(\mathbf{G}) = \arg \min_{\breve{\mathbf{B}}_i \in \mathcal{B}} \text{tr}\left[\overline{\text{MSE}}(\breve{\mathbf{B}}_i)\right]. \tag{5.14}$$

The relationship between $\mathbf{G}$ and $\mathbf{G}'$ in (5.11) suggests that the precoding matrix for $\mathbf{G}$ is related to that for $\mathbf{G}'$. Let $\breve{\mathbf{B}}' = \mathbf{Q}_2 \breve{\mathbf{B}}$ be the precoding matrix for $\mathbf{G}'$. In [46, 82], for $\mathbf{H}[k]$ in $\mathbf{G}'$ (5.8), the optimal precoding matrix on the subcarrier k is $\breve{\mathbf{B}}'_{\text{opt}}[k] = \mathbf{V}'_C[k]$, where $\mathbf{V}'_C[k]$ is formed from the first M_C columns of the right matrix $\mathbf{V}'[k]$ yielded by the SVD of the $\mathbf{H}[k]$. Since $\mathbf{G}'$ is a block-diagonal matrix, $\breve{\mathbf{B}}'_{\text{opt}} = \mathbf{V}'_C = \text{diag}\left[\mathbf{V}'_C[0] \ldots \mathbf{V}'_C[N-1]\right]$ is also an $NM_T \times NM_C$ block-diagonal matrix, and the desired overall optimal precoding matrix is $\breve{\mathbf{B}} = \mathbf{Q}_2^H \breve{\mathbf{B}}'$.

5.1.1.2 Maximum Singular Value (MSV) Criterion

A selection criterion based on the minimum SNR is difficult to implement since it requires the computation of the SNR for every OFDM symbol interval. With pre-equalization by $\breve{\mathbf{B}}$, the system experiences an $NM_R \times NM_C$ effective channel matrix $\mathbf{G}\breve{\mathbf{B}}$. Since the minimum SNR for a ZF receiver is lower bounded by the minimum singular value of the effective channel [46, 54], $\breve{\mathbf{B}}$ can be selected such that the minimum singular value is as large as possible. The optimization problem therefore is

$$\mathcal{P}(\mathbf{G}) = \arg \max_{\breve{\mathbf{B}}_i \in \mathcal{B}} \gamma_{\min}\left(E_s \breve{\mathbf{B}}^H \mathbf{G}^H \mathbf{R}_{WW}^{-1} \mathbf{G} \breve{\mathbf{B}}\right). \tag{5.15}$$

Similar to the MMSE criterion, the solution is given by $\breve{\mathbf{B}}_{\text{opt}} = \mathbf{Q}_2^H \mathbf{V}'_C$.

5.1.1.3 Maximum Mutual Information (MMI) Criterion

The mutual information under an average transmit power constraint is given by [83]

$$C(\breve{\mathbf{B}}) = \frac{1}{N}\log_2\left[\det(\mathbf{I}_{NM_C} + E_s\breve{\mathbf{B}}^H\mathbf{G}^H\mathbf{R}_{WW}^{-1}\mathbf{G}\breve{\mathbf{B}})\right]. \tag{5.16}$$

The mutual information (5.16) can be maximized by the selection of the feedback matrix $\breve{\mathbf{B}}$ according to

$$\mathcal{P}(\mathbf{G}) = \arg\max_{\breve{\mathbf{B}}_i\in\mathcal{B}} C(\breve{\mathbf{B}}_i). \tag{5.17}$$

The optimization problem (5.17) is equivalent to

$$\mathcal{P}(\mathbf{G}) = \arg\min_{\breve{\mathbf{B}}_i\in\mathcal{B}} \det(\overline{\mathrm{MSE}}(\breve{\mathbf{B}}_i)). \tag{5.18}$$

Similar to the MMSE criterion (5.14), the solution is $\breve{\mathbf{B}}_{\text{opt}} = \mathbf{Q}_2^H\mathbf{V}'_C$.

5.1.2 Matrix Selection Criterion for Maximum-Likelihood Receiver

Now the precoding matrix selection criterion for an OSTBC MIMO OFDM with an ML receiver is considered. Each user has an ML receiver. The user's index u is omitted here for simplicity.

To minimize the system BER given the channel matrix $\mathbf{G}$, the Frobenius norm of the effective channel $\mathbf{G}\breve{\mathbf{B}}$ must be maximized [55]. The precoding matrix from the codebook $\mathcal{B}$ is therefore chosen according to

$$\mathcal{P}(\mathbf{G}) = \arg\max_{\breve{\mathbf{B}}_i\in\mathcal{B}} \|\mathbf{G}\breve{\mathbf{B}}_i\|_F = \|\mathbf{S}\mathbf{Q}_1\mathbf{G}'\mathbf{Q}_2\breve{\mathbf{B}}_i\|_F. \tag{5.19}$$

This selection criterion can be easily implemented by performing a matrix multiplication and computing a Frobenius norm for each of the K codebook matrices. With the SVD of $\mathbf{G}'$ in (5.10), the optimal $\breve{\mathbf{B}}_{\text{opt}}$ is given by $\breve{\mathbf{B}}_{\text{opt}} = \mathbf{Q}_2^H\mathbf{V}'_C$. The receiver performs ML decoding on the effective channel $\mathbf{G}\breve{\mathbf{B}}_{\text{opt}}$.

Similarly as proven in [55], limited-feedback precoding in OSTBC systems achieves full-diversity order. The proposed LFB-TH precoder thus can be used in a generalized OSTBC system with an arbitrary number of transmit antennas and with full diversity.

5.1.3 Limited-Feedback Precoding Design

To find the optimal precoding matrix $\breve{\mathbf{B}}_{\text{u,opt}} = \mathbf{Q}_2^H \mathbf{V}'_{u,C}$, we need to look for $\mathbf{V}'_{u,C}$. Since $\mathbf{V}'_{u,C}$ is a block diagonal matrix, we can build up a codebook $\mathcal{B} = \{\breve{\mathbf{B}}_1, \ldots, \breve{\mathbf{B}}_K\}$ to find $\breve{\mathbf{B}}'_{\text{u,opt}}[k]$ at a subcarrier level. Therefore, in our codebook $\mathcal{B}$, each complex matrix $\breve{\mathbf{B}}_i$ has a size of $M_T \times M_C$, rather than $NM_T \times NM_C$. The optimal $\breve{\mathbf{B}}'_{\text{u,opt}}[k]$ is chosen from the codebook $\mathcal{B}$ at the u-th user's receiver according to the current channel conditions. After the optimal $\mathbf{V}'_{u,C}[k]$ for all subcarriers are obtained, the $NM_T \times NM_C$ optimal precoding matrix $\breve{\mathbf{B}}_{\text{u,opt}} = \mathbf{Q}_2^H \text{diag}\left[\breve{\mathbf{B}}'_{\text{u,opt}}[0] \ldots \breve{\mathbf{B}}'_{\text{u,opt}}[N-1]\right]$ can be constructed. The overall precoding matrix is built up as follows:

$$\breve{\mathbf{B}}_{\text{opt}} = \left[\breve{\mathbf{B}}_{1,\text{opt}}, \ldots, \breve{\mathbf{B}}_{\text{U,opt}}\right]. \tag{5.20}$$

The effective overall channel therefore becomes

$$\mathbf{G}\breve{\mathbf{B}}_{\text{opt}} = \begin{bmatrix} \mathbf{G}_1\breve{\mathbf{B}}_{1,\text{opt}} & \cdots & \mathbf{G}_1\breve{\mathbf{B}}_{\text{U,opt}} \\ \vdots & \ddots & \vdots \\ \mathbf{G}_U\breve{\mathbf{B}}_{1,\text{opt}} & \cdots & \mathbf{G}_U\breve{\mathbf{B}}_{\text{U,opt}} \end{bmatrix}. \tag{5.21}$$

Since the codebook is known at both the transmitter and each user, only the index of the selected precoding matrix needs to be fed back to the BS transmiter. The BS transmitter broadcasts every user's precoding index such that each user will also knows other users' precoding matrix. At the u-th user's receiver, the effective channel is $\mathbf{G}_u \sum_{u=1}^{U} \breve{\mathbf{B}}_{\text{u,opt}}$. Since the index of $\breve{\mathbf{B}}_{\text{u,opt}}$, $\forall\ u$, is available at each user's receiver, the transmitted signal can be detected. For the single-user case, the overall $NM_T \times NM_C$ precoding matrix is $\breve{\mathbf{B}}_{\text{opt}} = \mathbf{Q}_2^H \text{diag}\left[\breve{\mathbf{B}}'_{\text{opt}}[0] \ldots \breve{\mathbf{B}}'_{\text{opt}}[N-1]\right]$. Zero-forcing detection can be used at the receiver with the assumption of $M_R \geq M_C$.

For each user, the total $N\lceil \log_2 K \rceil$ feedback bits are required for a codebook with K precoding matrices. When a better performance is required, a larger codebook can be constructed, i.e., more bits can be sent to the transmitter. To reduce the total amount of the feedback information, we can exploit the correlation of precoding matrices on adjacent subcarriers. The significant correlations between adjacent subcarriers lead to substantial correlation between the precoders corresponding to neighboring subcarriers. The neighboring subcarriers can therefore be combined into a group

and use the precoding matrix corresponding to the center subcarrier for all the subcarriers in the group. If the N subcarriers are divided into N_b groups, each group includes N/N_b subcarriers. Since the subcarriers near the group boundary may experience performance degradation, an interpolation scheme can be used to improve the performance due to grouping. Interpolation introduces a unitary matrix $\mathbf{Q}_I$ which takes the unitary-invariance of the optimal precoding matrix into consideration. The optimal $\mathbf{Q}_I$ can be determined by the same criteria used for precoding selection, and a codebook $\mathcal{Q}$ can be built up for optimal interpolation matrix selection. Naturally, a larger size of the codebook $\mathcal{Q}$ will lead to a better BER performance. The details of interpolation schemes can be found in [81, 82].

The following subsections develop the matrix selection criteria for both SM and OSTBC MIMO OFDM systems and propose the codebook design schemes.

5.1.4 Codebook Design

The construction of the precoding codebook $\mathcal{B} = \{\breve{\mathbf{B}}_1, \ldots, \breve{\mathbf{B}}_K\}$ is now considered. Frequency offsets have been first shown to have no impact on the codebook design, which makes precoding on per-subcarrier basis possible. Next, the codebook design criterion which is valid only for flat-fading MIMO channels in [53–56] is generalized to OFDM systems with frequency offset. The user index is omitted here.

5.1.4.1 Impact of the ICI Matrix

Since the ICI matrix $\mathbf{S}$ is a unitary matrix, the singular value matrix and the right matrix in (5.11) are actually generated from the eigenvalue decomposition (EVD) of the channel gain matrix $\mathbf{H}^H\mathbf{H}$:

$$\mathbf{G}^H\mathbf{G} = \mathbf{H}^H\mathbf{H} = \mathbf{Q}_2^H\mathbf{G}'^H\mathbf{Q}_1^H\mathbf{Q}_1\mathbf{G}'\mathbf{Q}_2 = \mathbf{Q}_2^H\mathbf{G}'^H\mathbf{G}'\mathbf{Q}_2 = \mathbf{V}\mathbf{\Gamma}^2\mathbf{V}^H. \tag{5.22}$$

We thus find

Lemma 1: In an OFDM system, if the values of frequency offsets only change on different receive antennas, $\breve{\mathbf{B}}'_{\text{opt}}[k] = \mathbf{V}'_C[k]$ is uniformly distributed on the set $\Theta(M_T, M_C)$, i.e., the frequency offset

does not have impact on the codebook design compared to an OFDM system without frequency offset.

Proof: If there is no frequency offset, the overall channel matrix is reduced to a block diagonal matrix $\mathbf{G}'$, and $\mathbf{V}' = \mathbf{Q}_2\mathbf{V} = \text{diag}\left[\mathbf{V}'[0]\ldots\mathbf{V}'[N-1]\right]$ is also a block diagonal matrix. Each subblock matrix is uniformly distributed on $\Theta(M_T, M_T)$ [84], where $\Theta(m,n)$ is the set of $m \times n$ matrices with n orthonormal columns. As in [54], the optimal precoding matrix on the subcarrier k $\breve{\mathbf{B}}'_{\text{opt}}[k] = \mathbf{V}'_C[k]$ is also uniformly distributed on the set $\Theta(M_T, M_C)$. □

5.1.4.2 Codebook Design Criteria

Since $\breve{\mathbf{B}}'_{\text{opt}}[k]$ is uniformly distributed over $\Theta(M_T, M_C)$, the codebook matrices are in the set of $\Theta(M_T, M_C)$. The set of all possible column spaces of the matrices $\breve{\mathbf{B}}_i$, $\forall\ i$, in $\Theta(M_T, M_C)$ is a complex Grassmannian manifold $\Xi(M_T, M_C)$, in which $\Xi(m,n)$ is the set of n-dimensional subspaces in an m-dimensional vector space. Since each codebook matrix generates a subspace, there is a set of subspaces yielded by the codebook matrices $\{\breve{\mathbf{B}}_1, \ldots, \breve{\mathbf{B}}_K\}$. These subspaces can be related by several different distances. The chordal distance between any two subspaces is defined as

$$\text{d}_{\text{chord}}\left(\breve{\mathbf{B}}_p,\ \breve{\mathbf{B}}_q\right) = \frac{1}{\sqrt{2}}\|\breve{\mathbf{B}}_p\breve{\mathbf{B}}_p^H - \breve{\mathbf{B}}_q\breve{\mathbf{B}}_q^H\|_F. \tag{5.23}$$

The projection two-norm distance between two subspaces is

$$\text{d}_{\text{norm}}\left(\breve{\mathbf{B}}_p,\ \breve{\mathbf{B}}_q\right) = \|\breve{\mathbf{B}}_p\breve{\mathbf{B}}_p^H - \breve{\mathbf{B}}_q\breve{\mathbf{B}}_q^H\|_2, \tag{5.24}$$

where $\|.\|_2$ is two-norm distance. The Fubini-Study distance between two subspaces is

$$\text{d}_{\text{FS}}\left(\breve{\mathbf{B}}_p,\ \breve{\mathbf{B}}_q\right) = \arccos|\det\left|\breve{\mathbf{B}}_p^H\breve{\mathbf{B}}_q\right||. \tag{5.25}$$

The codebook can be designed according to a specific precoding selection criterion. This set of subspaces is a packing of subspaces in $\Xi(M_T, M_C)$. In OSTBC MIMO OFDM, a packing can be described by the its minimum chordal distance on the Grassmann manifold

$$\text{d}_{\text{min}} = \min_{1\le p<q\le K}\text{d}_{\text{chord}}\left(\breve{\mathbf{B}}_p,\ \breve{\mathbf{B}}_q\right). \tag{5.26}$$

As in [56], we need to minimize

$$\rho = \max_{1 \le p < q \le K} \|\mathbf{B}_p^{\dagger} \breve{\mathbf{B}}_q\|_F, \tag{5.27}$$

which is related to a packing in a complex Grassmannian space. Since minimizing ρ in (5.27) is equivalent to maximizing the minimum distance of (5.23), the codebook design criterion turns out to be the problem of Grassmannian subspace packing. The set of K subspaces must therefore be chosen in $\Xi(M_T, M_C)$ such that $\mathrm{d}_{\min}$ is as large as possible. Each precoding matrix in the set $\breve{\mathcal{B}}$ is given as $\breve{\mathbf{B}}_i = \mathbf{\Phi}^{i-1}\breve{\mathbf{B}}_1$, where $\breve{\mathbf{B}}_1$ is formed by the first M_C columns of a unitary matrix in the set of $\Theta(M_T, M_C)$, and $\mathbf{\Phi}$ is an $M_T \times M_T$ diagonal unitary matrix and $\mathbf{\Phi}^K = \mathbf{I}$, i.e., $\mathbf{\Phi}$ is a K-th root of unity. The parameter set $\mathbf{\Psi} = \{\varphi_1, \ldots, \varphi_{M_T}\}$ is selected to achieve

$$\min_{0 \le \varphi_1, \ldots, \varphi_{M_T} \le K-1} \rho = \min_{0 \le \varphi_1, \ldots, \varphi_{M_T} \le K-1} \max_{i=2,\ldots,K} \left\| \breve{\mathbf{B}}_1^{\dagger} \breve{\mathbf{B}}_i \right\|_F, \tag{5.28}$$

i.e., the parameter set $\mathbf{\Psi}$ of the diagonal entries of $\mathbf{\Phi}$ is

$$\mathbf{\Psi} = \arg\max \min_{1 \le i \le K-1} \mathrm{d}\left(\breve{\mathbf{B}}_1,\ \mathbf{\Phi}^{i-1}\breve{\mathbf{B}}_1\right). \tag{5.29}$$

Geometrically, this construction rotates an initial M_T-dimensional subspace using a K-th root of unity to form K different M_C-dimensional subspaces.

In SM MIMO OFDM, for MSV and MMSE selection criteria, the codebook can be designed by maximizing the minimum projection two-norm distance between any pair of codeword matrix column space. For capacity selection criterion, the codebook can be designed by maximizing the minimum Fubini-Study distance between any pair of codeword matrix column space [54]. Once the codebook is designed, the matrix on the k-th subcarrier $\breve{\mathbf{B}}[k] \in \mathcal{B}$ using the performance criteria in (5.14), (5.15) or (5.18) is chosen at the receiver. Its index is then delivered to the transmitter using only $\lceil \log_2 K \rceil$ bits.

5.1.5 Non-Linear Tomlinson-Harashima Precoding

The linear pre-distortion $\mathbf{B} = \breve{\mathbf{B}}^{\dagger}$ is equivalent to the feedback structure in Fig. 2. THP can therefore be proposed for limited-feedback precoding. The design of THP is described in Chapter

2. For better clarification, $\mathbf{B}$ is named as the feedback matrix of THP in the rest of the chapter, while $\breve{\mathbf{B}}$ as the precoding matrix.

Specific design targets for linear precoding are considered in Section 5.1.1 to improve the overall system performance. If the input sequence $a[k]$ is a sequence of i.i.d. symbols with variance E_a, the output of the modulo arithmetic feedback structure is also a sequence of i.i.d. random variables, and the real and imaginary parts are independent, i.e., $X[k]$ with variance $E_s = \mathrm{E}\left[|X[k]|^2\right], \forall\, k$ can be assumed. The linear precoding design criteria in (5.14), (5.15) and (5.16) can thus be applied to our non-linear precoding selection criteria. Similarly, the feedforward matrix $\mathbf{D} = \left[\mathbf{G}\breve{\mathbf{B}}\right]^{\dagger}$.

5.2 Limited-Feedback Precoding for Spatially Correlated Channels

The section focuses on OFDM in spatially correlated fading environments. Insufficient scattering around antennas of the BS transmitter and/or the receiver makes the channels spatially correlated [85]. The precoding matrix is restrained to lie in the codebook $\mathcal{B} = \{\breve{\mathbf{B}}_1, \breve{\mathbf{B}}_2, \ldots, \breve{\mathbf{B}}_K\}$. The receiver chooses the matrix as a function of the channel conditions to minimize the error rate or maximize the capacity. The correlated MIMO channel model has been introduced in Section 3.3.

5.2.1 Receive Antenna Correlations Only

First consider the case that each pair of transmit antennas has sufficient distance, i.e., only the effect of receive correlations needs to be analyzed. The channel is given by

$$\mathbf{G}_R = \mathbf{S}\mathbf{Q}_1\mathbf{G}'_R\mathbf{Q}_2, \tag{5.30}$$

where $\mathbf{G}'_R = \left(\mathbf{I}_N \otimes \mathbf{R}_R^{1/2}\right)\mathbf{G}'$ is a block diagonal matrix, and $\mathbf{G}'$ is given by (5.8). The k-th subblock on the main diagonal of $\mathbf{G}'_R$ is $\mathbf{H}_{Rc}[k] = \mathbf{R}_R^{1/2}\mathbf{H}_w[k]$. Thus, precoding can be designed on a subcarrier basis. The SVD of $\mathbf{H}_{Rc}[k]$ is $\mathbf{H}_{Rc}[k] = \mathbf{U}_{Rc}[k]\mathbf{\Gamma}_{Rc}[k]\mathbf{V}_{Rc}^H[k]$ with singular values of $\gamma_{Rc,1}[k] \geq \ldots \geq \gamma_{Rc,M_T}[k]$. The following lemma describes the distribution of $\mathbf{V}_{Rc}[k]$.

Lemma 2: $\mathbf{V}_{Rc}[k]$ is a uniformly distributed unitary matrix over $\Theta(M_T, M_C)$ and is independent

of $\mathbf{\Gamma}_{Rc}[k]$, if the channel gain matrix $\mathbf{H}_w[k]$ (5.6) has i.i.d. $\mathcal{CN}(0,1)$ entries.

Proof: The entries $H_{u,v}[k]$ of the channel gain matrix $\mathbf{H}_w[k]$ are i.i.d. complex Gaussian random variables with zero mean and unity variance (see details in Section 3.1). The distribution of an uniformly distributed unitary matrix is unchanged when the matrix is multiplied by any deterministic unitary matrix. $\mathbf{H}_{Rc}[k]$ is thus a right-rotationally invariant random matrix, and $\mathbf{V}_{Rc}[k]$ is thus uniformly distributed on $\Theta(M_T, M_T)$ [84], i.e., $\mathbf{\Omega}\mathbf{V}_{Rc}[k]$ is also uniformly distributed if $\mathbf{\Omega} \in \Theta(M_T, M_T)$ [86]. $\square$

Thus, the matrix which is formed by the first M_C columns of $\mathbf{V}_{Rc}[k]$ is uniformly distributed on the set $\Theta(M_T, M_C)$. The codebook design criterion in Section 5.1 is also available for the case that only receive antenna array is correlated. The feedback matrix can be chosen from the codebook $\mathcal{B}$ by (5.14) or (5.16) for SM MIMO OFDM and (5.19) for OSTBC MIMO OFDM.

5.2.2 Both Receive and Transmit Antenna Correlations

This subsection considers the fully correlated channel model (5.31). The overall channel matrix $\mathbf{G}$ can be given by

$$\mathbf{G} = \mathbf{S}\mathbf{Q}_1\mathbf{G}'\mathbf{Q}_2, \tag{5.31}$$

where the $NM_R \times NM_T$ spatially-correlated channel gain matrix is $\mathbf{G}' = \text{diag}\left[\mathbf{H}[0] \ldots \mathbf{H}[N-1]\right]$ with $\mathbf{H}[k] = \mathbf{R}_R^{1/2}\mathbf{H}_w[k]\mathbf{R}_T^{1/2}$. We first need to find the optimal matrix $\mathbf{B}'_{\text{opt}}[k]$ for $\mathbf{H}[k]$, and the desired overfall optimal precoding matrix is $\mathbf{B}_{\text{opt}} = \mathbf{Q}_2^H\mathbf{B}'_{\text{opt}}$.

Intuitively, we want to choose a precoding matrix with the effective channel $\mathbf{H}[k]\breve{\mathbf{B}}'[k]$ to provide a performance approaching to that given by $\mathbf{H}[k]\breve{\mathbf{B}}'_{\text{opt}}[k]$. Since improvement of probability of error or capacity is relative to maximize $\|\mathbf{H}[k]\breve{\mathbf{B}}'[k]\|_F$, we will attempt to minimize

$$\vartheta = \text{E}\left[\|\mathbf{H}[k]\breve{\mathbf{B}}'_{\text{opt}}[k]\|_F^2 - \|\mathbf{H}[k]\breve{\mathbf{B}}'[k]\|_F^2\right]. \tag{5.32}$$

Eq. (5.32) can be bounded as

$$\begin{aligned}\vartheta &= \text{E}\left[\|\mathbf{H}[k]\breve{\mathbf{B}}'_{\text{opt}}[k]\|_F^2 - \|\mathbf{G}_R[k]\mathbf{R}_T^{1/2}\breve{\mathbf{B}}'[k]\|_F^2\right] \\ &\leq \text{E}\left[\|\mathbf{H}[k]\breve{\mathbf{B}}'_{\text{opt}}[k]\|_F^2 - \gamma_{Rc,1}^2\|\breve{\mathbf{B}}_{Rc,\text{opt}}^H[k]\mathbf{R}_T^{1/2}\breve{\mathbf{B}}'[k]\|_F^2\right],\end{aligned} \tag{5.33}$$

where $\breve{\mathbf{B}}_{Rc,\text{opt}}[k]$ is the $M_T \times M_C$ optimal precoding matrix of $\mathbf{H}_{Rc}[k]$ in $\mathbf{G}'_R$ (5.30). Since $\mathbf{V}_{Rc}[k]$ is a uniformly distributed unitary matrix over $\Theta(M_T, M_C)$ and independent of the singular value matrix, the distribution of (5.33) only has one term which depends on the codebook. As a consequence, it is sufficient to only consider $\mathbf{R}_T^{H/2}\breve{\mathbf{B}}_{Rc,\text{opt}}[k]$, which is a subspace correlation as it only depends on the column space of $\breve{\mathbf{B}}_{Rc,\text{opt}}[k]$, $\breve{\mathbf{B}}_{Rc,\text{opt}}[k] \in \Theta(M_T, M_C)$. All column spaces in $\Theta(M_T, M_C)$ generate the complex Grassmannian manifold $\Xi(M_T, M_C)$. As shown in Section 5.1, the Grassmannian subspace packing problem in uncorrelated channels can be described by designing a codebook $\mathbb{B} = \{\mathbf{b}_1, .., \mathbf{b}_K\}$ to maximize the minimum distance

$$\mathrm{d}_{\min} = \min_{1 \le m \le n \le K} \mathrm{d}(\mathbf{b}_m, \mathbf{b}_n). \tag{5.34}$$

The proposed codebook in correlated channels from multiplying each element of $\mathbb{B}$ by $\mathbf{R}_T^{1/2}$ can be obtianed. Therefore, we design the codebook $\mathcal{B}$ by picking $\{\mathbf{b}_1, .., \mathbf{b}_K\}$ that maximize (5.34) and normalize the codebook to meet the average transmit power constraint

$$\breve{\mathbf{B}}_i = \frac{\mathbf{R}_T^{H/2}\mathbf{b}_i}{\|\mathbf{R}_T^{H/2}\mathbf{b}_i\|}. \tag{5.35}$$

This design criterion adapts the precoder to the correlated-channel conditions. The transmit spatial correlation matrix $\mathbf{R}_T$ can be estimated at the transmitter so that no feedback for the correlation matrix is needed.

5.3 Simulation Results

The BER performance of the proposed precoders is simulated. The codebook is known a priori at both the transmitter and the receiver. A MIMO 4-QAM-OFDM system with 64 subcarriers over a 6-tap Rayleigh fading channel is considered. The vehicular B channel specified by ITU-R M. 1225 [73] is used. For many wireless systems, the multipath channels fade slowly. Thus the fading gains can be assumed constant over several OFDM symbol intervals. Each user has M_u receive antennas and different frequency offsets. M_R different values of normalized frequency offsets are assumed to be uniformly distributed in two intervals $\mathcal{I} = (0, 0.1]$ and $\mathcal{II} = (0.1, 0.3]$.

5.3.1 Spatially Multiplexed OFDM

This subsection considers spatially uncorrelated MIMO channels.

5.3.1.1 Perfect CSI at the Receiver

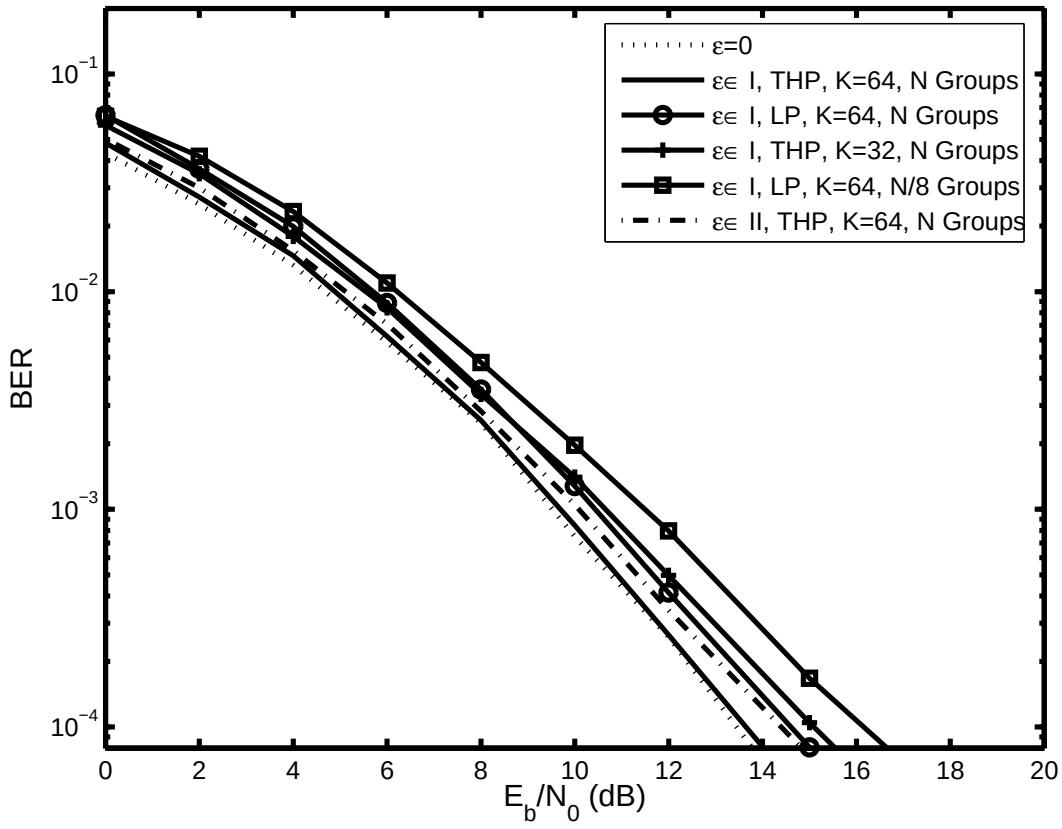

Figure 5.2: BER of LFB-THP and LFB linear precoding (LFB-LP) with MMSE codebook selection criterion as a function of the SNR for different values of the normalized frequency offset and 64-subcarrier 2-user 4-QAM-OFDM; perfect CSI at the receiver; $M_T = 4$, $M_C = 2$, $M_u = 2$.

Here, the receiver has perfect CSI, including frequency offset and channel gains. Fig. 5.2 shows the BER of 2-user 4-QAM OFDM for two groups; $M_T = 4$, $M_C = 2$, $M_u = 2$. First, the codebook consists of 64 matrices, i.e., 6 bits are transferred to the transmitter; while 32 matrices are included in the second group. The BER of an OFDM system with zero-frequency offset is shown as the reference. MMSE precoders are used. The BER is improved notably: even with

normalized frequency offsets in the interval $\mathcal{II}$, OFDM with the proposed precoder performs as well as the zero-frequency offset reference, i.e., the BER increase due to ICI has been reduced completely. Our non-linear LFB-THP outperforms its linear counterpart. The system has lower BER when the number of feedback bits increases. The case is also considered when grouping with the interpolation scheme is used. The N subcarriers are divided into 8 groups, and each group has 8 subcarriers. The size of the codebook $\mathcal{Q}$ for interpolation is 4 as in [81]. Thus, the total number of feedback bits is $8 \times (\log 64 + \log 4) = 64$ bits. If the grouping scheme is not used, $64 \times \log 64 = 384$ bits are needed. Due to grouping, there is 2.5 dB performance loss at the BER of 10^{-4}. However, more than 80% feedback bits are saved. The optimal higher-order interpolation design (large-size of $\mathcal{Q}$ is more complicated and still under investigation).

5.3.1.2 Impact of Inaccurate Channel Estimation

Fig. 5.3 presents BER when the receiver has imperfect knowledge of channel gains and frequency offset. The MMSE selection criterion is used and the size of the codebook is 64. Section 3.4 provides the details of channel estimation and frequency offset estimation are introduced. The BER of OFDM with zero-frequency offset is also shown as a benchmark. Clearly, limited-feedback linear precoding is more sensitive to estimation errors than the proposed THP. Compared with the ideal case of zero-frequency offset, the BER degradation is small for the imperfect channel and frequency offset estimates. Consequently, even with imperfect CSI, the proposed precoders improve BER significantly.

5.3.1.3 Different Performance Criteria

The BERs of two-user 4-QAM uncoded and coded OFDM systems with non-linear limited-feedback precoding are shown in Fig. 5.4. The codebook size K is set to 64. Each user has 2 receive antennas. The BER of OFDM with zero-frequency offset is shown as a reference. In Fig. 5.4, the MMSE, MSV and MMI selection criteria are used in an SM MIMO OFDM system with $M_T = 3,\ M_C = 2,\ M_R = 2$. As before, the proposed precoder reduces ICI significantly; even for

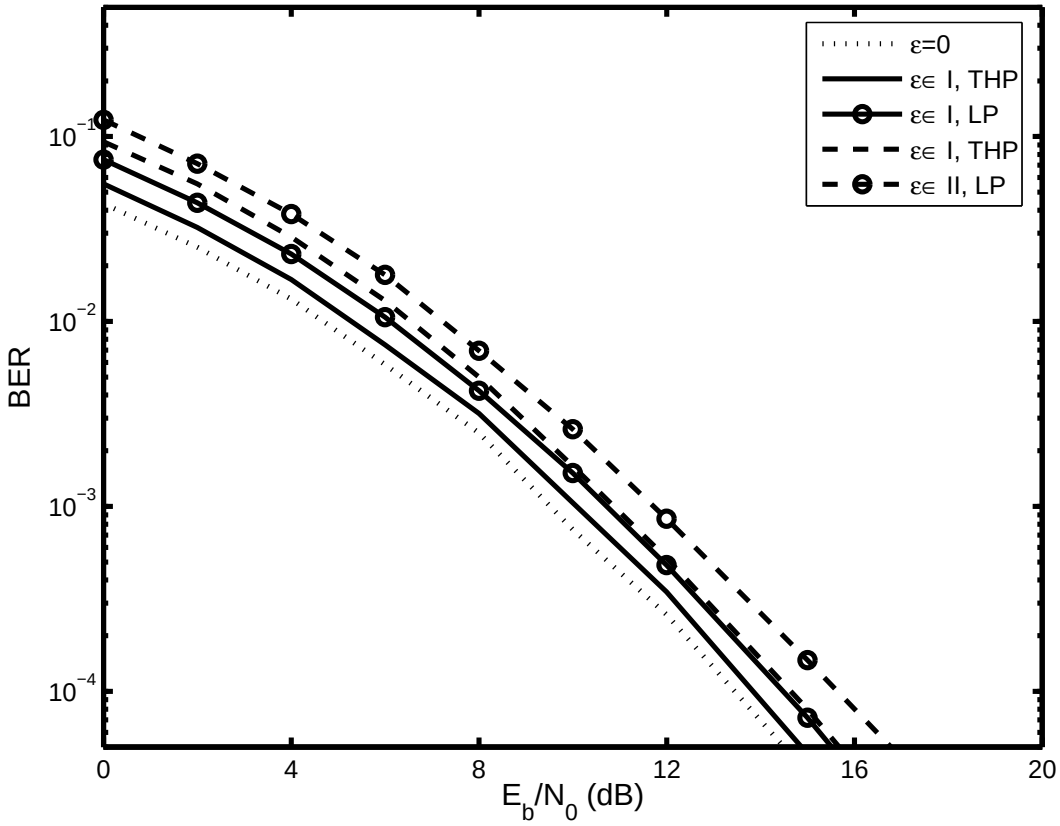

Figure 5.3: BER of LFB-THP and LFB linear precoding (LFB-LP) with MMSE codebook selection criterion as a function of the SNR for different values of the normalized frequency offset and 64-subcarrier 2-user 4-QAM-OFDM; $M_T = 4$, $M_C = 2$, $M_u = 2$; estimated CSI at the receiver. $K = 64$.

the normalized frequency offsets in the interval $\mathcal{II}$, the BER is significantly improved. Furthermore, the MMSE based system outperforms the MSV and the MMI ones by 0.6 and 1.8 dB at a BER of 10^{-4} with normalized frequency offsets in $\mathcal{I}$.

5.3.2 OSTBC OFDM

Fig. 5.5 presents the BER of 2×4 and 3×4 single-user OFDM with the MMSE criterion and shows that the proposed precoder can be used in OSTBC systems. The Alamouti code is considered. The BER increase due to ICI is significantly reduced by the porposed precoder, and the Alamouti-coded OFDM achieves a 3 dB gain over the uncoded SM MIMO OFDM at a BER of 10^{-4} in 2×4

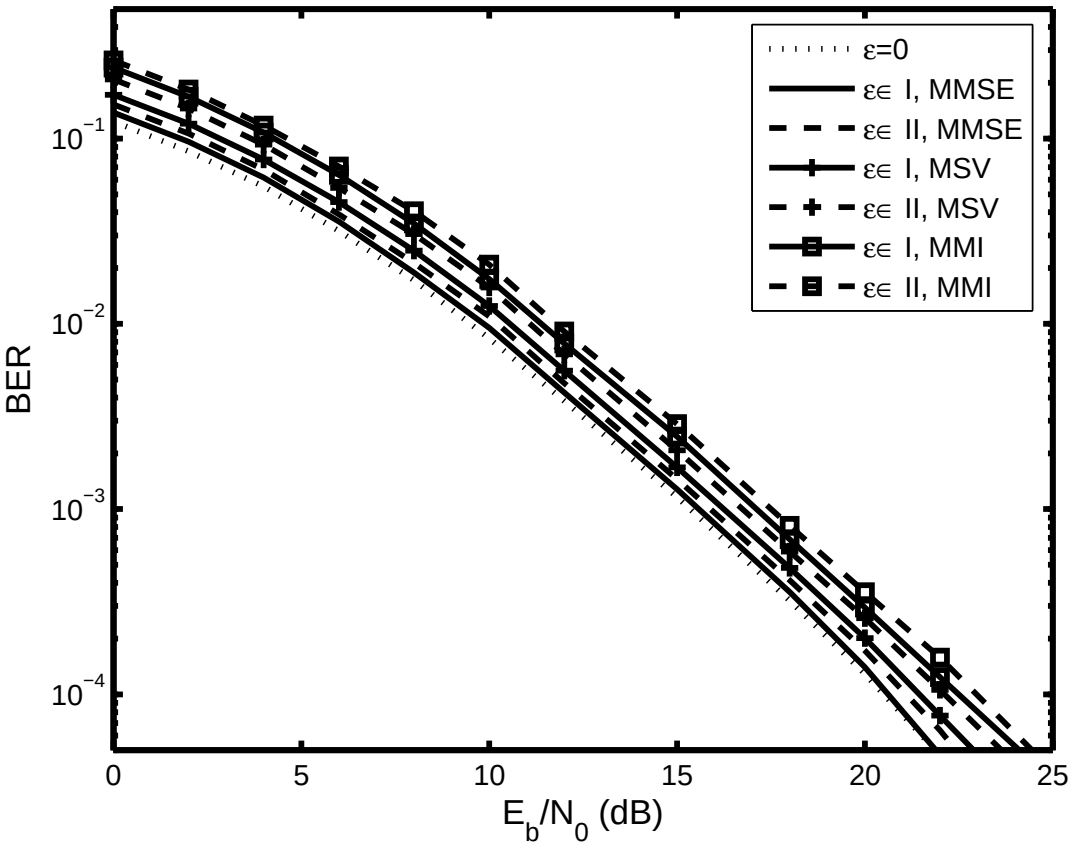

Figure 5.4: BER for LFB-THP as a function of the SNR for different values of the normalized frequency offset and 64-subcarrier 2-user 4-QAM SM OFDM; $M_T = 3$, $M_C = 2$, $M_u = 2$. The MMSE, MSV and MMI codebook selection criteria are compared.

systems. In 3×4 Alamouti-coded OFDM, once again, ICI is almost completely suppressed. As a result, our precoder can be used for OSTBC MIMO OFDM with an arbitrary number of transmit antennas.

5.3.3 Spatially Correlated MIMO Channels

In Fig. 5.6, a correlated Rayleigh fading channel is simulated for two-user OFDM system; $M_T = 3,\ M_C = 2,\ M_u = 2$. The MMSE selection criterion is used and the codebook size is 64. The angle of arrival spread Δ in (3.20) is set to 0.1; the transmit and receive antenna spacing 4λ and 0.45λ, respectively. The transmit antenna correlation matrix $\mathbf{R}_T$ is known at both the transmitter

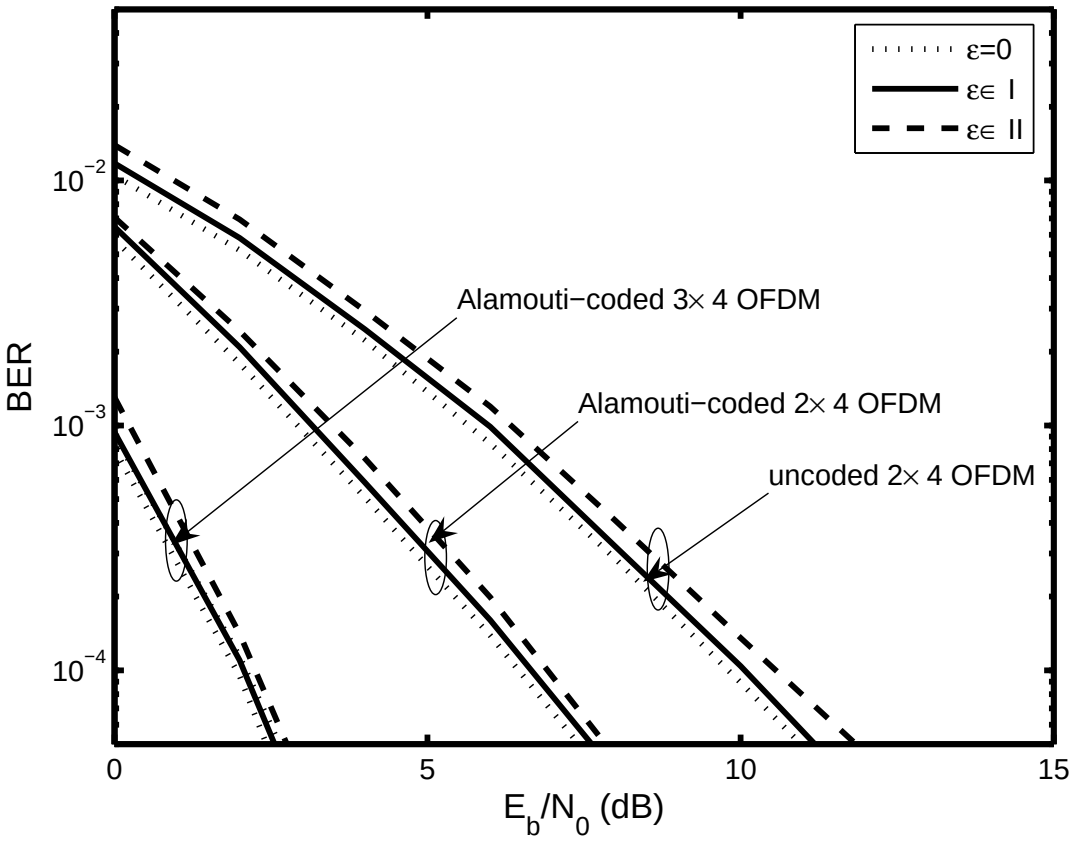

Figure 5.5: BER of LFB-THP with the MMSE selection criterion as a function of the SNR for different values of the normalized frequency offset and 64-subcarrier 2×4 4-QAM uncoded (SM) OFDM, 4-QAM Alamouti-coded OFDM, and 3×4 4-QAM Alamouti-coded OFDM.

and the receiver. The proposed LFB-TH precoder reduces ICI due to frequency offset. Although marginal BER loss occurs as a result of antenna correlations, the proposed LFB-THP performs quite well.

5.4 Summary

Linear and non-linear limited-feedback precoding have been developed for both SM and OSTBC MIMO OFDM with frequency offsets. The ICI matrix does not influence precoding, which makes precoding design on per-subcarrier basis possible. Exploiting this property, the limited-feedback codebook design algorithm and the precoding matrix selection criteria have been derived. The

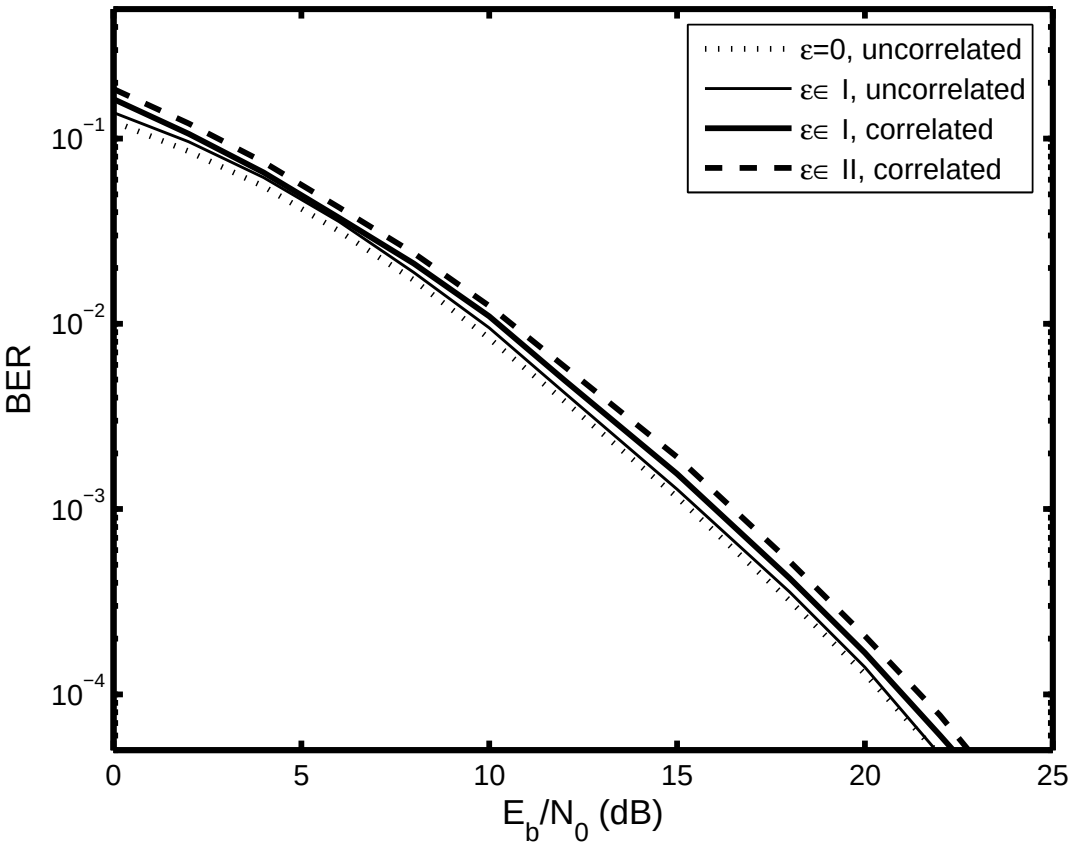

Figure 5.6: BER for LFB-THP with the MMSE criterion as a function of the SNR for different values of the normalized frequency offset and 64-subcarrier 4-QAM SM MIMO OFDM in spatially correlated channels; $M_T = 3$, $M_C = 2$, $M_u = 2$.

proposed limited-feedback precoders reduce the feedback requirement and non-linear precoding outperforms linear precoding. The results demonstrate that it significantly reduces the BER degradation due to frequency offset. Furthermore, our precoder can also be used in OSTBC MIMO OFDM systems with an arbitrary number of transmit antennas and spatially correlated MIMO channels.

Chapter 6

Covariance Precoding Schemes for MIMO OFDM over Transmit-Antenna and Path-Correlated Channels

MIMO OFDM systems can achieve capacity increase or diversity gain, when antenna and path correlations are negligible [85]. However, these correlations are not negligible in practice because of many reasons such as insufficient antenna spacing, the presence of scatterers far from the transmit antenna array in a narrow angular range, and other reasons. Spatial correlations significantly reduce the system capacity [72] and increase the system BER [87]. Thus, techniques are required to mitigate the impact of correlations on SM and space-time coding (STC) systems. Precoding/beamforming can mitigate capacity loss in SM MIMO systems [88] or improve BER for OSTBC systems in spatially correlated flat-fading channels [47, 48, 51, 89, 90], if the channel correlation matrices are available at the transmitter. For SM OFDM over antenna and path-correlated frequency-selective channels, precoding enables pre-processing of the signals at a subcarrier level and improves capacity [91]. However, precoders designed to improve the error rate in OSTBC OFDM have not been studied yet. Precoders are derived to mitigate the impact of transmit-antenna and path correlations.

Several schemes that switch between SM and STC and adaptive schemes have been investigated in the literature. The fundamental diversity-multiplexing trade-off in the high SNR region has been analyzed in [20]. A switching algorithm between SM and STC is proposed in [92]. Reference [93]

presents an antenna selection scheme to choose transmit antennas for SM or selection diversity combining mode. A multi-mode linear precoder with limited feedback is proposed in [94]. These approaches [92–94] employ selection diversity combining to improve error rate in high data-rate transmission over spatially-uncorrelated fading channels. In [95], an adaptive scheme is developed to achieve maximum-possible capacity subject to a pre-defined BER value. However, these schemes do not deal with OFDM, assuming only flat-fading MIMO channels, and [92, 95] do not consider precoding.

This chapter considers covariance based linear precoding and non-linear THP for MIMO OFDM systems. The main objective is to design precoders to mitigate the impact of transmit-antenna and path correlations. First, the impact of path correlations on the pairwise error probability (PEP) is analyzed, and closed-form, waterfilling-based linear and non-linear precoders are derived to minimize the worst-case PEP in OSTBC OFDM. Second, an adaptive transmission strategy is also developed for switching between precoded SM OFDM and precoded OSTBC OFDM. The system is designed to achieve a low BER with a target fixed transmission rate. The switching criterion is the minimum Euclidean distance of the received codebook. A lower complexity switching criterion is also developed. The switching decision sent to the transmitter requires one feedback bit per subcarrier. To reduce the number of feedback bits, the switching decision can be made for groups of neighboring subcarriers. The proposed precoders considerably reduce the error rate in antenna and path-correlated channels; non-linear precoders perform better than linear precoders. The adaptive strategy outperforms either SM or OSTBC individually in terms of the BER.

The remainder of this chapter is organized as follows. Section 6.1 briefly describes the system model of SM OFDM and OSTBC OFDM over transmit-antenna and path-correlated channels. The impact of the path correlations on the error rate of OSTBC OFDM is analyzed. Section 6.2 derives new linear and non-linear precoders for OSTBC OFDM in correlated channels. In Section 6.3 a selection criterion is developed for switching between SM-based and OSTBC-based precoding modes, along with adaptive linear and non-linear precoders. The simulation results and conclusions

are given in Sections 6.4 and 6.5.

6.1 System Model

This section will introduce the system model of an N-subcarrier OFDM system with M_T transmit antennas and M_R receive antennas in the presence of transmit-antenna and path correlations. The downlink case is analyzed where spatial correlations exist between the transmit antennas, but none between the receive antennas. At the receiver (mobile station), a sufficiently uncorrelated set of antennas can be assumed if antenna spacing is half wavelength of the carrier or more [85]. This condition is easily satisfied by practical systems that use a high carrier frequency in the order of GHz. The impact of path correlations in OSTBC OFDM is also analyzed.

6.1.1 Transmit-Antenna and Path Correlations in OFDM

The channel between the v-th transmit antenna and u-th receive antenna is a wideband frequency-selective fading channel with L resolvable paths. The l-th path gain is a zero-mean complex Gaussian random variable (Rayleigh fading) with variance σ_l^2. The set of the l-th path gains can be represented by an $M_R \times M_T$ matrix $\mathbf{H}_l$ with entries $h_{u,v}[l]$, $\forall\, l$. The channel gains remain constant over several OFDM symbol intervals. As in [91], the path gain matrices $\mathbf{H}_l$ can be represented as

$$\left[\mathbf{H}_0 \cdots \mathbf{H}_{L-1}\right] = \mathbf{H}_w \left[\mathbf{R}_P^T \otimes \mathbf{R}_T\right]^{1/2}, \tag{6.1}$$

where $\mathbf{H}_w$ is an $M_R \times M_T L$ matrix of i.i.d zero mean complex Gaussian random variables with unit variance. The $L \times L$ path correlation matrix $\mathbf{R}_P$ is defined as (3.19) with the $\{m, n\}$th entry

$$R_P(m,n) = \sigma_m \sigma_n p^{|m-n|} e^{\jmath\, \theta_{m,n}}, \quad 0 < p \leq 1 \tag{6.2}$$

where p is the path correlation factor and $\theta_{m,n}$ is the phase of the path correlation between the m-th and the n-th path. The entries of the transmit-antenna correlation matrix $\mathbf{R}_T$ are given in (3.20).

At the receiver, the $M_R \times M_T$ channel on the k-th subcarrier can be represented as

$$\mathbf{H}[k] = \sum_{l=0}^{L-1} \mathbf{H}_l e^{-\jmath \frac{2\pi}{N} kl}. \tag{6.3}$$

If the path gain matrices $\mathbf{H}_l$ satisfy (6.1), (6.3) can be re-written as

$$\mathbf{H}[k] = \mathbf{H}_w \left(\mathbf{R}_P^{T/2} \mathbf{F}[k] \otimes \mathbf{R}_T^{1/2} \right) = \mathbf{H}_w \mathbf{R}_{PT}^{1/2}[k], \tag{6.4}$$

where $\mathbf{F}[k] = \left[e^{-\jmath \frac{2\pi}{N} k0} \dots e^{-\jmath \frac{2\pi}{N} k(L-1)} \right]^T$ is an L-element vector; $\mathbf{R}_{PT}^{1/2}[k] = \mathbf{R}_P^{T/2} \mathbf{F}[k] \otimes \mathbf{R}_T^{1/2}$ is an $M_T L \times M_T$ matrix. The k-th received signal vector thus can be given by

$$\mathbf{Y}[k] = \mathbf{H}[k]\mathbf{X}[k] + \mathbf{W}[k]. \tag{6.5}$$

With SM OFDM, M_T independent data symbols are transmitted at each time slot on the k-th subcarrier. Since the space-time code rate is defined as P/T, where P is the number of symbols transmitted over the T time slots, SM OFDM has a rate of $R_{\text{SM}} = M_T$.

6.1.2 Impact of Path Correlations

Correlated fading can significantly affect the wireless performance. In SM OFDM, the achievable spectral efficiency (in bits/sec/Hz) can decrease due to path correlations and transmit-antenna correlations [91]. The latter has been shown to increase the BER in OSTBC OFDM [87]. We now show the impact of path correlations on PEP in OSTBC OFDM.

The PEP is the probability that a transmitted signal matrix $\mathbf{X}[k]$ is erroneously decoded as a matrix $\hat{\mathbf{X}}[k]$. For an ML receiver that uses the Euclidean distance metric, the output decision is given by

$$\hat{\mathbf{X}}[k] = \arg \min_{\mathbf{X}[k]} \|\mathbf{Y}[k] - \mathbf{H}[k]\mathbf{X}[k]\|_F^2, \tag{6.6}$$

where $\|.\|_F$ is the Frobenius norm. The PEP for the k-th subcarrier can be upper bounded as [87]

$$P_e \left(\mathbf{X}[k] \longrightarrow \hat{\mathbf{X}}[k] \right) \leq \exp \left(-\frac{\|\mathbf{H}[k]\boldsymbol{\emptyset}\|_F^2}{4\sigma_W^2} \right), \tag{6.7}$$

where $\boldsymbol{\emptyset} = \mathbf{X}[k] - \hat{\mathbf{X}}[k]$ is the codeword difference matrix. As in [50], by taking the expectation of (6.7) over the channel statistics, the average PEP can be bounded by

$$\log \bar{P}_e \leq -M_R \log \det \left| \mathbf{Q}[k] \right|, \tag{6.8}$$

where $\mathbf{Q}[k] = \frac{\boldsymbol{\Theta}\boldsymbol{\Theta}^H}{4\sigma_W^2}\mathbf{R}_{PT}[k] + \mathbf{I}_{M_T}$; $\mathbf{R}_{PT}[k] = \mathbf{R}_{PT}^{H/2}[k]\mathbf{R}_{PT}^{1/2}[k]$ is an $M_T \times M_T$ matrix, and depends on $\mathbf{R}_T^{1/2}$ and $\mathbf{R}_P^{1/2}$, given by (6.4). For OSTBC, $\boldsymbol{\Theta}\boldsymbol{\Theta}^H = \mu\mathbf{I}_{M_T}$ is a diagonal matrix [12], where μ is the distance between the codewords in a pair, depending on the specific codeword pair. Since μ dominates the error probability exponent, the minimum distance over all pairs of the codewords, $\mu_{\min}$, primarily determines the worst system performance in an OSTBC system. Minimizing the worst average PEP is hence equivalent to maximizing the below function of $\mathbf{Q}$:

$$\mathfrak{L}(\mathbf{Q}) = \log\det\left|\mathbf{Q}_{\min}[k]\right| = \log\det\left|\frac{\mu_{\min}}{4\sigma_W^2}\mathbf{R}_{PT}[k] + \mathbf{I}_{M_T}\right|. \tag{6.9}$$

To analyze the impact of $\mathbf{R}_P^{1/2}$, the two correlation matrices are decomposed by using the SVD as follows:

$$\begin{aligned}\mathbf{R}_P^{T/2}\mathbf{F}[k] &= \mathbf{U}_P\boldsymbol{\Gamma}_P\mathbf{V}_P^H \\ \mathbf{R}_T^{1/2} &= \mathbf{U}_T\boldsymbol{\Gamma}_T\mathbf{V}_T^H,\end{aligned} \tag{6.10}$$

where $\mathbf{U}_T$ and $\mathbf{V}_T$ are $M_T \times M_T$ unitary matrices. $\boldsymbol{\Gamma}_T$ is the singular value matrix of $\mathbf{R}_T^{1/2}$. Since $\mathbf{R}_P^{T/2}\mathbf{F}[k]$ is an $L \times 1$ vector, $\mathbf{U}_P$ is an $L \times 1$ vector and $\mathbf{U}_P^H\mathbf{U}_P = 1$; $\mathbf{V}_P = 1$ and the $\boldsymbol{\Gamma}_P$ is a rank-one matrix with the only entry $\gamma_{p_k} = \mathbf{F}^H[k]\mathbf{R}_P\mathbf{F}[k]$. The matrix $\mathbf{R}_T^{1/2}[k]$ in (6.4) can therefore be represented as

$$\mathbf{R}_{PT}^{1/2}[k] = \mathbf{R}_P^{T/2}\mathbf{F}[k] \otimes \mathbf{R}_T^{1/2} = \left(\mathbf{U}_P\gamma_{p_k}\right) \otimes \left(\mathbf{U}_T\boldsymbol{\Gamma}_T\mathbf{V}_T^H\right) = \gamma_{p_k}\tilde{\mathbf{U}}\boldsymbol{\Gamma}_T\mathbf{V}_T^H, \tag{6.11}$$

where $\tilde{\mathbf{U}} = \mathbf{U}_P \otimes \mathbf{U}_T$ is an $LM_T \times M_T$ matrix, and $\tilde{\mathbf{U}}^H\tilde{\mathbf{U}} = \mathbf{I}_{M_T}$ because $\mathbf{U}_T$ is a unitary matrix. The correlation matrix $\mathbf{R}_{PT}[k]$ can thus be given by

$$\mathbf{R}_{PT}[k] = \gamma_{P_k}^2\mathbf{V}_T\boldsymbol{\Gamma}_T^H\tilde{\mathbf{U}}^H\tilde{\mathbf{U}}\boldsymbol{\Gamma}_T\mathbf{V}_T^H = \gamma_{P_k}^2\mathbf{V}_T\boldsymbol{\Gamma}_T^2\mathbf{V}_T^H. \tag{6.12}$$

The performance degradation due to the path correlation is shown in Fig. 6.1. The transmit antenna correlation parameter ζ_T is set to zero, i.e., $\mathbf{R}_T = \mathbf{I}_{M_T}$. Perfect channel estimates are assumed available at the receiver. Three groups of BERs are provided for different values of the path correlation factor p and phase $\theta_{m,n}$ at SNRs of 5 dB, 10 dB and 15 dB, respectively; the

impact of p and $\theta_{m,n}$ on the path correlation matrix $\mathbf{R}_P$ is shown by (6.2). In each group, when $\theta_{m,n} = 0, \forall\, m, n$, the BER monotonously increases as p grows. Compared with the BER of zero phase, the random phase can mitigate the impact of path correlations, especially at the high path correlation ($p \to 1$). However, the BER at a positive value of p is always higher than the BER at zero p, i.e, the propagation path correlation always degrades the error rate.

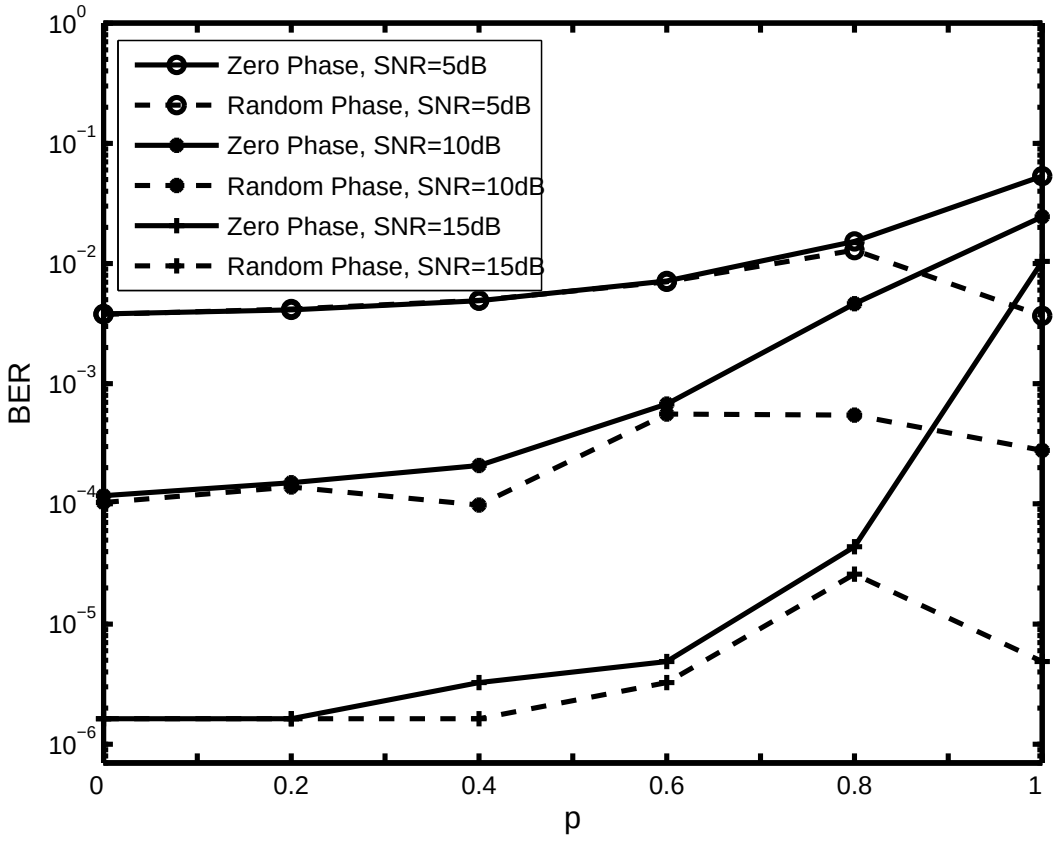

Figure 6.1: BER as a function of the path-correlation factor p for different values of SNR for a 2×2 4-QAM Alamouti-coded 64-subcarrier OFDM system with perfect channel estimation.

6.2 Precoding Schemes for OSTBC MIMO OFDM

This section develops covariance linear precoding and non-linear THP to mitigate the performance degradation of OSTBC OFDM over transmit-antenna and path-correlated channels. Capacity-

optimal precoding is discussedfor SM OFDM.

In covariance precoding systems, the correlation matrices are known to the transmitter. The transmit-antenna correlation matrices depend on transmit antenna spacing, which changes slower than the channel response or even does not change at all. As well, transmit-antenna spacing is known at the transmitter, i.e., feedback for $\mathbf{R}_T$ is not needed. The feedback load in covariance precoding is thus significantly reduced.

6.2.1 Optimal Precoding Scheme for OSTBC OFDM

With an $M_T \times M_T$ precoding matrix $\mathbf{E}_{\text{ST}}[k]$ on the k-th subcarrier the transmitted signal vector on the k-th subcarrier is $\mathbf{E}_{\text{ST}}[k]\mathbf{X}[k]$, instead of $\mathbf{X}[k]$. The cost metric $\mathfrak{L}(\mathbf{Q})$ (6.9) becomes

$$\begin{aligned}\mathfrak{L}(\mathbf{Q}) &= \log\det\left|\tfrac{\mathbf{E}_{\text{ST}}[k]\boldsymbol{\emptyset}\boldsymbol{\emptyset}^H\mathbf{E}_{\text{ST}}^H[k]}{4\sigma_W^2}\mathbf{R}_{PT}[k] + \mathbf{I}_{M_T}\right| \\ &= \log\det\left|\tfrac{\mu_{\min}\mathbf{E}_{\text{ST}}[k]\mathbf{E}_{\text{ST}}^H[k]}{4\sigma_W^2}\mathbf{R}_{PT}[k] + \mathbf{I}_{M_T}\right|.\end{aligned} \tag{6.13}$$

The optimal precoding matrix is thus given by

$$\mathbf{E}_{\text{ST}}[k]_{\text{opt}} = \arg\max_{\text{tr}(\mathbf{Z}[k])=M_T} \log\det\left|\xi\mathbf{Z}[k]\mathbf{R}_{PT}[k] + \mathbf{I}_{M_T}\right|, \tag{6.14}$$

where $\xi = \frac{\mu_{\min}}{4\sigma_W^2}$, $\mathbf{Z}[k] = \mathbf{E}_{\text{ST}}[k]\mathbf{E}_{\text{ST}}^H[k]$, and $\text{tr}(\cdot)$ denotes the matrix trace. Substituting (6.12) into (6.14) and applying the determinant identity [96], the optimal precoding matrix is given by

$$\begin{aligned}\mathbf{E}_{\text{ST}}[k]_{\text{opt}} &= \arg\max_{\text{tr}(\mathbf{Z}[k])=M_T} \log\det\left|\xi\gamma_{P_k}^2\boldsymbol{\Gamma}_T\mathbf{V}_T^H\mathbf{Z}[k]\mathbf{V}_T\boldsymbol{\Gamma}_T + \mathbf{I}_{M_T}\right| \\ &= \arg\max_{\text{tr}\left(\tilde{\mathbf{Z}}[k]\right)=\xi M_T} \log\det\left|\tilde{\boldsymbol{\Gamma}}_T\tilde{\mathbf{Z}}[k]\tilde{\boldsymbol{\Gamma}}_T + \mathbf{I}_{M_T}\right|,\end{aligned} \tag{6.15}$$

where $\tilde{\boldsymbol{\Gamma}}_T = \gamma_{p_k}\boldsymbol{\Gamma}_T$ and $\tilde{\mathbf{Z}}[k] = \xi\mathbf{V}_T^H\mathbf{Z}[k]\mathbf{V}_T$. As in [45], a waterfilling solution can be derived from (6.15). The optimal main-diagonal entries in $\tilde{\mathbf{Z}}[k]_{\text{opt}}$ will then be

$$\tilde{Z}_{kvv} = \left(\rho - \tilde{\gamma}_{vv}^{-2}\right)_+, \quad v = 1, \ldots, M_T, \tag{6.16}$$

where $(a)_+$ denotes $\max(a, 0)$; the parameter ρ is chosen to satisfy $\text{tr}\left(\tilde{\mathbf{Z}}[k]\right) = \xi M_T$; $\tilde{\gamma}_{vv}$ are the main-diagonal entries of $\tilde{\boldsymbol{\Gamma}}_T$. Hence, the optimal precoding matrix can be obtained by

$$\mathbf{E}_{\text{ST}}[k]_{\text{opt}} = \sqrt{\mathbf{Z}[k]_{\text{opt}}} = \sqrt{\frac{1}{\xi}\mathbf{V}_T\tilde{\mathbf{Z}}[k]_{\text{opt}}\mathbf{V}_T^H}\mathbf{K}, \tag{6.17}$$

where $\mathbf{K}$ can be any $M_T \times M_T$ unitary matrix, and hence the optimal precoder may not be unique [97]. In this chapter, $\mathbf{K}$ is chosen as the identity matrix $\mathbf{I}_{M_T}$.

The precoder (6.17) requires singular values of the corelation matrices and is based on the classical waterfilling optimization. With this precoder, the effective channel matrix on the k-th subcarrier becomes $\mathbf{H}[k]\mathbf{E}_{\text{ST}}[k]$, with which the receiver performs ML decoding. The precoder only needs the correlation matrices of $\mathbf{R}_{PT}^{1/2}$, i.e, only covariance feedback.

6.2.2 Non-Linear Tomlinson-Harashima Precoding

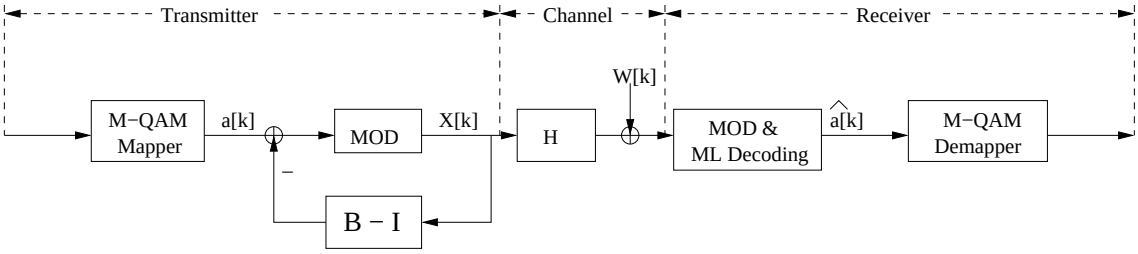

Figure 6.2: Tomlinson-Harashima precoding in OSTBC OFDM.

The transmitter in Fig. 6.2 includes a modulo arithmetic feedback structure employing matrix $\mathbf{B}[k]$, with which the transmitted symbols $X[k]$ are successively calculated for the data symbols $a[k]$ drawn from the initial M-ary QAM signal constellation. The feedback structure alone (without the modulo device, the purpose of which is to constrain the range of $X[k]$) is equivalent to $\mathbf{B}^{-1}[k]$, which can be optimally designed as in (6.17), $\mathbf{B}[k]_{\text{opt}} = \mathbf{E}_{\text{ST}}^{-1}[k]_{\text{opt}}$. The effective channel is $\mathbf{H}[k]\mathbf{E}_{\text{ST}}[k]_{\text{opt}}$ and ML decoding is used at the receiver. The overall precoding matrix can be written as $\mathbf{B} = \text{diag}\left[\mathbf{B}[0] \ldots \mathbf{B}[N-1]\right]$.

6.2.3 Precoding in SM OFDM

We have not been able to derive error-rate-minimization covariance precoders for SM OFDM. Instead, a result from [91] is adopted for capacity-suboptimal precoding for SM OFDM with only covariance feedback of CSI for transmit-antenna and path-correlated channels. The capacity-optimal

solution can loosely be considered as an MMSE-optimal solution, which can be considered as an indirect way of reducing the error rate.

The capacity-suboptimal solution of the $M_T \times M_T$ precoding matrix $\mathbf{E}_{\text{SM}}[k]$ is given by [91]

$$\left\{\mathbf{E}_{\text{SM}}[k]_{\text{opt}}\right\}_{k=0}^{N-1} = \arg \max_{\text{tr}(\tilde{\mathbf{Z}}_{\text{SM}}[k])=M_T} \frac{1}{N} \sum_{k=0}^{N-1} \log \det \left| \mathbf{I}_{M_T} + \tfrac{\eta_k M_R}{M_T} \mathbf{\Gamma}_T \tilde{\mathbf{Z}}_{\text{SM}}[k] \mathbf{\Gamma}_T \right|, \tag{6.18}$$

where $\eta_k = \frac{E_s \gamma_{p_k}}{\sigma_W^2}$, $\tilde{\mathbf{Z}}_{\text{SM}}[k] = \mathbf{V}_T^H \mathbf{Z}_{\text{SM}}[k] \mathbf{V}_T$, $\mathbf{V}_T$ and $\mathbf{\Gamma}_T$ are given in (6.10), and $\mathbf{Z}_{\text{SM}}[k] = \mathbf{E}_{\text{SM}}[k] \mathbf{E}_{\text{SM}}^H[k]$. Diagonal matrices of $\left\{\tilde{\mathbf{Z}}_{\text{SM}}[k]\right\}_{k=0}^{N-1}$ achieve optimality. This fact can be easily proven by assuming the fixed power is allocated to each of $\tilde{\mathbf{Z}}_{\text{SM}}[k]$ and applying the proof in [98]. The optimization entries of $\left\{\tilde{\mathbf{Z}}_{\text{SM}}[k]\right\}_{k=0}^{N-1}$ can be found by useing water-filling technique [98]. The suboptimal solution is more practical and efficient; it not only avoids numerical optimization, but also leads to almost the same capacity as the optimal solution [91]. Similarly, non-linear precoding can be used for SM OFDM with $\mathbf{B}_{\text{SM}}[k] = \mathbf{E}_{\text{SM}}^{-1}[k]_{\text{opt}}$, which can be designed according to (6.18). Using THP the entire capacity of the underlying MIMO channel can be achieved [60]. Detailed discussion of how THP can be applied to reach MIMO capacity is included in [60].

Clearly, the precoders in (6.17) and (6.18) need covariance feedback only, not the full CSI at the transmitter. They are designed for either capacity improvement in SM OFDM or error-rate improvement in OSTBC OFDM. We next show how to effectively exploit the two precoding modes for OFDM over transmit-antenna and path-correlated channels.

6.3 Adaptive Dual-Mode Precoding

This section develops an adaptive strategy which switches between precoded SM OFDM and OSTBC OFDM. For each subcarrier, the minimum Euclidean distance of the received codebook is computed for SM and OSTBC and is used to select the transmission mode. A lower complexity switching criterion is also derived. The selection decision is sent to the transmitter at a cost of one feedback bit per subcarrier. To reduce the number of feedback bits, the choice of SM or OSTBC can also be made for groups of neighboring subcarriers. At the receiver, ML decoding is used for

both modes.

The system is designed to maintain a fixed desired transmission rate of R bits per codeword, or R/T bits per symbol, where T is the number of symbols per codeword. In the case of Alamouti coding for diversity $T = 2$, and for SM $T = 1$. If minimum bandwidth Nyquist pulses are used for transmission, R/T is also equal to spectral efficiency in bits/s/Hz.

6.3.1 Euclidean-Distance Based Selection of Precoding-Mode

With a precoder $\mathbf{E}[k]$ at the transmitter (either (6.17) or (6.18)), the effective channel is $\mathbf{H}_{\text{eff}}[k] = \mathbf{H}[k]\mathbf{E}[k]$.

In an SM OFDM system, the squared minimum Euclidean distance of the received codebook, d^2_{SM}, can be found by exhaustive search over all possible codewords, as follows

$$d^2_{\text{SM}} = \min_{\mathbf{X}[k] \neq \mathbf{X}'[k]} \left\| \mathbf{H}[k]\mathbf{E}_{\text{SM}}[k]_{\text{opt}} \left(\mathbf{X}[k] - \mathbf{X}'[k] \right) \right\|^2 . \tag{6.19}$$

In the SM mode the codeword is the transmitted signal vector. In a full-rate OSTBC system with precoding (6.17), the minimum Euclidean distance is given by [99]

$$d^2_{\text{ST}} = \frac{d^2_{\text{min,st}}}{M_T} \|\mathbf{H}[k]\mathbf{E}_{\text{ST}}[k]_{\text{opt}}\|^2_F, \tag{6.20}$$

where $d_{\text{min,st}}$ is the minimum Euclidean distance of the transmit constellation of the OSTBC system. The precoding mode which offers a larger minimum distance for each channel realization is selected. When d_{SM} is greater than or equal to d_{ST}, the precoder (6.18) is used with SM OFDM; otherwise the precoder (6.17) with OSTBC OFDM. The decision is then conveyed to the transmitter by one bit per subcarrier; hence the total number of feedback bits is N.

The decisions on several neighboring subcarriers are typically highly correlated. This suggests the grouping of neighboring subcarriers, i.e., all the subcarriers are divided into N_b groups, and each group has N/N_b subcarriers. A single mode decision is thus made for each subcarrier group, rather than for each single subcarrier. This arrangement reduces the total number of feedback bits to N_b, and simulations results are provided to evaluate the resulting performance loss.

The basic structure of the proposed system is shown in Fig. 6.3. The transmitter switches between the precoding modes (6.17) and (6.18) for OSTBC OFDM and SM OFDM. The receiver unit contains the corresponding ML decoder and a mode selection unit. A low-bandwidth feedback link exists from the receiver to the transmitter. If non-linear precoding is included in either SM OFDM or OSTBC OFDM, the THP structure in Fig. 6.2 is applied to the precoding unit in Fig. 6.3; the receiver structure changes accordingly.

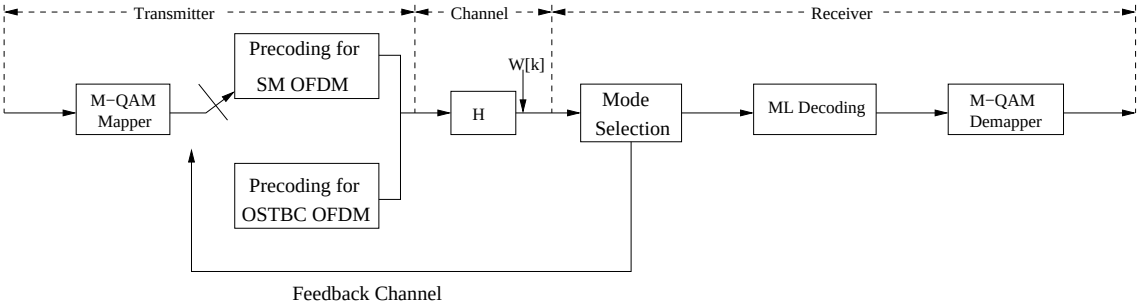

Figure 6.3: The adaptive dual-mode precoder.

6.3.2 Suboptimal Metric

Exhaustive search required to calculate the minimum distance (6.19) for SM may be prohibitive for a large constellation and a large number of transmit antennas. The calculation requirements can be reduced by finding a tight lower bound of the minimum distance. The received minimum Euclidean distance is lower bounded by [92]

$$d^2_{\text{SM}} \geq \gamma^2_{\min}\left(\mathbf{H}_{\text{eff}}[k]\right) \frac{d^2_{\text{min,sm}}}{M_T}, \tag{6.21}$$

where $\gamma_{\min}\left(\mathbf{H}_{\text{eff}}[k]\right)$ is the smallest singular value of $\mathbf{H}_{\text{eff}}[k]$ and $d_{\text{min,sm}}$ is the minimum Euclidean distance of the transmit constellation for SM. The equality holds if and only if the effective channel gain matrix is unitary. Since the lower bound in (6.21) is the worst case in precoded SM OFDM, it is used for mode selection.

Eq. (6.20) gives the maximum achievable minimum Euclidean distance of space-time coding [99]. The comparison of (6.20) and (6.21) reveals when the worst case of (6.18) in SM OFDM

is better than the best case of (6.17) in OSTBC OFDM. Therefore, the precoding mode (6.18) is selected when

$$\begin{aligned} \frac{d^2_{\text{min,st}}}{M_T}\|\mathbf{H}_{\text{eff}}[k]\|_F^2 &\leq \gamma^2_{\min}\left(\mathbf{H}_{\text{eff}}[k]\right)\frac{d^2_{\text{min,sm}}}{M_T}, \\ \text{or} \qquad \varsigma = \frac{\|\mathbf{H}_{\text{eff}}[k]\|_F}{\gamma_{\min}\left(\mathbf{H}_{\text{eff}}[k]\right)} &\leq \frac{d_{\text{min,sm}}}{d_{\text{min,st}}}, \end{aligned} \tag{6.22}$$

and SM OFDM is used for transmission; otherwise, (6.17) is applied for OSTBC OFDM. Although the suboptimal criterion (6.22) avoids potential large-scale search, thereby reducing the computational requirements, it may result in some BER increase.

6.4 Simulation Results

This section presents simulation results to show how our proposed precoders improve the system performance in OFDM over transmit-antenna and path-correlated channels. The vehicular B channel specified by ITU-R M. 1225 [73] is used. ML decoding is used. The transmitter only knows the correlation matrices $\mathbf{R}_T$ and $\mathbf{R}_P$ with the antenna-correlation parameter $\zeta_T = \Delta\frac{d_T}{\lambda}$ and path-correlation factor p, respectively; the path-correlation phase $\theta_{m,n}$ in (6.2) is zero. The angle of arrival spread is assumed 12°, i.e., $\Delta \approx 0.2$.

The simulation cases consider both perfect and imperfect channel estimation. ML estimation is assumed. The estimation error affects the power loading of the precoders and the variance of the estimation error Ω_e is known at both the transmitter and the receiver. As channel estimation becomes accurate, i.e., the variance of estimation errors Ω_e becomes negligible, the CSIR approaches the actual channel.

6.4.1 PEP-Optimal Precoding for OSTBC OFDM

This subsection demonstrates how the proposed linear and non-linear precoders $\mathbf{E}_{\text{ST}}[k]_{\text{opt}}$ (6.17) reduce the system BER for OSTBC OFDM in transmit-antenna and path-correlated channels.

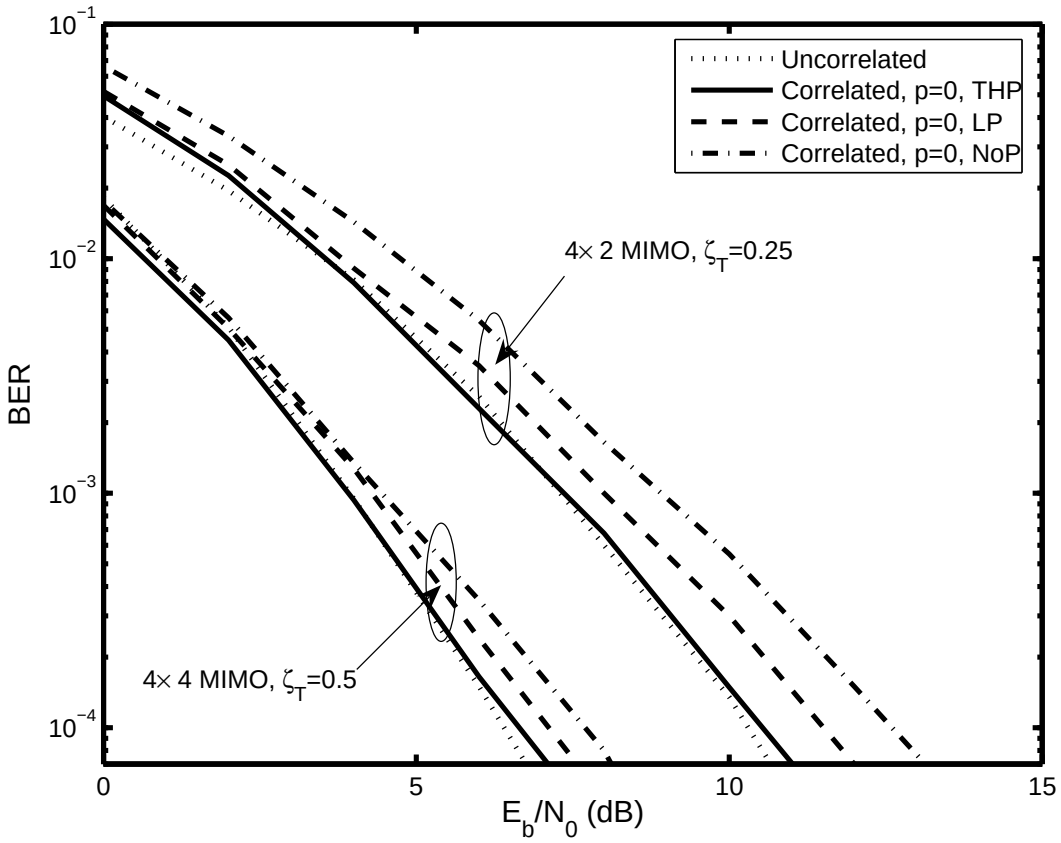

Figure 6.4: BER with linear precoding (LP), THP and no precoding (NoP) as a function of the SNR for different values of the normalized transmit-antenna spacing for 4×2 and 4×4 16-QAM $1/2$-rate OSTBC systems in transmit-antenna correlated channels with perfect channel estimation, $N = 1$, $L = 1$, and $p = 0$. Vehicular B channel is considered.

6.4.1.1 Flat-Fading MIMO Channels

The special case with $N = 1$ and $L = 1$ is first considered, where the channel model (6.4) is reduced to a flat-fading MIMO channel. Only transmit-antenna correlations need to be considered and perfect channel estimation is assumed. The BERs of 16-QAM 4×2 systems and 4×4 systems are shown in Fig. 6.4, and antenna-correlation parameter ζ_T is set to 0.25 and 0.5, respectively. The code rate R_{ST} of the OSTBC matrix is $1/2$ as in [12]. The BER for uncorrelated MIMO channels is shown as reference. Clearly, the transmit-antenna correlations significantly degrade the BER performance. As they become high (antenna spacing and/or the angle of arrival spread

decreases), the degradation becomes severe. Both linear precoding and non-linear THP mitigate the degradation. The TH precoder almost completely cancels it. At a BER of 10^{-4}, the linear precoding obtains 0.5 dB gain in 4×4 systems and 1 dB gain in 4×2 systems; THP achieves 0.8 dB and 1.8 dB, respectively.

6.4.1.2 Frequency-Selective Fading MIMO Channels

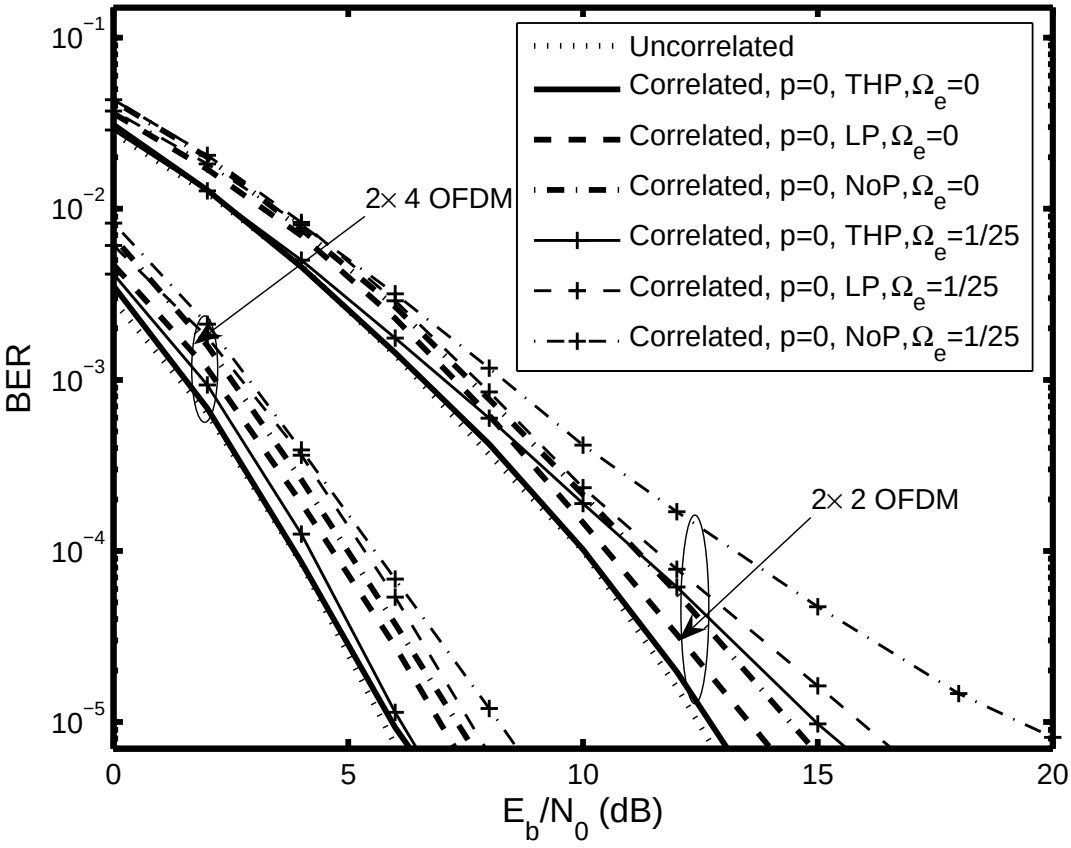

Figure 6.5: BER with linear precoding (LP), THP and no precoding (NoP) as a function of the SNR for 2×2 and 2×4 4-QAM Alamouti-coded 64-subcarrier OFDM systems in transmit-antenna correlated channels with perfect and imperfect channel estimation, $\zeta_T = 0.25$, $\Omega_e = 1/25$, and $p = 0$. Vehicular B channel is considered.

64-subcarrier 4-QAM OSTBC OFDM over the vehicular B channel [73] is now considered. In Fig. 6.5, 2×2 and 2×4 Alamouti-coded OFDM systems with perfect and imperfect channel estimation are considered. The variance of the estimation error is $\Omega_e = 1/25$. The path-correlation

factor is zero, and ζ_T is 0.25. Both linear and non-linear precoders suppress the BER increase due to the transmit-antenna correlations. Compared with the perfect CSI case, channel estimation errors result in additional performance degradation, but our precoders still offer BER gains over the no-precoding case. The non-linear TH precoder outperforms linear precoding.

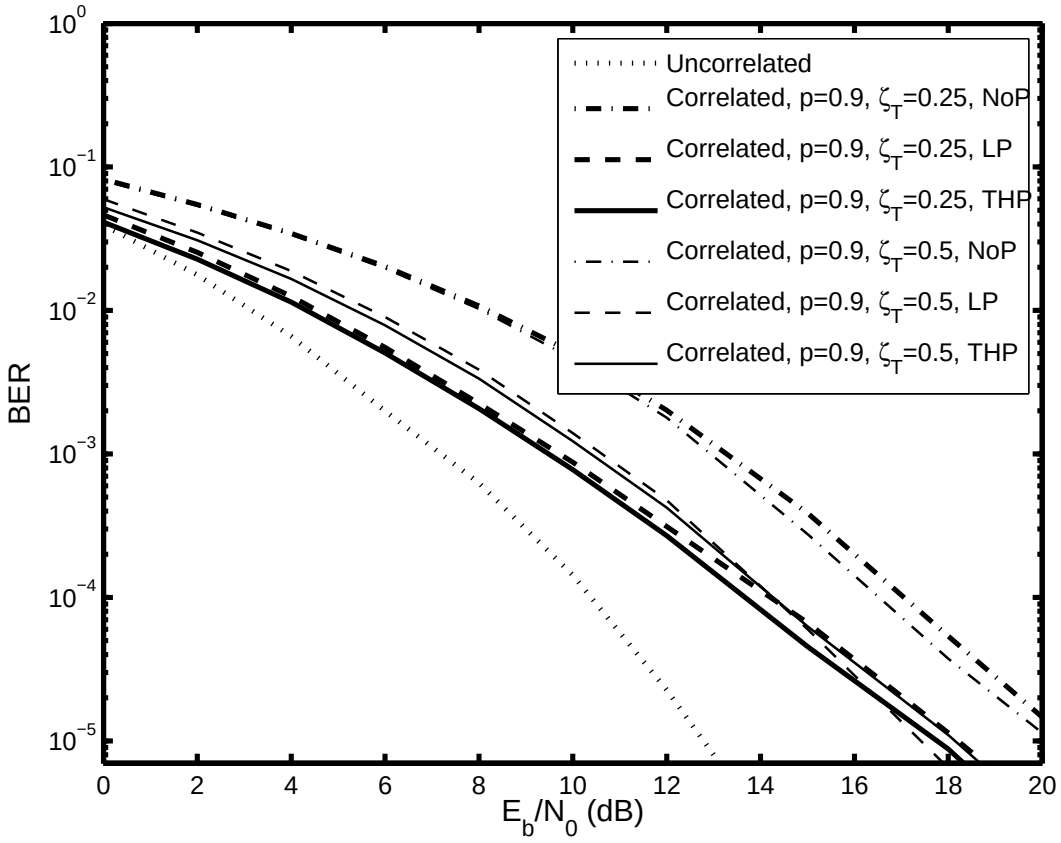

Figure 6.6: BER with linear precoding (LP), THP and no precoding (NoP) as a function of the SNR for different values of the normalized transmit-antenna spacing for 2×2 4-QAM Alamouti-coded 64-subcarrier OFDM systems in antenna and path-correlated channels with perfect channel estimation, $p = 0.9$. Vehicular B channel is considered.

Fig. 6.6 assumes the path correlation coefficient $p = 0.9$ and perfect CSI at the receiver (CSIR); ζ_T is set to 0.25 and 0.5. Although the BER substantially increases in this case, both the linear and non-linear precoders mitigate the impact of path correlations.

6.4.2 Adaptive Dual-Mode Precoding

This subsection shows how our new adaptive precoders improve the BER of MIMO OFDM in transmit-antenna and path-correlated channels. For simplicity, the Alamouti code for 2 transmit antennas is considered. In the simulation, the transmission rate R/T is fixed to 4 bits/s/Hz in both cases. With 2 transmit antennas, the adaptive precoding selects between precoding for spatial multiplexing (6.18) in 4-QAM SM OFDM and precoding for diversity (6.17) in 16-QAM Alamouti-coded OFDM.

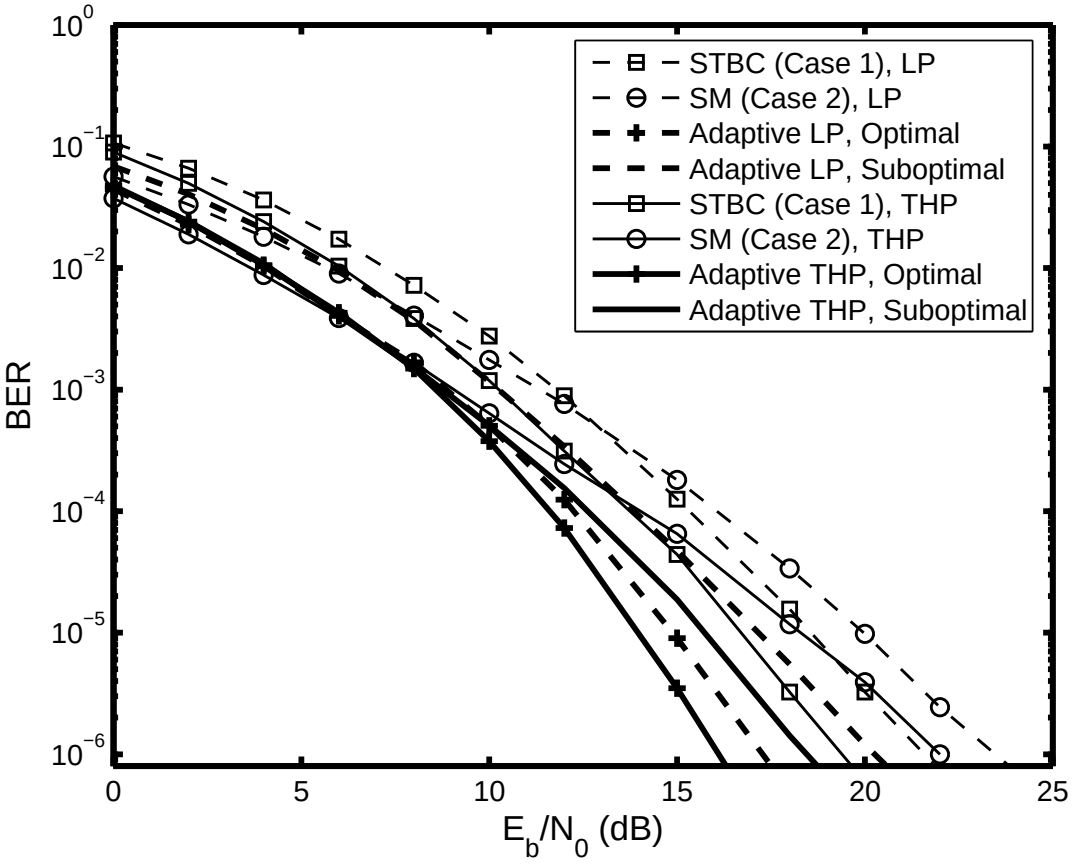

Figure 6.7: BER as a function of SNR for linear and non-linear precoding with and without the adaptive structure in 2×2 64-subcarrier OFDM systems in transmit-antenna correlated channels with perfect CSIR. One subcarrier per group ($N_b = N$), $R = 4$ bits/s/Hz and $p = 0$, $\zeta_T = 0.25$. Adaptive precoders use the optimal (exhaustive search) and suboptimal (metric (6.22)) criteria.

Fig. 6.7 illustrates the BERs of adaptive dual-mode precoding in 2×2 64-subcarrier OFDM,

where the path-correlation factor is zero and the antenna-correlation parameter ζ_T is 0.25. Both linear and non-linear precoders with perfect CSIR are considered. In adaptive precoding, the mode-selection decision is sent back for each subcarrier. The optimal switching criterion using exhaustive search and the suboptimal criterion using the metric (6.22) are considered. The BERs of precoding (6.17) for 16-QAM Alamouti-coded OFDM (Case 1) and precoding (6.18) for 4-QAM SM OFDM (Case 2) in spatially-correlated channels are also separately given for reference. The linear precoder or TH precoder in the both cases do not have adaptive structure. Different diversity orders of spatial multiplexing and Alamouti coding (for the 2×2 MIMO system they are two versus four, respectively) change the slope of the average BER curves of Case 1 and 2 at high SNR. The curves of Case 1 and Case 2 cross approximately at the SNR of 13 dB in the case of linear precoding, and at 14 dB for THP. The curves represent the average BER over all channel realizations. In our adaptive precoding, the better precoding mode is chosen for each channel realization, which offers additional selection diversity gain. When using the suboptimal criterion, almost 1 dB improvement over Case 1 and 3 dB gain over Case 2 in the high SNR region are obtained. Non-linear adaptive THP outperforms linear adaptive precoding. The suboptimal criterion saves on computational complexity, but suffers a diversity gain loss. Exhaustive search with the optimal criterion offers about 1.5 dB over the suboptimal metric at a BER of 10^{-5}.

Fig. 6.8 shows the BERs of adaptive linear/non-linear precoding in 2×2 64-subcarrier OFDM with imperfect channel estimation. The variance of the estimation error Ω_e is $1/25$, ζ_T is 0.25, and the path-correlation factor is zero. The suboptimal criterion is used. The selection decision is sent back per subcarrier (N groups) and per pair of subcarriers ($N/2$ groups). Clearly, the estimation errors degrade the system performance, but our proposed precoding still outperforms cases 1 and 2 implemented individually. The group-wise decision feedback results in 1 dB degradation for linear or non-linear adaptive precoding. However, 50% on the feedback requirements are saved. Clearly, there is a trade-off between the feedback requirement and performance.

The BERs of proposed adaptive precoding with perfect CSIR are shown in Fig. 6.9. The

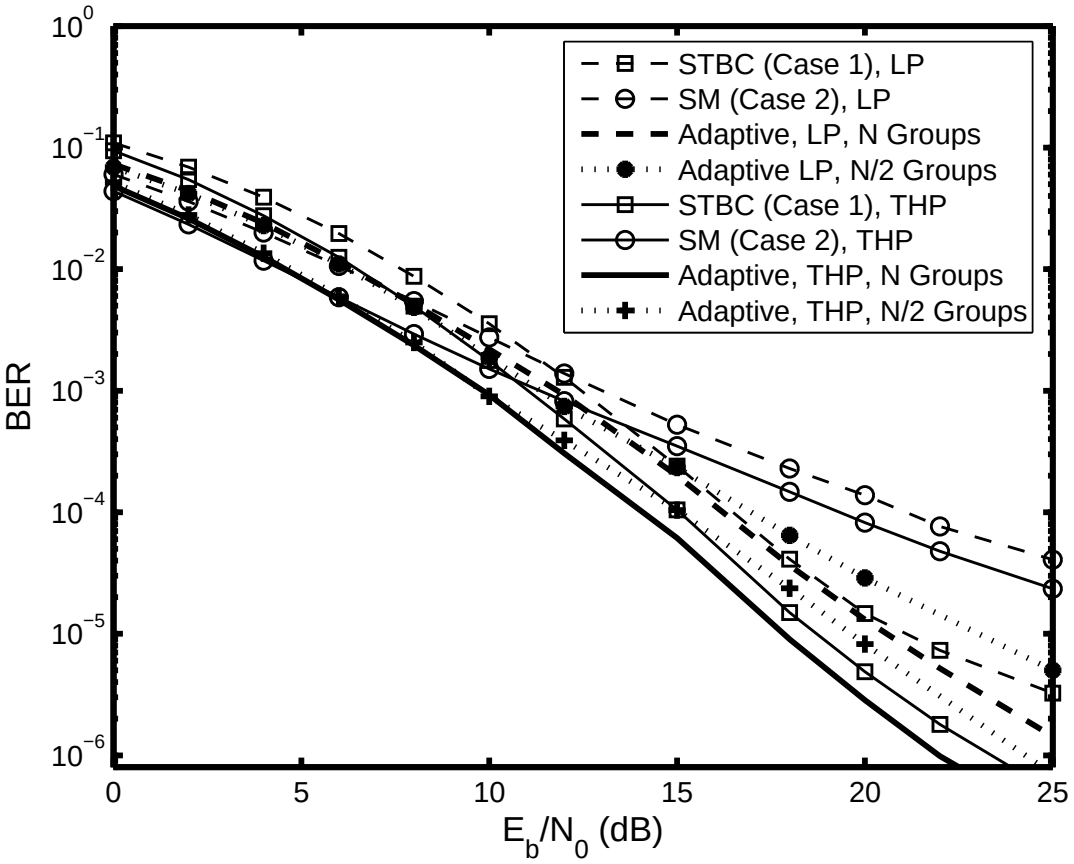

Figure 6.8: BER as a function of SNR for linear and non-linear precoding with and without the adaptive structure in 2×2 64-subcarrier OFDM systems over transmit-antenna correlated channels with imperfect CSIR. One or two subcarriers per group ($N_b = N$, $N_b = N/2$), $R = 4$ bits/s/Hz, $\Omega_e = 1/25$, $p = 0$, and $\zeta_T = 0.25$. Vehicular B channel is considered. Adaptive precoding uses the suboptimal criterion.

path-correlation factor is 0.9 and the antenna-correlation parameter ζ_T is 0.25. The optimal and suboptimal criteria are considered for adaptive precoding, and the selection decision is fed back on a subcarrier basis ($N_b = N$). The proposed linear and non-linear precoders are compared to precoding without adaptive structure in Case 1 and Case 2. The linear and non-linear adaptive precoders individually outperform their non-adaptive counterparts in Case 1 and 2. The non-linear adaptive THP outperforms linear adaptive precoding: at a BER of 10^{-5}, there is 1.2 dB gain. Adaptive precoding suffers a BER increase for MIMO OFDM with both transmit-antenna and path correlations compared to that for MIMO OFDM with only transmit-antenna correlations in

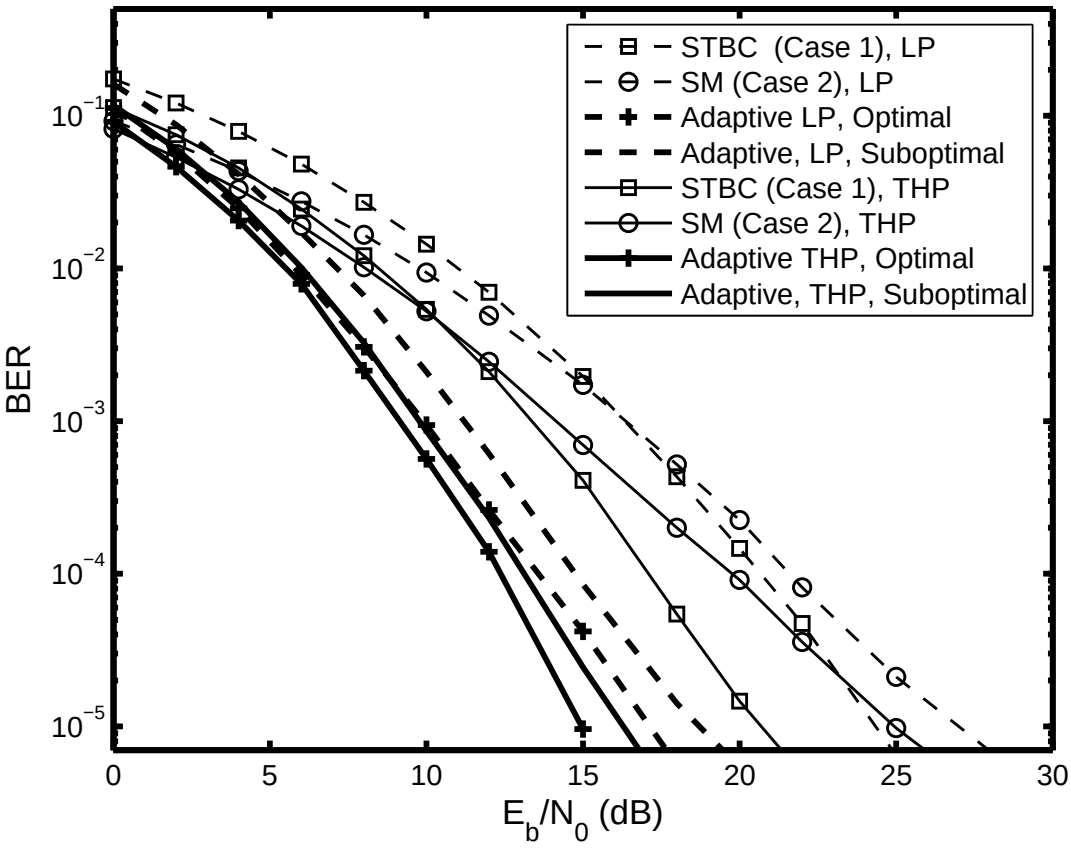

Figure 6.9: BER as a function of SNR for linear and non-linear precoding with and without the adaptive structure in 2×2 64-subcarrier OFDM systems over antenna and path-correlated channels with perfect CSIR. One subcarrier per group ($N_b = N$), $R = 4$ bits/s/Hz, $\zeta_T = 0.25$ and $p = 0.9$. Vehicular B channel is considered. Adaptive precoding uses the optimal and suboptimal criteria.

Fig. 6.7. The suboptimal selection criterion leads to about 1 dB loss at a BER of 10^{-5}.

Fig. 6.10 shows the performance of adaptive linear and non-linear precoding using the optimal selection criterion. Both perfect and imperfect channel estimation are considered. The variance of estimation error is $1/25$. The number of subcarrier groups is N or $N/2$. The path-correlation factor is 0.9 and the antenna-correlation parameter ζ_T is 0.5. When the mode decision is sent back every two subcarriers ($N/2$ groups), there is almost 1dB degradation, but the required feedback bandwidth is reduced by 50%. Imperfect channel estimation increases the system BER.

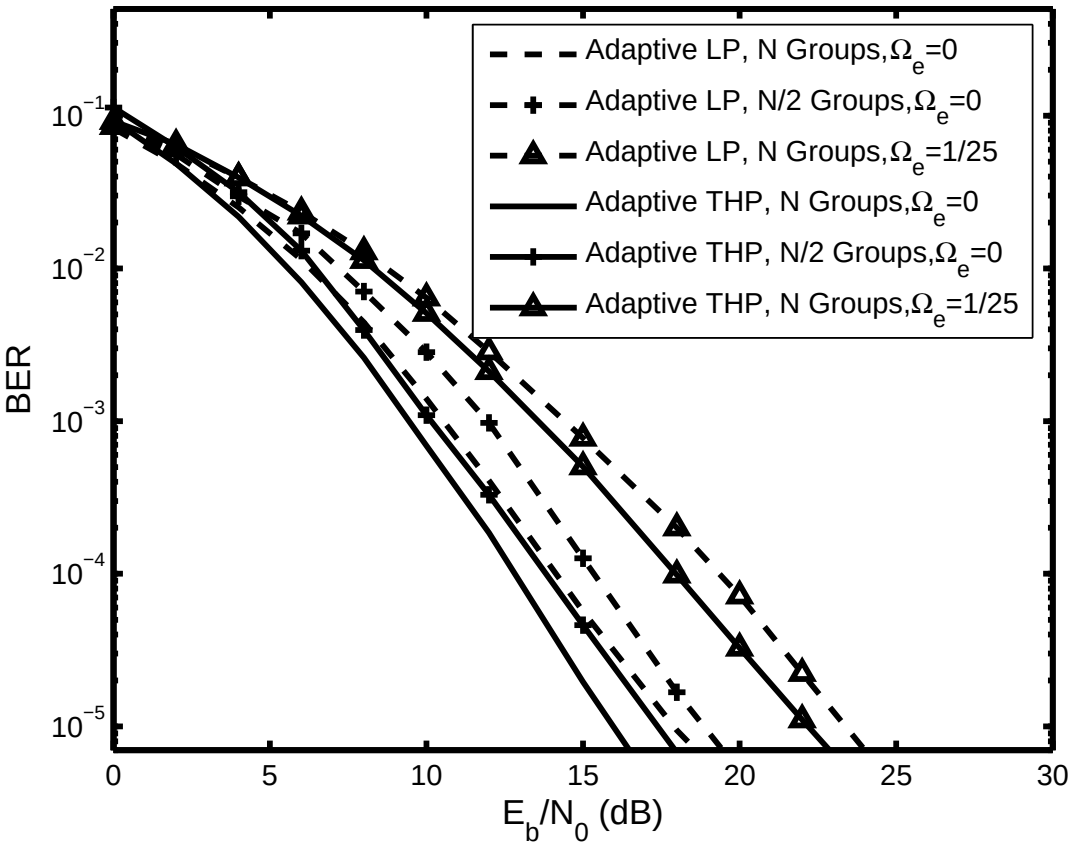

Figure 6.10: BER as a function of SNR for linear and non-linear adaptive precoding using the optimal switching criterion in 2×2 64-subcarrier OFDM systems over antenna and path-correlated channels with perfect and imperfect channel estimation. One or two subcarriers per group ($N_b = N$, $N_b = N/2$), $R = 4$ bits/s/Hz, $\zeta_T = 0.5$ and $p = 0.9$. Vehicular B channel is considered.

6.5 Summary

Covariance-based linear precoding and non-linear Tomlinson-Harashima precoding have been developed for a MIMO OFDM wireless link over transmit-antenna and path-correlated channels. The impact of path correlations on the PEP was analyzed. Closed-form, waterfilling-based linear and non-linear precoders that minimize the worst-case PEP in OSTBC OFDM are derived. An adaptive strategy that switches between precoded SM OFDM and precoded OSTBC OFDM has also been developed. For each subcarrier, the minimum Euclidean distance of the received codebook was used to select between SM and OSTBC. A lower complexity selection criterion was

also derived. To reduce the number of feedback bits, mode selection could be based on groups of neighboring subcarriers. Our proposed precoders significantly reduce the impact of antenna and path-correlated channels; non-linear precoders perform better than linear precoders. The adaptive strategy outperforms either SM or OSTBC individually in terms of the BER.

Chapter 7

Precoding for OSTBC OFDM Downlink: Mean or Covariance Feedback?

7.1 Introduction

This chapter considers precoding for MIMO OSTBC OFDM downlink, where both the conditional mean of the channel gain matrix (the first-order channel statistics) and the channel gain covariance matrix (the long-term/ second-order channel statistics) are available at the transmitter (these two cases are referred to as *mean-feedback* and *covariance precoding*, respectively). The application of the original OSTBC is constrained by insufficient antenna spacing at the transmitter, which leads to transmit-antenna correlations. Precoding which can optimize the MIMO transmission is thus needed to offer the original OSTBC the flexibility of adapting to correlated MIMO channels [47, 100, 101].

A typical precoding design needs either the channel covariance matrix [47, 101, 102] or full CSIT [50, 103–105]. CSIT thus can be an outdated (due to channel time variations) and imperfect (due to estimation and feedback errors) estimate. Given CSIT and channel statistics, the conditional mean of the actual channel gain matrix can be calculated, and used for mean-feedback precoding. On the other hand, since the channel covariance matrix is primarily determined by the antenna correlation, which can be readily evaluated at the transmitter, the feedback requirement for covariance precoding in Chapter 6 is much smaller than for mean-feedback precoding. Naturally,

the quality of mean-feedback precoding will be degraded due to estimation errors, and in general it is more sensitive to the channel time variations and feedback delay than covariance precoding. In contrast, covariance precoding may become less effective when mean feedback is accurate.

Mean-feedback precoders have been developed for OSTBC systems over an uncorrelated flat-fading MIMO channel in [50, 103] with the assumption of perfect CSIR or imperfect CSIT with additive estimation noise but no feedback delay. A more general model has not been considered yet. If mean feedback and channel covariance matrix are available, [104] studies precoding schemes designed to approach capacity in spatially-uncorrelated flat-fading MIMO channels and multiple-input single-output (MISO) OFDM downlink (each user has one receive antenna). However, from available results it is still not clear whether mean feedback could be helpful to reduce error rates. This paper aims to examine whether and when mean feedback is necessary to achieve a lower error rate when considering precoding strategies for a general OSTBC-OFDM system with channel estimation errors and feedback delay over a spatially-correlated frequency-selective fading MIMO channel. We assume that the long-term channel statistics, including the variance of the estimation error and feedback delay, are available at the transmitter. In the mean-feedback model, the complete channel matrix is sent back so that the transmitter can calculate the conditional mean of the actual channel matrix given the channel statistics. In the covariance precoding model, the channel covariance matrix is available at the transmitter; complete CSIT is not necessary.

7.1.1 Contributions

Precoders are developed to effectively exploit mean feedback and channel covariance for error-rate improvement in OSTBC MIMO OFDM downlink. Our contributions are summarized as follows:

1. *A general system model* is derived, in which the receiver imperfectly estimates CSI and sends the inaccurate estimates back to the transmitter via a feedback channel, which introduces delay. The conditional mean and covariance of the channel matrix are derived.

2. *Mean-feedback precoding* is proposed to maximize the SNR in a general OSTBC OFDM

system; SNR determines the error rate in OSTBC systems. Both linear precoding and non-linear THP are considered. The proposed precoders take into account the estimation errors and channel time variations over feedback delay and offer optimal power allocation. We confirm the intuition of the fundamental trade-off between mean-feedback and covariance precoding. As mean feedback becomes accurate, mean-feedback precoding can achieve a lower BER than covariance precoding considered in Chapter 6, i.e., mean feedback is helpful. Non-linear precoding is shown to outperform linear precoding.

3. *Adaptive dual-mode precoding* which switches between the proposed mean-feedback precoding and covariance precoding in Chapter 6 is also developed. The maximum achievable SNR is derived and used as the precoding-mode selection metric. The receiver calculates the metric and decides whether mean feedback is necessary or not. The decision is sent back to the transmitter using only one bit per subcarrier. Our adaptive precoding significantly reduces the required capacity of the feedback link since only the channel covariance matrix available at the transmitter is used when the channel conditions become severe, and it outperforms both mean-feedback and covariance precoding applied individually.

7.1.2 Organization

The remainder of this chapter is organized as follows. In Section 7.2, the system model of OSTBC OFDM with transmit-antenna correlations is briefly described. The model of mean feedback is introduced, and the conditional mean and variance of the channel matrix is derived. Section 7.3 proposes mean-feedback precoding. Both linear precoding and non-linear precoding are considered. covariance precoding is also reviewed. In Section 7.4, the maximum achievable SNRs are derived for both mean-feedback and covarianc precoding. The metric for switching between the two precoding modes is developed. Simulation results for proposed precoding are given in Section 7.5. Section 7.6 concludes the chapter.

7.2 System Model

This section will introduce the system model of an N-subcarrier OFDM downlink system with M_T transmit antennas and M_R receive antennas in the presence of transmit antenna correlations. The path correlation is not considered.

7.2.1 MIMO OFDM with Transmit-Antenna Correlations

At the time i, the set of the l-th path spatial gains can be represented by an $M_R \times M_T$ matrix $\mathbf{H}_{w,l}[i]$ with entries $h_{u,v,l}[i]$ which are i.i.d zero mean complex Gaussian random variables with unit variance. The sum of channel tap power gains is normalized to unity. Similar to (6.4), the $M_R \times M_T$ channel on the k-th subcarrier at the time i can be represented as [72]

$$\mathbf{H}[k,i] = \sum_{l=0}^{L-1} \mathbf{H}_{w,l}[i] e^{-\jmath \frac{2\pi}{N} kl} \mathbf{R}_T^{1/2}. \tag{7.1}$$

$\mathbf{R}_T$ is the transmit antenna correlation matrix with entries which are expressed by (3.20)

$$R_T(p,q) = \mathcal{J}_0\left(2\pi |p-q| \zeta_T\right), \tag{7.2}$$

where $\zeta_T = \Delta \frac{d_T}{\lambda_c}$. $\mathbf{R}_T = \mathbf{R}_T^H$.

At the receiver, the k-th received signal vector can thus be given by

$$\mathbf{Y}[k,i] = \mathbf{H}[k,i]\mathbf{X}[k,i] + \mathbf{W}[k,i]. \tag{7.3}$$

Stacking all the N received signal vectors, the $NM_R \times NM_T$ overall channel matrix is then

$$\mathbf{H}[i] = \text{diag}\left[\mathbf{H}[1,i] \ \ldots \ \mathbf{H}[N,i]\right]. \tag{7.4}$$

This chapter considers the structure described by (7.3), for which precoding can be designed individually for each subcarrier.

7.2.2 Models for Mean Feedback and Channel Covariance

Here we introduce general MIMO channel models accounting for imperfect channel estimates, multiplicative time-varying effects, and transmit-antenna correlations. The conditional mean and covariance of the channel matrix are derived by exploiting the channel statistics.

7.2.2.1 Channel Covariance Model

For simplicity, the sum of the channel tap power gains is normalized to unity. The channel gain matrix on the subcarrier k in (7.1) is assumed to be a zero-mean complex Gaussian matrix with autocovariance

$$\mathbf{C_{HH}}[k] = \mathrm{E}\left[\mathbf{H}^H[k,i]\mathbf{H}[k,i]\right] = \mathbf{R}_T. \tag{7.5}$$

Hence, the autocovariance matrix is independent of the subcarrier indexes. $\mathbf{R}_T$ is mainly dependent on the angle of arrival spread and antenna spacing, which are easily available at the transmitter. $\mathbf{C_{HH}}[k]$ can also be readily determined at the receiver from the channel estimates. Evaluation of $\mathbf{C_{HH}}[k]$ needs to be done very infrequently, because of the very low rate of change of $\mathbf{R}_T$.

7.2.2.2 Mean Feedback Model

In this model, the complete complex channel gain matrix is sent back to the transmitter and the transmitter calculates the conditional mean of the actual channel matrix given the channel statistics. It is called mean feedback in the rest of the chapter. The receiver has inaccurate estimates $\mathbf{H}_R[k,i]$ of the current actual, but unknown, channel gain matrix $\mathbf{H}[k,i]$. The imperfect estimates are sent to the transmitter via a feedback channel which introduces a delay τ. The transmitter thus has the inaccurate estimate $\mathbf{H}_T[k,i]$ of the actual (unknown) but outdated channel matrix $\mathbf{H}[k,i-\tau]$, which is τ seconds older than the current channel matrix $\mathbf{H}[k,i]$. The variance of the estimation error and feedback delay are available at both the transmitter and the mobile receiver.

The time-variant frequency-selective channel is modeled as follows:

- The entries in a tap gain vector for the $\{u,v\}$th antenna pair $\mathbf{h}_{u,v}[i] = \left[h_{u,v,0}[i],\ldots,h_{u,v,L-1}[i]\right]^T$

are time-varying according to Clarke's 2-D isotropic scattering model with maximum Doppler shift f_D [85]. Since $\mathbf{h}_{u,v}[i-\tau]$ is a delayed version of $\mathbf{h}_{u,v}[i]$, they are jointly Gaussian with an autocovariance matrix

$$\mathrm{E}\left[\mathbf{h}_{u,v}[i]\mathbf{h}_{u,v}^{H}[i-\tau]\right] = J\mathbf{R}_P, \tag{7.6}$$

where $\mathbf{R}_P = \mathrm{diag}\left[\sigma_0^2, \ldots, \sigma_{L-1}^2\right]$, $J = \mathcal{J}_0(2\pi\epsilon)$ is the normalized autocovariance and $\epsilon = f_D\tau$ is the normalized maximum Doppler shift with respect to the feedback delay τ. From (7.5) and by analogy to (7.6), the following covariance matrix can be obtained:

$$\mathbf{C}_T = \mathrm{E}\left[\mathbf{H}^H[k, i-\tau]\mathbf{H}[k,i]\right] = J\mathbf{R}_T. \tag{7.7}$$

- The channel estimates at the receiver can be expressed as

$$\mathbf{H}_R[k,i] = \mathbf{H}[k,i] + \mathbf{E}_{\text{err}}[k], \tag{7.8}$$

where $\mathbf{E}_{\text{err}}[k]$ is the estimation error matrix with i.i.d. entries $E_{u,v}[k] \sim \mathcal{CN}(0,\ \Omega_e)$, $\forall\, i,k$; $\mathbf{E}_{\text{err}}[k]$ is independent of all other stochastic processes. Therefore, the cross-covariance matrix of $\mathbf{H}[k,i]$ and $\mathbf{H}_R[k,i]$ can be shown as

$$\mathbf{C}_{\mathbf{H}\mathbf{H}_R} = \mathrm{E}\left[\mathbf{H}^H[k,i]\mathbf{H}_R[k,i]\right] = \mathbf{R}_T. \tag{7.9}$$

The channel matrix estimate $\mathbf{H}_T[k,i]$ available at the transmitter can be modeled by

$$\mathbf{H}_T[k,i] = \mathbf{H}_R[k,i-\tau] = \mathbf{H}[k,i-\tau] + \mathbf{E}_{\text{err}}[k]. \tag{7.10}$$

Obviously, $\mathbf{H}[k,i] \neq \mathbf{H}_T[k,i-\tau] \neq \mathbf{H}_R[k,i]$. The cross-covariance of $\mathbf{H}_T[k,i]$ and $\mathbf{H}_R[k,i]$ can be obtained similarly to (7.5), (7.6) and (7.7)

$$\begin{aligned} \mathbf{C}_{\mathbf{H}_T\mathbf{H}_R} &= J\mathbf{R}_T + \Omega_e\mathbf{I}_{M_T}; \\ \mathbf{C}_{\mathbf{H}_T\mathbf{H}} &= J\mathbf{R}_T. \end{aligned} \tag{7.11}$$

- Given $\mathbf{H}_T[k,i]$, the transmitter can obtain the conditional mean and covariance matrices of the user following the approach in [79, pp.324] as

$$\begin{aligned} \mathbf{H}_{\mathbf{H}|\mathbf{H}_T}[k,i] &= J\mathbf{H}_T[k,i]\left(\mathbf{R}_T + \Omega_e\mathbf{I}_{M_T}\right)^{-1}\mathbf{R}_T, \\ \mathbf{C}_{\mathbf{H}|\mathbf{H}_T} &= \mathbf{R}_T - J^2\mathbf{R}_T\left(\mathbf{R}_T + \Omega_e\mathbf{I}_{M_T}\right)^{-1}\mathbf{R}_T. \end{aligned} \tag{7.12}$$

A more detailed derivation of (7.12) can be found in the Appendix and [105]. Since the receiver has the information $\mathbf{H}_R[k, i-\tau] = \mathbf{H}_T[k, i]$, the conditional mean of the channel matrix at the transmitter $\mathbf{H}_T[k, i]$ can be calculated at both the transmitter and the receiver, and the variance is dependent on the correlation matrix $\mathbf{R}_T$. Similarly, given $\mathbf{H}_R[k, i]$, the conditional channel and covariance matrices can be obtained as

$$\begin{aligned} \mathbf{H}_{\mathbf{H}|\mathbf{H}_R}[k, i] &= \mathbf{H}_R[k, i] \left(\mathbf{R}_T + \Omega_e \mathbf{I}_{M_T}\right)^{-1} \mathbf{R}_T \\ \mathbf{C}_{\mathbf{H}|\mathbf{H}_R} &= \Omega_e \mathbf{R}_T \left(\mathbf{R}_T + \Omega_e \mathbf{I}_{M_T}\right)^{-1} \mathbf{R}_T. \end{aligned} \tag{7.13}$$

The conditional means $\mathbf{H}_{\mathbf{H}|\mathbf{H}_T}[k, i]$ and $\mathbf{H}_{\mathbf{H}|\mathbf{H}_R}[k, i]$ can be described as equivalent channels exploiting the channel statistics and uncertainty structure to mitigate the impact of imperfect CSI at the transmitter and the receivers [106, 107]. The conditional covariance matrices $\mathbf{C}_{\mathbf{H}|\mathbf{H}_T}$ and $\mathbf{C}_{\mathbf{H}|\mathbf{H}_R}$ indicate the CSIT and CSIR channel uncertainty given by the equivalent channels, respectively. Clearly, the CSIR uncertainty is determined by the transmit antenna correlation matrix and the estimation error. At the transmitter, beside $\mathbf{R}_T$ and estimation errors, the CSIT uncertainty also depends on the autocovariance J, which is the function of the normalized maximum Doppler shift. As the maximum Doppler shift increases, which may be caused by increasing velocity of the user, the mean-feedback uncertainty becomes significant.

7.3 Precoding with Mean Feedback and Channel Covariance

This section proposes mean-feedback precoding to maximize SNR in the general OSTBC OFDM system. By exploiting the conditional channel mean and covariance, our precoders take into account the channel uncertainty due to estimation errors and channel time variations. Both linear precoding and non-linear THP are presented. The THP structure is shown in Fig. 6.2.

7.3.1 Mean-Feedback Precoding

Here a general case with multiplicative time-varying effects and imperfect CSIR is considered. With the precoding matrix $\mathbf{E}_{\text{MF}}[k]$, the effective transmitted signal is $\mathbf{E}_{\text{MF}}[k]\mathbf{X}[k]$. For simplicity, the time index is omitted.

If the channel's mean and covariance matrices are available, given $\mathbf{H}_T[k,i]$ the transmitter can calculate $\mathbf{H}_{\mathbf{H}|\mathbf{H}_T}[k,i]$ of the actual channel matrix (7.12), and perform SVD, which yields $\mathbf{H}_{\mathbf{H}|\mathbf{H}_T}[k] = \widetilde{\mathbf{U}}[k]\widetilde{\mathbf{\Gamma}}[k]\widetilde{\mathbf{V}}^H[k]$. $\widetilde{\mathbf{U}}[k]$ and $\widetilde{\mathbf{V}}[k]$ are unitary matrices, and the diagonal singular value matrix $\widetilde{\mathbf{\Gamma}}[k]$ has real, non-negative entries. As in [103] and [46], a general form of the precoding matrix $\mathbf{E}_{\text{MF}}[k]$ can be given by

$$\mathbf{E}_{\text{MF}}[k] = \widetilde{\mathbf{V}}[k]\mathbf{\Lambda}_{\text{MF}}[k]\widetilde{\mathbf{V}}^H[k], \tag{7.14}$$

where $\mathbf{\Lambda}_{\text{MF}}[k]$ is an $M_T \times M_T$ diagonal matrix representing the power distribution with the main diagonal entries. In OSTBC systems, the minimum SNR (which should be maximized) determines the BER performance. With precoding (7.14), the SNR on the k-th subcarrier in OSTBC OFDM can be given by [99]

$$\text{SNR}_{\text{MF}}[k] = \frac{E_s}{\sigma_W^2}\text{E}\left[\text{tr}\left(\mathbf{\Lambda}_{\text{MF}}^H[k]\widetilde{\mathbf{V}}^H[k]\mathbf{H}^H[k]\mathbf{H}[k]\widetilde{\mathbf{V}}[k]\mathbf{\Lambda}_{\text{MF}}[k]\right)\right], \tag{7.15}$$

where E_s is the average energy of the transmitted symbols; $\text{tr}(\cdot)$ denotes the trace of a matrix. Since the actual channel has the conditional mean $\mathbf{H}_{\mathbf{H}|\mathbf{H}_T}[k]$ and covariance $\mathbf{C}_{\mathbf{H}|\mathbf{H}_T}$ as shown in (7.12), the error-rate minimization problem becomes

$$\mathbf{\Lambda}_{\text{MF}}[k]_{\text{opt}} = \arg\max_{\mathbf{\Lambda}_{\text{MF}}[k]} \text{tr}\left[\mathbf{\Lambda}_{\text{MF}}^H[k]\widetilde{\mathbf{V}}^H[k]\left(\mathbf{H}_{\mathbf{H}|\mathbf{H}_T}^H[k]\mathbf{H}_{\mathbf{H}|\mathbf{H}_T}[k] + \mathbf{C}_{\mathbf{H}|\mathbf{H}_T}\right)\widetilde{\mathbf{V}}[k]\mathbf{\Lambda}_{\text{MF}}[k]\right], \tag{7.16}$$

subject to $\text{tr}\left(\mathbf{E}_{\text{MF}}^H[k]\mathbf{E}_{\text{MF}}[k]\right) = \text{tr}\left(\mathbf{\Lambda}_{\text{MF}}^2[k]\right) = M_T$, which is a normalization condition guaranteeing that precoding will not increase the transmitted power. The function in (7.16) is linear and therefore it is concave in $\mathbf{\Lambda}_{\text{MF}}[k]$. The objective of (7.16) is to find the power allocation $\mathbf{\Lambda}_{\text{MF}}[k]$ that maximizes the SNR. This maximum SNR will depend on the quality of the conditional mean $\mathbf{H}_T[k]$. As $\mathbf{H}_T[k]$ approaches the actual channel matrix $\mathbf{H}[k]$, $\widetilde{\mathbf{V}}[k]$ approaches $\mathbf{V}[k]$ (the right unitary matrix from the SVD of the actual channel matrix) and $\mathbf{\Lambda}_{\text{MF}}[k]$ is primarily determined by the singular values of the channel matrix. The optimization problem of (7.16) can be solved numerically or analytically. Furthermore, it has been shown that for some specific uncertainties, the problem can be simplified and closed-form solutions exist [50, 103]. Several software packages

are available including *optimization toolbox* in MATLAB. For example, the function *fmincon* can be used, which offers efficient computation within a polynomial time.

7.3.2 Non-Linear Tomlinson-Harashima Precoding

Mean-feedback THP is proposed for SNR maximization in OSTBC MIMO OFDM downlink. Ignoring the modulo device, the user's feedback structure is equivalent to $\mathbf{B}^{-1}[k]$, which can be optimally designed as in (7.16), $\mathbf{B}[k]_{\text{opt}} = \mathbf{E}_{\text{MF}}^{-1}[k]_{\text{opt}}$. The effective channel is $\mathbf{H}[k]\mathbf{E}_{\text{MF}}[k]$ and ML decoding is used at the receiver.

7.3.3 Covariance Precoding

When mean feedback is not available, the transmitter knows only the channel covariance matrix (7.5). The PEP optimal covariance precoding introduced in Chapter 6 has the following form

$$\mathbf{E}_{\text{CP}_{\text{opt}}} = \mathbf{V}_T \mathbf{\Lambda}_{\text{CP}} \mathbf{V}_T^H, \tag{7.17}$$

where $\mathbf{V}_T$ is the right $M_T \times M_T$ unitary matrix from SVD of the transmit-antenna correlation matrix $\mathbf{R}_T$. The optimal $\mathbf{\Lambda}_{\text{CP}}$ can be found as discussed in Chapter 6.

The precoding design, involving either mean-feedback (7.16) or covariance precoding (7.17), aims to minimize the system error rate, which is determined by SNR in OSTBC systems. Mean-feedback precoding requires a high capacity feedback link, and is more sensitive to the channel time variations and feedback delay. On the other hand, covariance precoding is a one-size-fits-all solution which does not reflect the instantaneous and varying channel conditions. Covariance precoding thus becomes less helpful when mean feedback can be accurate. Naturally, the quality of the mean and covariance matrices used in precoding determines the achievable error probability.

7.4 Mean-Feedback Precoding or Covariance Precoding?

This section develops adaptive precoding which switches between mean-feedback (7.16) and covariance precoding (7.17). The maximum achievable SNR in both cases of (7.16) and (7.17) is

derived. The SNRs are calculated at the receiver and used as the selection metric, according to which the precoding mode is chosen.

7.4.1 Maximum Achievable SNR

In a precoded OSTBC system, the maximized SNR on k-th subcarrier can be given by

$$\text{SNR}[k] = \frac{E_s}{\sigma_W^2}\text{E}\left[\text{tr}\left(\mathbf{H}^H[k]\mathbf{H}[k]\right)\right] = \frac{E_s}{\sigma_W^2}\text{tr}\left[\mathbf{E}_{\text{opt}}^H\left(\mathbf{H}_{\mathbf{H}|\mathbf{H}_T}^H[k]\mathbf{H}_{\mathbf{H}|\mathbf{H}_T}[k] + \mathbf{C}_{\mathbf{H}|\mathbf{H}_T}\right)\mathbf{E}_{\text{opt}}\right]. \quad (7.18)$$

If only the channel covariance matrix is available, $\mathbf{C}_{\mathbf{H}|\mathbf{H}_T} = \mathbf{C}_{\mathbf{HH}}$ and the conditional mean is an all-zero matrix. The SNR is then

$$\text{SNR}_{\text{CP}} = \frac{E_s}{\sigma_W^2}\text{tr}\left(\mathbf{E}_{\text{CP}_{\text{opt}}}^H\mathbf{C}_{\mathbf{HH}}\mathbf{E}_{\text{CP}_{\text{opt}}}\right). \quad (7.19)$$

Substituting the covariance from (7.5) and the precoding matrix (7.17) into (7.19), the SNR of a covariance precoded system is identical for all subcarriers, and becomes

$$\text{SNR}_{\text{CP}} = \frac{E_s}{\xi\sigma_W^2}\text{tr}\left(\mathbf{V}_T\mathbf{\Lambda}_{\text{CP}}\mathbf{V}_T^H\mathbf{R}_T\mathbf{V}_T\mathbf{\Lambda}_{\text{CP}}\mathbf{V}_T^H\right) = \frac{E_s}{\xi\sigma_W^2}\text{tr}\left(\mathbf{\Gamma}_T^2\mathbf{\Lambda}_{\text{CP}}^2\right), \quad (7.20)$$

where $\mathbf{R}_T = \mathbf{V}_T\mathbf{\Gamma}_T^2\mathbf{V}_T^H$. Clearly, the SNR of covariance precoded OSTBC OFDM is independent of the index of subcarriers and the channel time variations. Different users will have identical SNRs.

When mean feedback is available, the transmitter can calculate the equivalent channel matrix $\mathbf{H}_{\mathbf{H}|\mathbf{H}_T}[k]$ and the SNR becomes

$$\text{SNR}_{\text{MF}}[k] = \frac{E_s}{\sigma_W^2}\text{tr}\left(\mathbf{E}_{\text{MF}}^H[k]_{\text{opt}}\left(\mathbf{H}_{\mathbf{H}|\mathbf{H}_T}^H[k]\mathbf{H}_{\mathbf{H}|\mathbf{H}_T}[k] + \mathbf{C}_{\mathbf{H}|\mathbf{H}_T}\right)\mathbf{E}_{\text{MF}}[k]_{\text{opt}}\right). \quad (7.21)$$

Substituting (7.12) into (7.21), we have

$$\begin{aligned}
&\text{SNR}_{\text{MF}}[k] \\
&= \frac{E_s}{\sigma_W^2}\text{tr}\left(J^2\mathbf{E}_{\text{MF}}^H[k]_{\text{opt}}\mathbf{R}_T\left(\mathbf{R}_T + \Omega_e\mathbf{I}_{M_T}\right)^{-1}\mathbf{H}_T^H[k]\mathbf{H}_T[k]\mathbf{R}_T\left(\mathbf{R}_T + \Omega_e\mathbf{I}_{M_T}\right)^{-1}\mathbf{E}_{\text{MF}}[k]_{\text{opt}}\right) \\
&+ \frac{E_s}{\sigma_W^2}\text{tr}\left(\mathbf{E}_{\text{MF}}^H[k]_{\text{opt}}\mathbf{R}_T\left(\mathbf{R}_T + \Omega_e\mathbf{I}_{M_T}\right)^{-1}\left((1-J^2)\mathbf{R}_T + \Omega_e\mathbf{I}_{M_T}\right)\mathbf{E}_{\text{MF}}[k]_{\text{opt}}\right).
\end{aligned} \quad (7.22)$$

The SNR for a mean-feedback precoded OSTBC system is a function of J. The precoding matrix (7.16) is determined by $\mathbf{H}_T[k]$ and $\mathbf{R}_T$ in (7.12), whose accuracy is dominated by J and Ω_e. SNR in (7.21) is sensitive to the channel estimation errors and channel variations.

7.4.2 When to Use Mean Feedback

The SNRs are used as an indicator of the accuracy needed for mean feedback to give a lower BER than covariance precoding. The accuracy of mean feedback can be gauged by its correlation with the actual channel matrix, which primarily depends on the normalized autocovariance J and estimation errors Ω_e. There may exist certain values of J and Ω_e such that for some channel realizations, the SNR of mean-feedback precoded systems given by (7.21) is greater than the SNR of covariance precoded systems given by (7.19), i.e., mean feedback is helpful to achieve a lower BER.

The mean-feedback precoding on the subcarrier k will outperform covariance precoding if

$$\text{SNR}_{\text{MF}}[k] > \text{SNR}_{\text{CP}}. \tag{7.23}$$

A simple case of perfect CSIR is first considered, i.e., the estimate error $\Omega_e = 0, \forall\, u$. The mean and variance of the actual channel are thus simplified to

$$\mathbf{H}_{\mathbf{H}|\mathbf{H}_T}[k] = J\mathbf{H}_T[k], \;\; \mathbf{C}_{\mathbf{H}|\mathbf{H}_T} = (1-J^2)\mathbf{R}_T. \tag{7.24}$$

Since from (7.14) $\mathbf{E}_{\text{MF}}[k]_{\text{opt}} = \widetilde{\mathbf{V}}[k]\mathbf{\Lambda}_{\text{MF}}[k]\widetilde{\mathbf{V}}^H[k]$ and $\mathbf{H}_T^H[k]\mathbf{H}_T[k] = \widetilde{\mathbf{V}}[k]\widetilde{\mathbf{\Gamma}}^2[k]\widetilde{\mathbf{V}}^H[k]$, we have

$$\begin{aligned} \text{SNR}_{\text{CP}} &= \frac{E_s}{\xi\sigma_W^2}\text{tr}\left(\mathbf{\Gamma}_T^2\mathbf{\Lambda}_{\text{CP}}^2\right) = \frac{E_s}{\xi\sigma_W^2}\sum_{m=1}^{M_T}\gamma_{T_m}^2\lambda_{\text{CP}_m}^2, \\ \text{SNR}_{\text{MF}}[k] &= \frac{E_s}{\sigma_W^2}\left[J^2\text{tr}\left(\mathbf{\Lambda}_{\text{MF}}^2[k]\widetilde{\mathbf{\Gamma}}^2[k]\right) + (1-J^2)\text{tr}\left(\mathbf{\Lambda}_{\text{MF}}[k]\widetilde{\mathbf{V}}^H[k]\mathbf{R}_T\widetilde{\mathbf{V}}[k]\mathbf{\Lambda}_{\text{MF}}[k]\right)\right]. \end{aligned} \tag{7.25}$$

Eq. (7.23) can now be simplified to

$$f - c < J^2(b-c), \tag{7.26}$$

with $f = \frac{1}{\xi}\sum_{m=1}^{M_T}\gamma_{T_m}^2\lambda_{\text{CP}_m}^2$, $b = \text{tr}\left(\mathbf{\Lambda}_{\text{MF}}^2[k]\widetilde{\mathbf{\Gamma}}^2[k]\right)$, and $c = \text{tr}\left(\mathbf{\Lambda}_{\text{MF}}[k]\widetilde{\mathbf{V}}^H[k]\mathbf{R}_T\widetilde{\mathbf{V}}[k]\mathbf{\Lambda}_{\text{MF}}[k]\right)$.

The mode selection inequality (7.23) is the selection criterion used by our proposed adaptive precoding scheme. The inequality depends on J and Ω_e, indicating when mean feedback has better performance. The receiver calculates (7.19) and (7.21), and adaptively selects the precoding mode which achieves a higher SNR. The same selection criterion is used for non-linear precoding. The decision is sent back to the transmitter; one bit per subcarrier is required. The transmitter allows different subcarriers to use different precoding modes. In an OFDMA system, different subcarriers may be assigned to different users, and suffer from different channel conditions. When the channel time variation is fast or the channel conditions are poor, covariance precoding may outperform mean-feedback precoding. The channel information then does not need to be sent back to the transmitter, which significantly reduces the feedback requirements. If mean feedback can be accurate, mean-feedback precoding may offer a higher SNR. The receiver can thus use mean feedback to achieve a lower error rate.

To further reduce the feedback load, subcarrier grouping with interpolation can be introduced. Higher-order interpolation design will lead to a better performance, but is more complex. There is a trade-off among complexity, performance, and the feedback load. It thus remains a future research topic to develop a simpler mode switching metric.

7.5 Simulation Results

This section presents simulation results to show how our proposed precoders improve the system performance in a 64-subcarrier OSTBC MIMO OFDM system with transmit-antenna correlations. The vehicular B channel specified by ITU-R M. 1225 [73] is used. ML decoding is used at the receiver. The BS and the user terminals know the correlation matrix $\mathbf{R}_T$ with the correlation parameter $\zeta_T = \Delta\frac{d_T}{\lambda}$; the angle of arrival spread is assumed 12°, i.e., $\Delta \approx 0.2$.

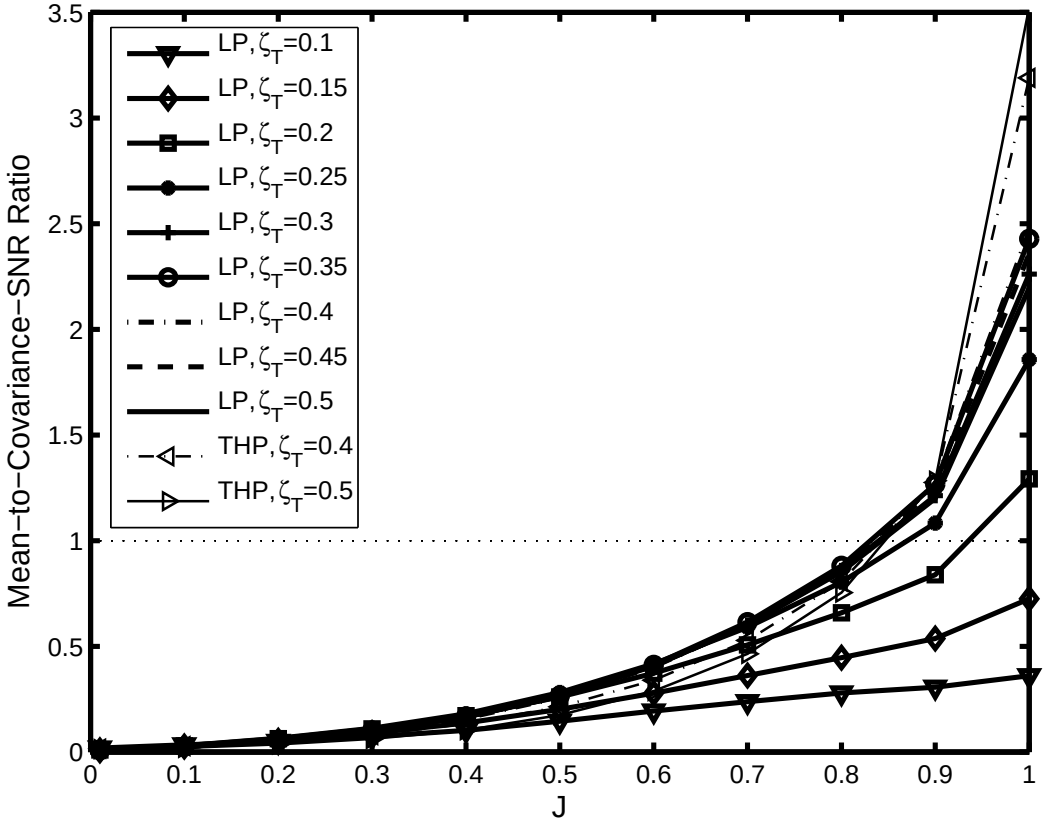

Figure 7.1: The mean-feedback SNR to covariance SNR ratio with linear precoding (LP) and THP as a function of the normalized autocovariance for 2×2 4-QAM Alamouti-coded 64-subcarrier MIMO OFDM systems over transmit-antenna-correlated channels with different values of ζ_T; $\Omega_e = 0$.

7.5.1 Maximum Achievable SNR

Fig. 7.1 compares the maximum achievable SNR of mean-feedback precoding and covariance precoding in Alamouti-coded OFDM systems. We considered 2 receive antennas and perfect CSIR, i.e., $J = \mathcal{J}_0(2\pi\epsilon)$, $\Omega_e = 0$. The mean-feedback SNR to covariance SNR ratio (MCSR) is used to show the gain that mean feedback can obtain over covariance precoding. Clearly, as $\mathcal{J}_0$ increases with decreasing user's speed, the MCSR monotonously increases. On the other hand, as the correlation parameter ζ_T increases, i.e., the transmit-antenna correlations weaken, the MCSR also increases. When ζ_T is greater than 0.2 and J is greater than 0.8, the value of MCSR is larger than

1, i.e., the proposed mean-feedback precoding achieves a higher SNR than covariance precoding. This tells us that in this case, mean feedback is sufficiently accurate to have a lower error rate. Furthermore, THP performs better than linear precoding.

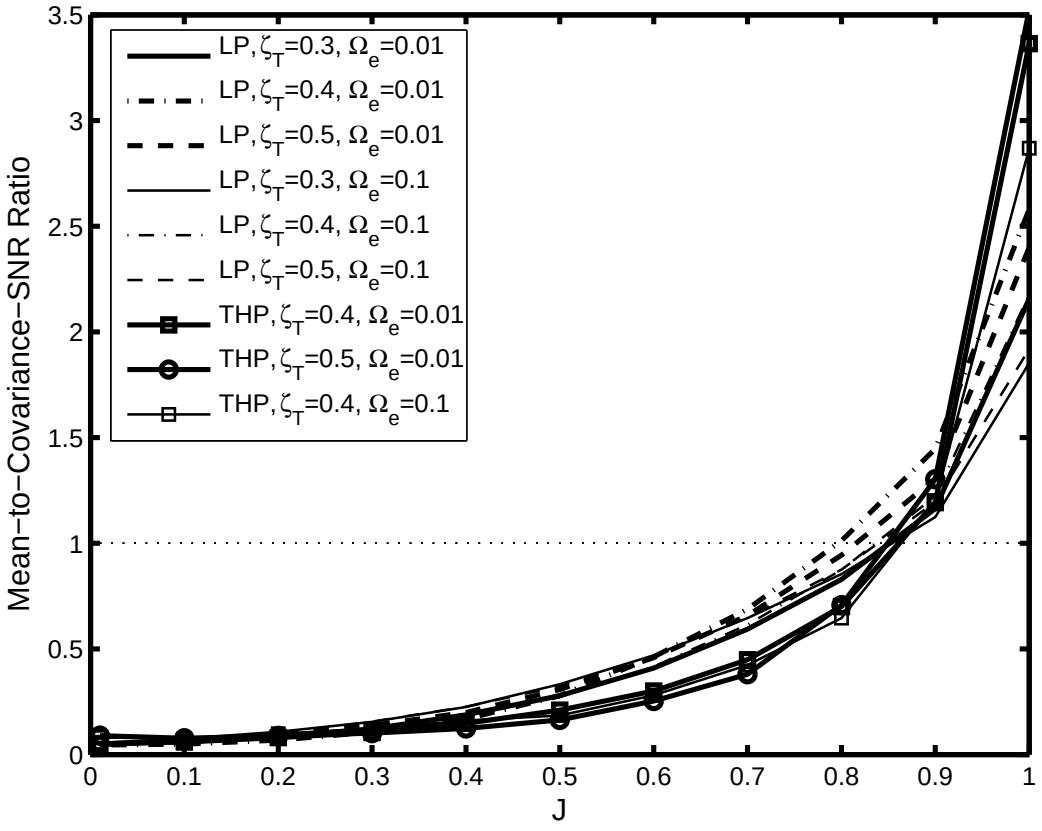

Figure 7.2: The mean-feedback SNR to covariance SNR ratio with linear precoding (LP) and THP as a function of the normalized autocovariance for 2×2 4-QAM Alamouti-coded 64-subcarrier MIMO OFDM systems over transmit-antenna-correlated channels with different values of ζ_T, $\Omega_e = 0.01$ and $\Omega_e = 0.1$.

Fig. 7.2 assumes that the variances of the estimation error are 0.1 and 0.01. As the variance becomes large, the gain of mean-feedback precoding over covariance precoding decreases. The values in Fig. 7.1 and 7.2 are comparable, i.e., the reasonable estimation errors do not have a significant impact on the SNR gain that mean feedback can achieve.

7.5.2 BER Performance

The interval $\mathcal{I} = [0.9, 1]$ is considered for the normalized autocovariance J, and the values are assumed to be uniformly distributed in this interval. In the interval $\mathcal{I} = [0.9, 1]$, the Doppler shifts $\epsilon = f_{D_u}\tau$ normalized with respect to feedback delays τ are in the range $[0, 0.1]$. This range of normalized Doppler shifts corresponds to the range of mobile velocities from zero to 216 km/h (at 5 GHz carrier frequency and $100\,\mu s$ feedback delay).

7.5.2.1 Mean-Feedback Precoding

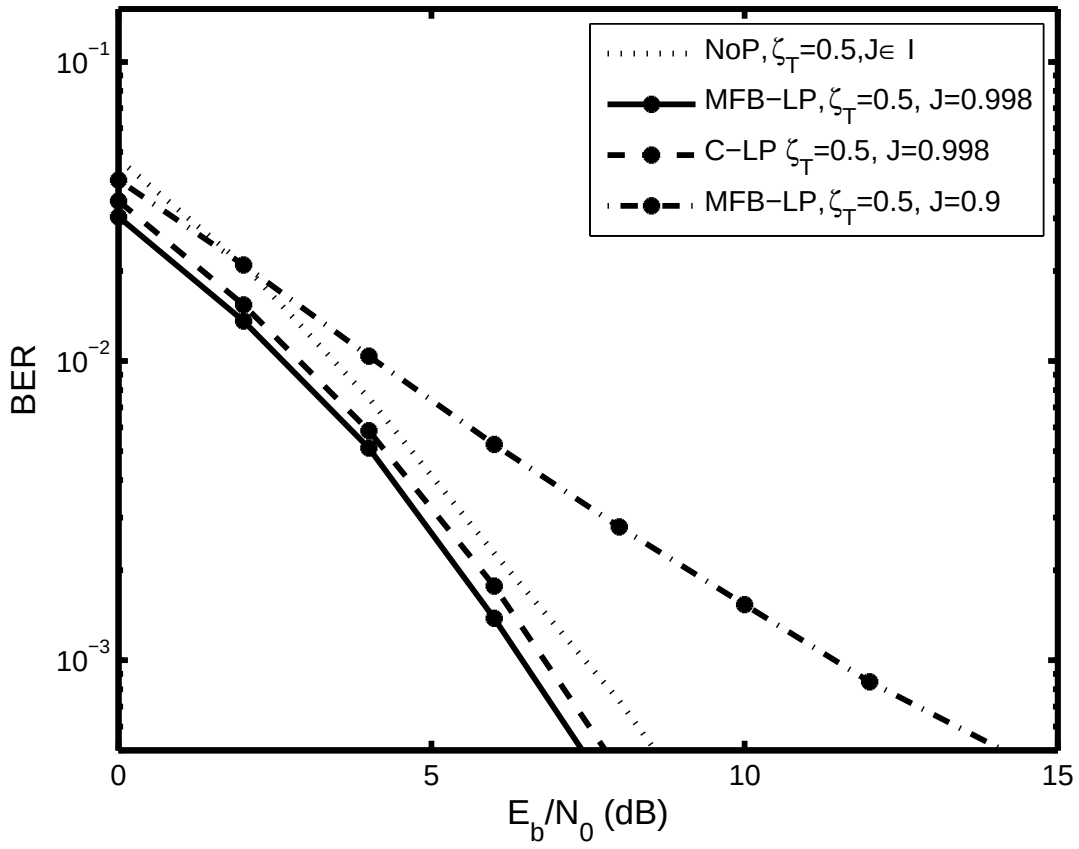

Figure 7.3: BER as a function of SNR for mean-feedback linear precoding (MFB-LP), covariance linear precoding (C-LP) and no precoding (NoP) in 64-subcarrier 4-QAM Alamouti-coded 2×2 OFDM systems with perfect feedback., $J \in \mathbb{I}$ and $J = 0.9$ and $J = 0.998$.

Fig. 7.3 shows the BERs of the proposed mean-feedback linear precoding (MFB-LP) in

Alamouti-coded 2×2 OFDM with perfect channel estimation. The normalized autocovariances J of 0.9 and 0.998 are considered. BER of the covariance linear precoding (C-LP) proposed in Chapter 6 is shown for reference. When the user is moving at the speed of 30 km/h ($J = 0.998$), the user's speed is around 30km/h (assuming 5 GHz carrier frequency and $\tau = 100\,\mu s$, as before). The value of J decreases as the speed increases. The proposed mean-feedback precoder offers a 0.4 dB gain over covariance precoding at the BER of 10^{-3}. Clearly, as CSIT becomes more accurate, mean-feedback precoding outperforms covariance precoding. The BER increases with decreasing J. At J of 0.9, the BER of mean-feedback precoding increases drastically, i.e., covariance precoding is more suitable in this case.

Fig. 7.4 shows the performance of our proposed mean-feedback linear precoding (MFB-LP), mean-feedback THP (MFB-THP) and the impact of imperfect channel estimation. 4-QAM Alamouti-coded 2×2 OFDM is considered. The variance of the channel estimation error Ω_e is $1/16$. Our MFB-THP outperforms the no-precoding case even if the channel's time-variation range is as high as $[0.9, 1]$. Clearly, non-linear precoding outperforms linear precoding. At a BER of 10^{-3}, covariance THP has 0.6 dB gain over covariance LP, and MFB-THP has about 1.2 dB gain over MFB-LP.

Fig. 7.5 shows the impact of the number of transmit antennas on the proposed mean-feedback precoding. We consider 16-QAM $1/2$-rate-OSTBC 4×2 OFDM and 4-QAM full-rate OSTBC 2x2 OFDM systems when the antenna correlation coefficient ζ_T is 0.3. Clearly, Fig. 7.5 confirms the intuition that a large number of transmit antennas improves the BER in the high SNR region and increases robustness against the channel estimation errors. Once again, non-linear THP outperforms linear precoding, in both perfect and imperfect CSIR cases.

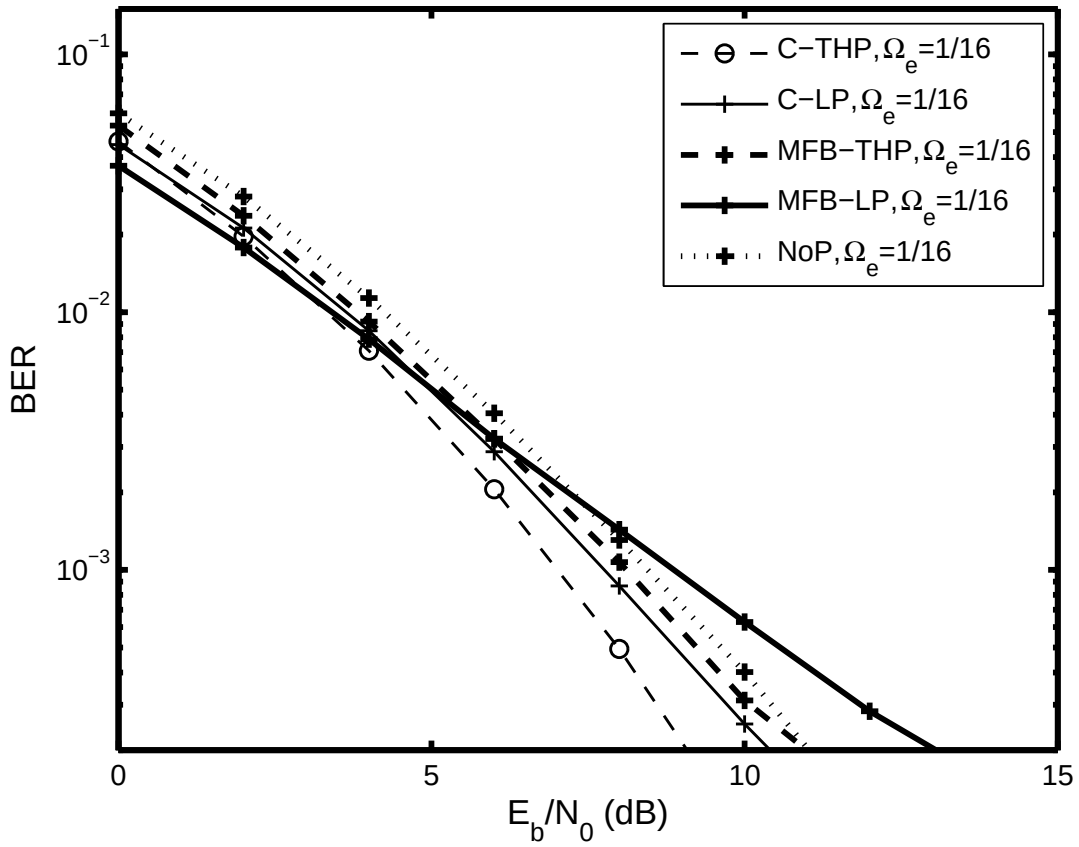

Figure 7.4: BER as a function of SNR for mean-feedback linear precoding (MFB-LP), MFB-THP, covariance linear precoding (C-LP), C-THP and no precoding (NoP) in 64-subcarrier 4-QAM Alamouti-coded 2×2 OFDM systems with perfect and imperfect channel estimation. $\zeta_T = \Delta\frac{d_T}{\lambda_c} = 0.4$, $J \in \mathbb{I}$.

7.5.2.2 Adaptive Precoding

This subsection now shows how our new adaptive precoding improves the BER in OSTBC OFDM with transmit-antenna correlations and imperfect channel estimation. Fig. 7.6 shows the BERs of the proposed adaptive linear precoder for 4-QAM Alamouti-coded 2×2 OFDM when the correlation parameter ζ_T is 0.5. Perfect CSIR is considered. Adaptive precoding switches between the mean-feedback and covariance precoding modes, which offers additional selection diversity. As a result, it achieves almost 1.5 dB improvement over covariance precoding. Also, adaptive precoding eliminates error floors at a BER of 10^{-4} present with mean-feedback precoding.

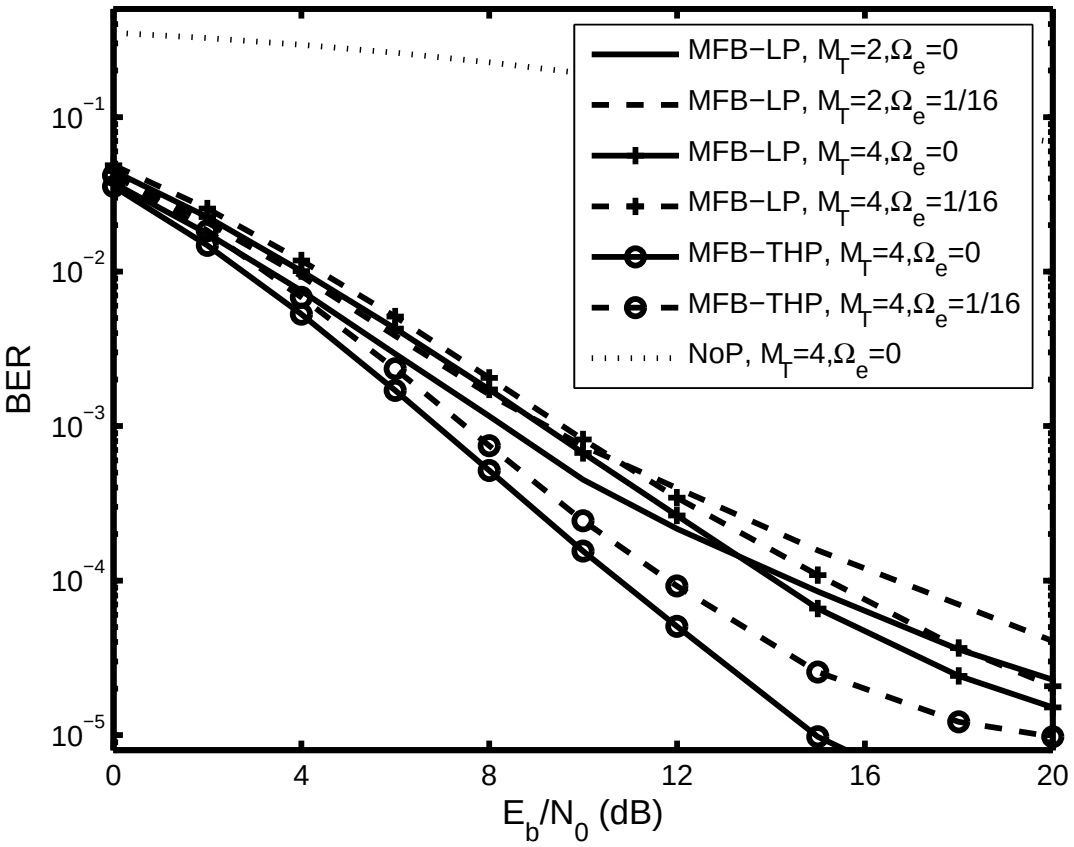

Figure 7.5: BER as a function of SNR for mean-feedback linear precoding (MFB-LP), MFB-THP and no precoding (NoP) in 64-subcarrier 16-QAM $1/2$-rate-OSTBC OFDM and 4-QAM Alamouti-coded OFDM systems with perfect and imperfect channel estimation. $\zeta_T = \Delta\frac{d_T}{\lambda_c} = 0.3$, $M_R = 2$, $J \in \mathbb{I}$.

Fig. 7.7 shows the BERs of our proposed adaptive THP in 16-QAM $1/2$-rate OSTBC 4-transmit-antenna OFDM with perfect and imperfect CSIR when ζ_T is 0.4. Adaptive precoding individually outperforms MFB-THP and C-THP for both perfect and imperfect channel estimation cases; non-linear THP outperforms linear precoding.

7.6 Summary

For a general transmit-antenna-correlated, frequency-selective fading MIMO channel model in an OSTBC OFDM downlink system with estimation errors and feedback delay, the conditional mean

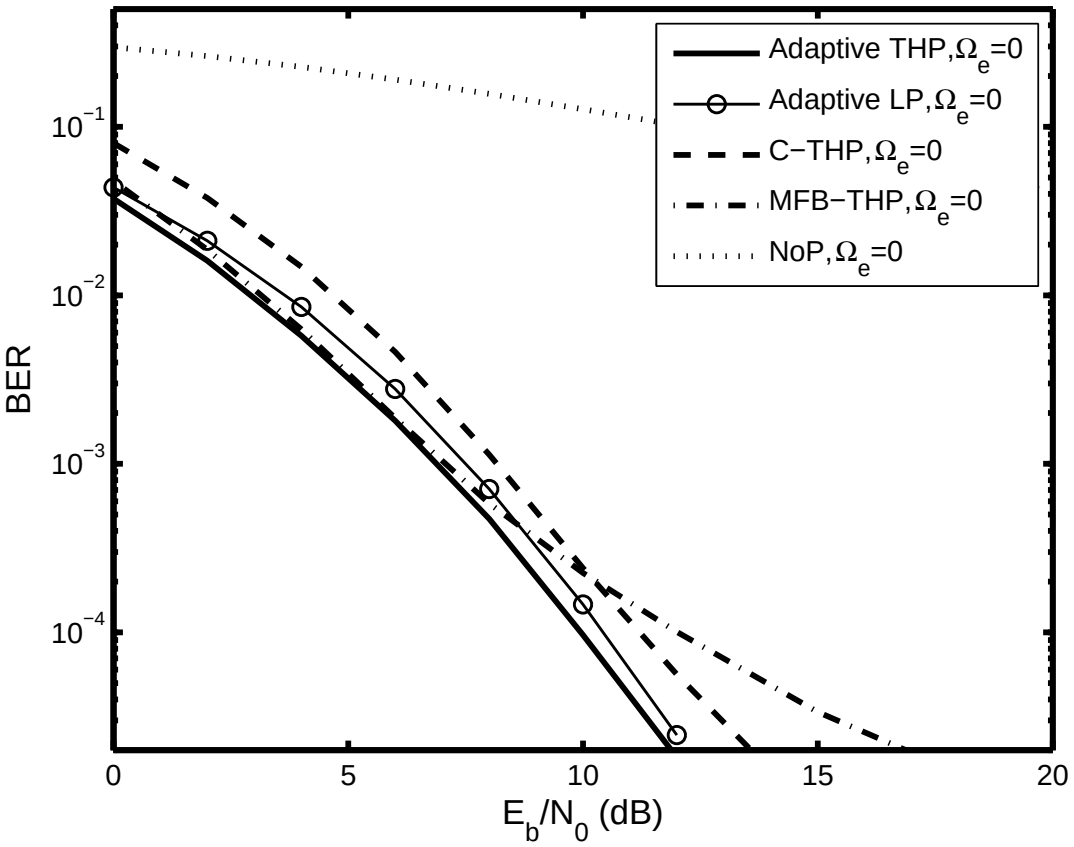

Figure 7.6: BER as a function of SNR for mean-feedback THP (MFB-THP), covariance THP (C-THP), adaptive LP and THP, and no precoding (NoP) in a 64-subcarrier 4-QAM Alamouti-coded 2×2 OFDM system. $\zeta_T = \Delta \frac{d_T}{\lambda_c} = 0.5$, $J \in \mathbb{I}$.

and covariance of the channel matrix have been derived. SNR-maximizing mean-feedback precoding has been proposed. Adaptive dual-mode precoding is also proposed, in which either new mean-feedback precoding or covariance precoding is adaptively chosen at the receiver according to the channel conditions. The receiver calculates the precoding-mode switching metric and decides whether mean feedback is necessary. We have confirmed the intuition that if mean feedback is sufficiently accurate, it improves the system performance. The proposed precoders, both the mean-feedback precoder and the dual-mode precoder, reduce the error rate. Adaptive precoding outperforms both mean-feedback precoding and covariance precoding individually applied.

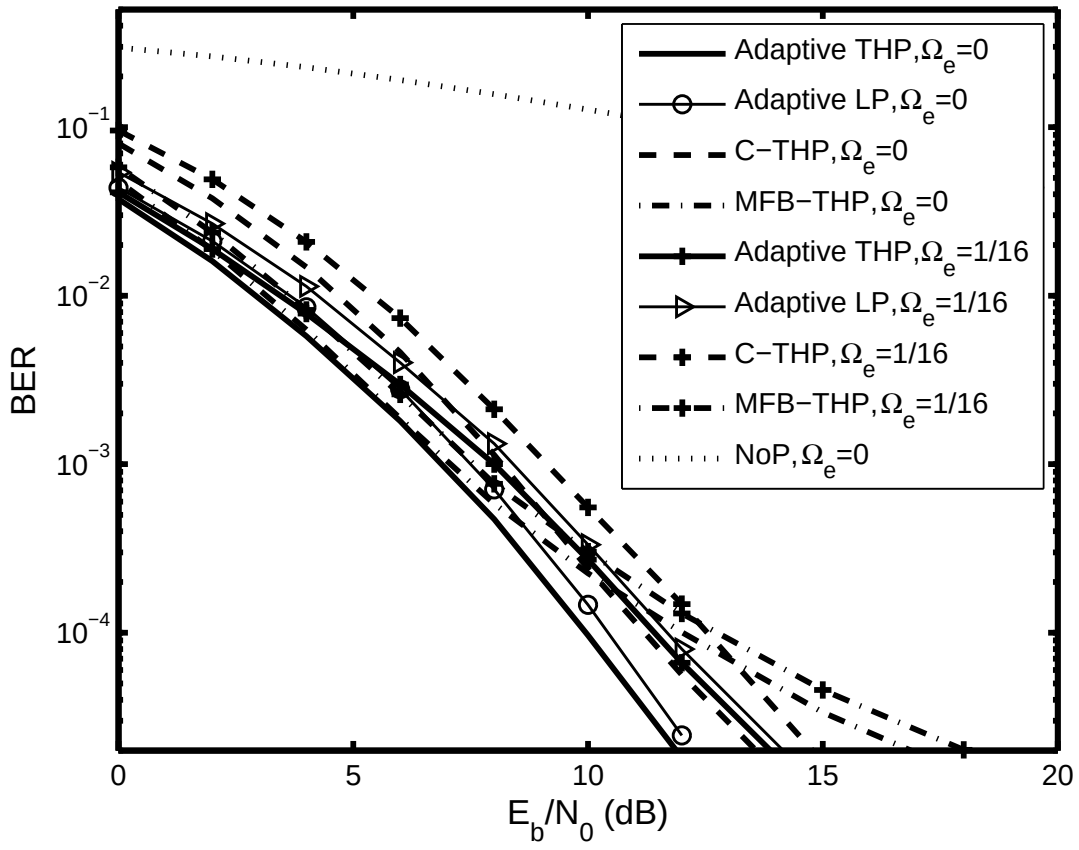

Figure 7.7: BER as a function of SNR for mean-feedback THP (MFB-THP), covariance THP (C-THP), adaptive non-linear precoding, adaptive linear precoding and no precoding (NoP) in 64-subcarrier 16-QAM $1/2$-rate OSTBC 4×2 OFDM systems with perfect and imperfect channel estimation. $\zeta_T = 0.4$, $J \in \mathcal{I}$.

Chapter 8

Conclusions and Future Work

8.1 Conclusions and Summary of Contributions

In this thesis, we have developed transmitter precoding schemes to mitigate ICI in closed-loop MIMO OFDM and multiuser MIMO OFDM downlink. We have also proposed precoders to reduce BER in MIMO OFDM systems with spatial correlations.

In Chapter 3, ICI reduction in closed-loop MIMO OFDM has been studied. A non-linear TH precoder has been proposed for closed-loop MIMO OFDM with frequency offsets. It has been shown that the ICI coefficient matrix is approximately unitary. Exploiting this property, the proposed TH precoder only needs partial CSI, channel gain matrix, at the transmitter. The knowledge of frequency offset hence does not need to be fed back to the transmitter, which reduces the feedback load and avoids possible frequency-offset transmitter mismatch. The proposed THP-OFDM significantly reduces the BER increase due to frequency offset. In addition, it has been shown that proposed THP also works well for spatially-correlated MIMO channels.

In multiuser OFDM downlink, if only post-processing techniques are used at each user's receiver to reduce MUI due to spatial multiplexing, the processing at the user level can hence be quite complex or even impossible. On the other hand, since the users are decentralized, the application of only transmitter precoding for ICI and MUI mitigation, which requires full CSI at the BS, is problematic. Chapter 4 has thus proposed two-stage transmitter/receiver processing to reduce ICI and MUI in downlink multiuser OFDM with multiple transmit antennas. The first stage

employs a TH precoder at the BS to mitigate multiuser interference in a spatial MIMO channel. The second stage applies a low-complexity linear MMSE equalizer to suppress ICI and MUI due to frequency offset at each user's receiver. The MMSE equalizer has low complexity due to the unitary property of the ICI matrix. Our proposed equalizer significantly reduces the BER increase due to frequency offset. Sending frequency offset information to the BS does not offer additional BER improvement.

In the previous two chapters, to apply precoding channel gains are needed at the transmitter. Chapter 5 has developed a LFB-TH precoder for closed-loop multiuser MIMO OFDM with frequency offset. Frequency offsets have been shown to have no impact on precoding, and hence precoding on per-subcarrier basis is possible. The limited-feedback codebook design algorithm is proposed, and the precoding matrix selection criteria are derived. With the limited-feedback feature, the precoding matrix is determined at the receiver, i.e., the CSI is not required at the transmitter. Since only a limited number of bits needs to be fed back, a low feedback rate can be maintained, which is desired for closed-loop system design. The proposed LFB-THP significantly reduces the BER degradation due to frequency offset in SM systems, OSTBC systems, and OFDM with spatial correlations.

MIMO OFDM systems are also constrained by limited antenna spacing, which may lead to correlations among antennas. The antenna correlation always reduces the system data rate and increases the error rate. Furthermore, the original space-time MIMO techniques have poor performance if they are directly employed over antenna-correlated channels. In Chapter 6, covariance-based linear precoding and non-linear Tomlinson-Harashima precoding have been developed for a MIMO OFDM wireless link over transmit-antenna and path-correlated channels. The impact of path correlations on the PEP is analyzed. Closed-form, waterfilling-based linear and non-linear precoders that minimize the worst-case PEP in OSTBC OFDM have been derived. An adaptive strategy that switches between precoded SM OFDM and precoded OSTBC OFDM has also been proposed. The system is designed to achieve a low BER with a target fixed transmission rate.

For each subcarrier, the minimum Euclidean distance of the received codebook is used to select between SM and OSTBC. A lower complexity selection criterion is also derived. To reduce the number of feedback bits, mode selection could be based on groups of neighboring subcarriers. The proposed precoders significantly reduce the impact of antenna and path-correlated channels; non-linear precoders perform better than linear precoders. The adaptive strategy outperforms either SM or OSTBC individually in terms of the BER.

Taking estimation errors and feedback delay into consideration, Chapter 7 has derived the conditional mean and covariance of the channel matrix in an OSTBC MIMO OFDM downlink system over a general transmit-antenna-correlated, frequency-selective fading MIMO channel model. SNR-maximizing mean-feedback precoding has been developed. This chapter has also proposed adaptive dual-mode precoding, in which either new mean-feedback precoding or covariance precoding is adaptively chosen at the receiver according to the channel conditions. The receiver calculates the precoding-mode switching metric and decides whether mean feedback is necessary. We have confirmed the intuition that if mean feedback is sufficiently accurate, it improves the system performance. The proposed precoders, both the mean-feedback precoder and the dual-mode precoder, reduce the error rate. Adaptive precoding outperforms both mean-feedback precoding and covariance precoding applied individually.

Our techniques have good performance, low feedback requirements and low complexity, which are desirable features in the future wireless systems.

8.2 Future Work

Future research may be carried out in the following three major directions.

8.2.1 Complexity Reduction

There is a trade-off between the amount of CSI fedback to the transmitter and the gain available from the using CSI. For precoding over MIMO OFDM systems, the feedback may need to be

on a subcarrier basis. To reduce the total amount of the feedback information, the correlation of precoding matrices on adjacent subcarriers can be explored. The significant correlations between adjacent subcarriers lead to substantial correlation between the precoders corresponding to neighboring subcarriers. The neighboring subcarriers can therefore be combined into a group and use the precoding matrix corresponding to the center subcarrier for all the subcarriers in the group. Since the subcarriers near the group boundary may experience performance degradation, an interpolation scheme can be used to improve the performance due to grouping. When a better performance is required, a smaller group can be used, i.e., more bits can be sent to the transmitter. Higher-order interpolation design will lead to a better performance, but is more complicated. It thus remains a future research topic to address the trade-off among the complexity of the interpolation design, performance, and the feedback load.

8.2.2 Robust Precoding in Multiuser OFDM

Precoding schemes need instantaneous CSI or long-term statistics at the transmitter. Accurate CSIT requires perfect channel estimation and time-invariant channel conditions. However, estimation errors introduce channel mismatch at both the transmitter and the receiver, i.e., the channel information which is available at the transmitter and the receiver differs from the actual channel at the time of transmission. The time variations and feedback noise lead to unbalanced CSI between the transmitter and the receiver and make CSIT mismatch more serious. As the CSI mismatch becomes severe, the performance of precoders significantly degrades. Thus, there is a need to solve the problem of imperfect and mismatched CSI at the transmitter and the receiver. A new precoder which is robust against estimation errors and feedback delay for multiuser OFDM over spatially-correlated MIMO channels is of interest to investigate. A key feature of future wireless system design is the quality of CSI at the transmitter and related feedback requirements. The robust precoder with limited feedback is also of interest to explore.

8.2.3 Precoding Design in Medium Access Control Layer

A successful broadband wireless system design must include an efficient co-designed MAC layer for reliable link performance over the wireless channel. The MAC layer design will involve automatic retransmission and fragmentation mechanism, where the transmitter breaks up packets into smaller sequentially sent subpackects. If a subpacket is received incorrectly, the transmitter requests re-transmission of it. This automatic retransmission request (ARQ) algorithm introduces time diversity (delay) into the system, which may help to recover the transmitted signals from noise, interference and fades. It is interesting to develop fundamental diversity-multiplexing-delay tradeoffs of a MIMO retransmission channel, and have insights into benefits of ARQ schemes for future multiuser MIMO OFDM systems.

Appendix

Proof of Unitary Property of the ICI Coefficient Matrix

For simplicity, in the following proof the subscript $\{u, v\}$ of (3.8) is omitted.

As $N \to \infty$, for $1 \leq k < \frac{N}{2}$ and $k \gg \varepsilon$, we have

$$S[k] \approx \frac{\sin \pi(\varepsilon + k)}{\pi(\varepsilon + k)} e^{j\pi(\varepsilon+k)} = \frac{\sin \pi\varepsilon}{\pi(\varepsilon + k)} e^{j\pi\varepsilon} \approx \frac{\sin \pi\varepsilon}{\pi k} e^{j\pi\varepsilon}. \tag{1}$$

Note that when $k = 0$, $S[0] \approx \frac{\sin \pi\varepsilon}{\pi\varepsilon} e^{j\pi\varepsilon}$. From (3.5), one can immediately get $S[N - k] = S[-k]$.

The proof includes two steps. Firstly, the diagonal entries of $\mathbf{Z} = \mathbf{S}^H\mathbf{S}$, $Z(m, m)$, are shown to approach unity. Secondly, off-diagonal terms are proven to vanish, i.e, $\frac{|Z(m,m)|^2}{|Z(m,n)|^2} \to \infty$ as $\varepsilon \to 0$.

Since $S[N - k] = S[-k]$, the $\{m, n\}$th entry of $\mathbf{Z}$ is hence given by

$$Z(m, n) = \sum_{k=-m}^{N-1-m} S[k]S^*[k + m - n] = \sum_{k=0}^{N-1} S[k]S^*[k + m - n]. \tag{2}$$

Let us first consider diagonal entries of $\mathbf{Z}$. When $m = n$, $Z(m, m)$ are the diagonal entries

$$Z(m, m) = \sum_{k=0}^{N-1} S[k]S^*[k] = S[0]S^*[0] + \sum_{k=1}^{N-1} S[k]S^*[k] = \frac{\sin^2 \pi\varepsilon}{(\pi\varepsilon)^2} + \frac{\sin^2 \pi\varepsilon}{\pi^2} \sum_{k=1}^{N-1} \frac{1}{k^2}, \tag{3}$$

where the second term in (3) is the Riemann's Zeta function, i.e., $\sum_{k=1}^{\infty} \frac{1}{k^2} = \frac{\pi^2}{6}$ [108]. When N is sufficiently large, the terms of $1/k^2$, $\forall\, k \geq N$, can be omitted. We thus have $\sum_{k=1}^{N-1} \frac{1}{k^2} \approx \frac{\pi^2}{6}$. The (3) can be approximated as $Z(m, m) \approx \sin^2(\pi\varepsilon) \left[\frac{1}{(\pi\varepsilon)^2} + \frac{1}{6}\right]$, and $\lim_{\varepsilon\to 0} Z(m, m) = 1$.

Now the off-diagonal terms are considered. When $m \neq n$, since $\mathbf{Z}$ is a Hermitian matrix, i.e., $Z(m, n) = Z^*(n, m)$, it is sufficient to consider the case of $m > n$:

$$\begin{aligned} Z(m, n) &= S[0]S^*[m - n] + \sum_{k=1}^{N-1} S[k]S^*[k + m - n] \\ &= \frac{\sin^2 \pi\varepsilon}{\pi^2} \left[\frac{1}{\varepsilon(m - n)}\right] + \frac{\sin^2 \pi\varepsilon}{\pi^2} \sum_{k=1}^{N-1} \frac{1}{k(k + m - n)} \\ &= \frac{\sin^2 \pi\varepsilon}{\pi^2(m - n)} \left(\frac{1}{\varepsilon} + \sum_{k=1}^{N-1} \frac{1}{k} - \sum_{k=1}^{N-1} \frac{1}{k + m - n}\right), \forall\, m > n. \end{aligned} \tag{4}$$

Obviously, only when $m-n=1$, $Z(m,n)$ can reach the maximum value $Z(m,n)_{\max}=\frac{\sin^2\pi\varepsilon}{\pi^2}\left(\frac{1}{\varepsilon}+1-\frac{1}{N}\right)$. The least power ratio of the diagonal entries to the non-diagonal entries can be given by

$$K=\frac{Z^2(m,m)}{Z^2(m,n)}>\left(\frac{1+\frac{\pi^2\varepsilon^2}{6}}{\varepsilon^2+\varepsilon}\right)^2. \tag{5}$$

As $\varepsilon\to 0$, $K\to\frac{1}{\varepsilon^2}$. The value of the normalized frequency offset has the dominant effect on the power ratio K. For instance, when $\varepsilon=0.3$, $K>11.1$, which means over 90% energy is concentrated on the main diagonal. K rapidly increases when ε decreases. Therefore, the ICI coefficient matrix **S** can be approximated as a unitary matrix.

Proof of (7.12)

Note that vec$(\mathbf{ABC}) = (\mathbf{C}^T \otimes \mathbf{A})vec(\mathbf{B})$, where vec$(\mathbf{A})$ is a vectorization of the matrix $\mathbf{A}$, and is denoted as $\vec{\mathbf{A}}$. We omit the time index i.

Proof of (7.5). Since $\mathbf{H}[k] = \mathbf{H}_w[k]\mathbf{R}_T^{1/2}$ given in (7.1), the covariance of the channel vector $\vec{\mathbf{H}}[k] = \text{vec}(\mathbf{H}[k])$ can be given by

$$\begin{aligned}\mathbf{C}_{\vec{\mathbf{H}}\vec{\mathbf{H}}} &= \mathrm{E}\left[\vec{\mathbf{H}}[k]\vec{\mathbf{H}}^H[k]\right] \\ &= \left((\mathbf{R}_T^{1/2})^T \otimes \mathbf{I}_{M_R}\right) \text{vec}(\mathbf{H}_w[k])\text{vec}^H(\mathbf{H}_w[k]) \left((\mathbf{R}_T^{1/2})^H \otimes \mathbf{I}_{M_R}\right) \\ &= \mathbf{R}_T \otimes \mathbf{I}_{M_R},\end{aligned} \tag{6}$$

where the entries of $\mathbf{H}_w[k]$ are i.i.d. Gaussian random variables with zero mean and variance normalized to unity. After expanding the left and right sides of (6), we can calculate the entries in the matrix $\mathbf{C}_{\vec{\mathbf{H}}\vec{\mathbf{H}}}$, and thus obtain (7.5).

The vectorization format of the channel matrix $\vec{\mathbf{H}}[k] = \text{vec}(\mathbf{H}[k])$ given $\mathbf{H}_T[k]$ with conditional mean and covariance [79, pp. 324]

$$\begin{aligned}\mathbf{H}_{\vec{\mathbf{H}}|\vec{\mathbf{H}}_T}[k] &= \mathbf{C}_{\vec{\mathbf{H}}\vec{\mathbf{H}}_T}\mathbf{C}^{-1}_{\vec{\mathbf{H}}_T\vec{\mathbf{H}}_T}\vec{\mathbf{H}}_T[k] \\ \mathbf{C}_{\vec{\mathbf{H}}|\vec{\mathbf{H}}_T} &= \mathbf{C}_{\vec{\mathbf{H}}\vec{\mathbf{H}}} - \mathbf{C}_{\vec{\mathbf{H}}\vec{\mathbf{H}}_T}\mathbf{C}^{-1}_{\vec{\mathbf{H}}_T\vec{\mathbf{H}}_T}\mathbf{C}_{\vec{\mathbf{H}}_T\vec{\mathbf{H}}},\end{aligned} \tag{7}$$

where $\mathbf{H}_{\vec{\mathbf{H}}|\vec{\mathbf{H}}_T}[k] = \text{vec}\left(\mathbf{H}_{\mathbf{H}|\mathbf{H}_T}[k]\right)$. $\mathbf{C}_{\vec{\mathbf{H}}|\vec{\mathbf{H}}_T}$ is the covariance of the vec$(\mathbf{H}[k])$ given vec$(\mathbf{H}_T[k])$.

The vectorization of $\mathbf{H}_{\mathbf{H}|\mathbf{H}_T}[k]$ in (7.12) is $\mathbf{H}_{\vec{\mathbf{H}}|\vec{\mathbf{H}}_T}[k]$, and can be expressed by

$$\begin{aligned}\mathbf{H}_{\vec{\mathbf{H}}|\vec{\mathbf{H}}_T}[k] &= \mathbf{C}_{\vec{\mathbf{H}}\vec{\mathbf{H}}_T}\mathbf{C}^{-1}_{\vec{\mathbf{H}}_T\vec{\mathbf{H}}_T}\vec{\mathbf{H}}_T[k] \\ &= J\left(\mathbf{R}_T^T \otimes \mathbf{I}_{M_R}\right)\left(\left(\mathbf{R}_T^T + \Omega_e\mathbf{I}_{M_T}\right) \otimes \mathbf{I}_{M_R}\right)^{-1}\vec{\mathbf{H}}_T[k] \\ &= J\left(\left(\mathbf{R}_T^T\left(\mathbf{R}_T^T + \Omega_e\mathbf{I}_{M_T}\right)^{-1}\right) \otimes \mathbf{I}_{M_R}\right)\vec{\mathbf{H}}_T[k].\end{aligned} \tag{8}$$

We thus have

$$\mathbf{H}_{\mathbf{H}|\mathbf{H}_T}[k] = J\mathbf{H}_T[k]\mathbf{R}_T\left(\mathbf{R}_T + \Omega_e\mathbf{I}_{M_T}\right)^{-1}. \tag{9}$$

Similarly, the conditional covariance of $\mathbf{H}_{\mathbf{H}|\mathbf{H}_T}[k]$ can be shown to be given by

$$\mathbf{C}_{\mathbf{H}|\mathbf{H}_T} = \mathbf{R}_T - J^2\mathbf{R}_T\left(\mathbf{R}_T + \Omega_e\mathbf{I}_{M_T}\right)^{-1}\mathbf{R}_T. \tag{10}$$

Bibliography

[1] D. Gesbert, M. Shafi, D. Shiu, P. J. Smith, and A. Naguib, "From theory to practice: an overview of MIMO space-time coded wireless systems," *IEEE J. Select. Areas Commun.*, vol. 21, no. 3, pp. 281–301, Apr. 2003.

[2] A. J. Paulraj, D. A. Gore, R. U. Nabar, and H. Bölcskei, "An overview of MIMO communications - a key to Gigabit wireless," *Proc. of IEEE, invited paper*, vol. 92, no. 2, pp. 198–218, Feb. 2004.

[3] R. T. Derryberry, S. D. Gray, D. M. Ionescu, G. Mandyam, and B. Raghothaman, "Transmit diversity in 3G CDMA systems," *IEEE Commun. Magazine*, vol. 40, no. 4, pp. 68–75, Apr. 2002.

[4] A. S. Dakdouki, V. L. Banket, N. K. Mykhaylov, and A. A. Skopa, "Downlink processing algorithms for multi-antenna wireless communications," *IEEE Commun. Magazine*, vol. 43, no. 1, pp. 122–127, Jan. 2005.

[5] G. L. Stüber, J. R. Barry, S. W. McLaughlin, Y. G. Li, M. A. Ingram, and T. G. Pratt, "Broadband MIMO-OFDM wireless communications," *Proc. of IEEE, invited paper*, vol. 92, no. 2, pp. 271–294, Feb. 2004.

[6] H. Yang, "A road to future broadband wireless access: MIMO-OFDM-based air interface," *IEEE Commun. Magazine*, vol. 43, no. 1, pp. 53–60, Jan. 2005.

[7] N. Seshadri and J. H. Winters, "Two signaling schemes for improving the error performance of frequency-division-duplex (FDD) transmission system using transmitter antenna diversity," in *Proc. IEEE VTC'93-Spring*, vol. 1, Secaucus, NJ, May 1993, pp. 508–511.

[8] D. Gore, S. Sundhu, and A. J. Paulraj, "Delay diversity codes for frequency selective channels," in *Proc. IEEE ICC*, New York, NY, May 2002, pp. 1949–1953.

[9] V. Tarokh, H. Jafarkhani, and A. R. Calderbank, "Space-time codes for high data rate wireless communication: performance criterion and code construction," *IEEE Trans. Inform. Theory*, vol. 44, no. 2, pp. 744–765, Mar. 1998.

[10] Cenk Köse and Richard D. Wesel, "Universal space time trellis codes ," *IEEE Trans. Inform. Theory*, vol. 49, no. 10, pp. 2717–2727, Oct. 2003.

[11] S. M. Alamouti, "A simple transmit diversity technique for wireless communications," *IEEE J. Select. Areas Commun.*, vol. 16, no. 8, pp. 1451–1458, Oct. 1998.

[12] V. Tarokh, H. Jafarkhani, and A. R. Calderbank, "Space-time block codes from orthogonal designs," *IEEE Trans. Inform. Theory*, vol. 45, no. 5, pp. 1456–1467, Jul. 1999.

[13] J. Mietzner, P. A. Hoeher, and M. Sandell,, "Compatible improvement of the GSM/EDGE system by means of space-time coding techniques," *IEEE Trans. Wireless Commun.*, vol. 2, no. 4, pp. 690–702, 2003.

[14] Telecommunications Industry Association, *TIA/EIA Physical Layer Standard for cdma2000 Spread Spectrum Systems, Revision C.* TIA/EIA/IS-2000-2.

[15] 3rd Generation Partnership Project, *Technical Specification Group Radio Access Network: Physical Channels and Mapping of Transport Channels onto Physical Channels (FDD) (release 1999).* v.3.2.0, 2000-2003.

[16] P. W. Wolniansky, G. J. Foschini, G. D. Golden, and R. A. Valenzuela, "V-BLAST: an architecture for realizing very high data rates over the rich-scattering wireless channel," in *Proc. ISSSE'98, invited paper*, vol. 6, Pisa, Italy, 1998.

[17] G. J. Foschini and M. J. Gans, "On limits of wireless communication in a fading environment when using multiple antennas," *Wireless Personal Commun.*, vol. 6, no. 3, pp. 311–335, Mar. 1998.

[18] G. J. Foschini, "Layered space-time architecture for wireless communication in a fading environment when using multiple antennas," *Bell Lab. Technol. J.*, pp. 41–59, Autumn 1996.

[19] M. Sellathurai and S. Haykin, "Turbo-BLAST for high-speed wireless communications: theory and experiments," *IEEE Trans. Signal Processing*, vol. 50, no. 10, pp. 2538–2546, Oct. 2002.

[20] L. Zheng and D. N. C. Tse, "Diversity and multiplexing: a fundamental tradeoff in multiple-antenna channels," *IEEE Inform. Theory*, vol. 49, no. 5, pp. 1073–1096, May 2003.

[21] LAN/MAN Standards Committee, *Wireless LAN Medium Access Control (MAC) and Physical Layer (PHY) Specifications: Amendment 4: Enhancements for Higher Throughput*. Dallas, Tx: IEEE Std. 802.11n, Nov. 2008.

[22] A. Bria, F. Gessler, O. Queseth, R. Stridh, M. Unbehaun, J. Wu, and J. Zander, "4th-generation wireless infrastructures: scenarios and research challenges," *IEEE Personal Commun.*, vol. 8, no. 6, pp. 25–31, Dec. 2001.

[23] R. W. Chang, "Synthesis of band-limited orthogonal signals for multichannel data transmission," *Bell Syst. Tech. J.*, vol. 45, pp. 1775–1796, Dec. 1966.

[24] B. R. Saltzberg, "Performance of an efficient parallel data transmission system," *IEEE Trans. Commun. Technol.*, vol. COM-15, pp. 805–811, Dec. 1967.

[25] M. L. Doelz, E. T. Heald, and D. L. Martin, “Binary data tranmission techniques for linear systems,” in *Proc. IRE*, vol. 45, May 1957, pp. 656–661.

[26] M. S. Zimmerman and A. L. Kirsch, “The AN/GSC-10 (KATHRYN) variable rate data modem for HF radio,” *IEEE Trans. Commun. Technol.*, vol. COM-15, no. 2, pp. 197–204, Apr. 1967.

[27] S. B. Weinstein and P. M. Ebert, “Data transmission by frequency division multiplexing using the discrete Fourier transform,” *IEEE Trans. Commun. Technol.*, vol. COM-19, no. 5, pp. 628–634, Oct. 1971.

[28] L. J. Cimini, “Analysis and simulation of a digital mobile channel using orthogonal frequency-division multiplexing,” *IEEE Trans. Commun.*, vol. 33, no. 7, pp. 665–675, 1985.

[29] J. A. C. Bingham, “Multicarrier modulation for data transmission: an idea whose time has come,” *IEEE Commun. Magazine*, pp. 5–14, May 1990.

[30] P. S. Chow, J. C. Tu, and J. M. Cioffi, “Performance evaluation of a multichannel transceiver system for ADSL and VHDSL services,” *IEEE J. Select. Areas Commun.*, vol. 9, no. 6, pp. 909–919, Aug. 1991.

[31] European Telecommunications Standard Institute, *Radio Broadcasting Systems; Digital Audio Broadcasting (DAB) to mobile, portable and fixed receivers*, 2nd ed. Sophia Antipolis, France: ETS 300401, May 1997.

[32] ——, *Digital Video Broadcasting: Frame Structure, Channel Coding, and Modulation for Digital Terrestrial Television*. Sophia Antipolis, France: ETS EN300-744, Aug. 1997.

[33] T. de Couasnon, R. Monnier, and J. B. Rault, “OFDM for digital TV broadcasting,” *Signal Processing*, vol. 39, no. 1-2, pp. 1–31, Sep. 1994.

[34] LAN/MAN Standards Committee, *Wireless LAN Medium Access Control (MAC) and Physical Layer (PHY) Specifications: High-Speed Physical Layer in the 5 GHz Band*. Piscataway, NJ: IEEE Std. 802.11a, Sep. 1999.

[35] ——, *Local and Metropolitan Area Networks-Part 16, Air Interface for Fixed Broadband Wireless Access Systems*. Piscataway, NJ: IEEE Std. 802.16a, Apr. 2002.

[36] R. V. Nee and R. Prasad, *OFDM for Wireless Multimedia Communication*. London: Artech House Publishers, Apr. 2000.

[37] P. Robertson and S. Kaiser, "Analysis of the loss of orthogonality through Doppler spread in OFDM systems," in *Proc. IEEE Globecom'99*, vol. 1, Rio de Janeiro, Brazil, Dec. 1999, pp. 701–706.

[38] H. Nikookar and R. Prasad, "On the sensitivity of multicarrier transmission over multipath channels to phase noise and frequency offset," in *Proc. IEEE PIMRC'96*, vol. 1, Taipei, Taiwan, Oct. 1996, pp. 68–72.

[39] M. Russell and G. L. Stüber, "Interchannel interference analysis of OFDM in a mobile environment," in *Proc. IEEE VTC'95-Spring*, vol. 2, Chicago, IL, Jul. 1995, pp. 820–824.

[40] T. Pollet, M. V. Bladel, and M. Moeneclaey, "BER sensitivity of OFDM systems to carrier frequency offset and Wiener phase noise," *IEEE Trans. Commun.*, vol. 43, no. 2/3/4, pp. 191–193, Feb./Mar./Apr. 1995.

[41] Israel Koffman and Vincentzio Roman, "Broadband wireless access solutions based on OFDM access in IEEE 802.16," *IEEE Commun. Magazine*, vol. 40, no. 4, pp. 96–103, Apr. 2002.

[42] P. W. C. Chan and R. S. Cheng, "Capacity maximization for zero-forcing MIMO-OFDMA downlink systems with multuser diversity ," *IEEE Trans. Wireless Commun.*, vol. 6, no. 5, pp. 1880–1889, May 2007.

[43] WiMAX Forum, “Mobile WiMAX C part I: A technical overview and performance evaluation,” [online] http://www.wimaxforum.org/technology.

[44] D. J. Love and R. W. Heath Jr., “What is the value of limited feedback for MIMO channels?” *IEEE Commun. Magazine*, vol. 42, no. 10, pp. 54–59, Oct. 2004.

[45] İ. E. Telatar, “Capacity of multi-antenna Gaussian channels,” *Eur. Trans. Telecomm. ETT*, vol. 10, no. 6, pp. 585–596, Nov. 1999.

[46] A. Scaglione, P. Stoica, S. Barbarossa, G. B. Giannakis, and H. Sampath, “Optimal designs for space-time linear precoders and decoders,” *IEEE Trans. Signal Processing*, vol. 50, no. 5, pp. 1051–1064, May 2002.

[47] M. Vu and A. J. Paulraj, “Optimal linear precoders for MIMO wireless correlated channels with nonzero mean in space-time coded systems,” *IEEE Trans. Signal Processing*, vol. 54, no. 6, pp. 2318–2332, Jun. 2006.

[48] A. Hjørungnes, D. Gesbert, and J. Akhtar, “Precoding of space-time block coded signals for joint transmit-receive correlated MIMO channels,” *IEEE Trans. Wireless Commun.*, vol. 5, no. 3, pp. 492–497, Mar. 2006.

[49] A. Hjørungnes and D. Gesbert, “Precoding of orthogonal space-time block codes over correlated Ricean MIMO channels,” in *Proc. IEEE VTC’05-Spring*, vol. 5, Stockholm, Sweden, May 2005, pp. 3024–3028.

[50] G. Jöngren, M. Skoglund, and B. Ottersten, “Combining beamforming and orthogonal space-time block coding,” *IEEE Trans. Inform. Theory*, vol. 48, no. 3, pp. 611–627, Mar. 2002.

[51] S. Zhou and G. B. Giannakis, “Optimal transmitter eigen-beamforming and space-time block coding based on channel correlations,” *IEEE Trans. Inform. Theory*, vol. 49, no. 7, pp. 1673–1689, 2003.

[52] A. Hjørungnes and D. Gesbert, “Precoding of space-time block codes in an arbitrary correlated MIMO channels: iterative and closed-form solutions,” *IEEE Trans. Wireless Commun.*, vol. 6, no. 3, pp. 1072–1082, Mar. 2007.

[53] D. J. Love and R. W. Heath Jr., “Grassmannian beamforming for multiple-input multiple-output wireless systems,” *IEEE Trans. Inform. Theory*, vol. 49, no. 10, pp. 2735–2747, Oct. 2003.

[54] ——, “Limited feedback precoding for spatial multiplexing systems,” *IEEE Trans. Inform. Theory*, vol. 51, no. 8, pp. 2967–2976, Aug. 2005.

[55] ——, “Limited feedback unitary precoding for orthogonal space-time codes,” *IEEE Trans. Signal Processing*, vol. 53, no. 1, pp. 64–73, Jan. 2005.

[56] B. M. Hochwald, T. L. Marzetta, T. J. Richardson, W. Sweldens, and R. Urbanke, “Systematic design of unitary space-time constellation,” *IEEE Trans. Inform. Theory*, vol. 46, no. 6, pp. 1962–1973, Sep. 2000.

[57] M. Tomlinson, “New automatic equalizer employing modulo arithmetic,” *Electron. Lett.*, vol. 7, pp. 138–139, Mar. 1971.

[58] H. Harashima and H. Miyakawa, “Matched-transmission technique for channels with intersymbol interference,” *IEEE Trans. Commun.*, vol. COM-20, pp. 774–780, Aug. 1972.

[59] G. D. Forney and M. V. Eyuboğlu, “Combined equalization and coding using precoding,” *IEEE Commun. Magazine*, vol. 29, no. 12, pp. 25–34, Dec. 1991.

[60] C. Windpassinger, R. F. H. Fischer, T. Vencel, and J. B. Huber, “Precoding in multiantenna and multiuser communications,” *IEEE Trans. Wireless Commun.*, vol. 3, no. 4, pp. 1305–1315, Jul. 2004.

[61] R. F. H. Fischer, *Precoding and Signal Shaping for Digital Transmission*. New York: Wiley, 2002.

[62] O. Simeone, Y. Bar-Ness, and U. Spagnolini, "Linear and nonlinear preequalization/equalization for MIMO systems with long-term channel state information at the transmitter," *IEEE Trans. Wireless Commun.*, vol. 3, no. 2, pp. 373–378, Mar. 2004.

[63] S. H. Müller-Weinfurtner, "Optimal Nyquist windowing in OFDM receivers," *IEEE Trans. Commun.*, vol. 49, no. 3, pp. 417–420, Mar. 2001.

[64] K. Sathananthan and C. Tellambura, "Partial transmit sequence and selected mapping schemes to reduce ICI in OFDM systems," *IEEE Commun. Lett.*, vol. 6, no. 8, pp. 313–315, Aug. 2002.

[65] A. Gorokhov and J. - P. Linnartz, "Robust OFDM receiver for dispersive time-varying channels: equalization and channel acquisition," *IEEE Trans. Commun.*, vol. 52, no. 4, pp. 572–583, Apr. 2004.

[66] P. Schniter, "Low-complexity equalization of OFDM in doubly selective channels," *IEEE Trans. Signal Processing*, vol. 52, no. 4, pp. 1002–1011, Apr. 2004.

[67] Y. Zhao and S. - G. Häggman, "Intercarrier interference self-cancellation scheme for OFDM mobile communication systems," *IEEE Trans. Commun.*, vol. 49, no. 7, pp. 1185–1191, July 2001.

[68] Y. Fu and C. C. Ko, "A new ICI self-cancellation scheme for OFDM systems based on a generalized signal mapper," in *Proc. IEEE WPMC'02*, Honolulu, Hawaii, Oct. 2002, pp. 995–999.

[69] A. Stamoulis, S. N. Diggavi, and A. Al-Dhahir, "Intercarrier interference in MIMO OFDM," *IEEE Trans. Signal Processing*, vol. 50, no. 10, pp. 2451–2464, Oct. 2002.

[70] P. H. Moose, “A technique for orthogonal frequency division multiplexing frequency offset correction,” *IEEE Trans. Commun.*, vol. 42, no. 10, pp. 2908 – 2914, Oct. 1994.

[71] R. A. Horn and C. R. Johnson, *Matrix Analysis*. New York: Cambridge University Press, 2002.

[72] D. Shiu, G. J. Foschini, M. J. Gans and J. M. Kahn, “Fading correlation and its effect on the capacity of multi-element antenna systems,” *IEEE Trans. Commun.*, vol. 48, no. 3, pp. 502–512, Mar. 2000.

[73] International Telecommunication Union, Recommendation ITU-R M. 1225, *Guidelines for Evaluation of Radio Transmission Technologies for IMT-2000*, Feb. 2002.

[74] Y. - S. Choi, P. J. Voltz, and F. A. Cassara, “On channel estimation and detection for multicarrier signals in fast and selective Rayleigh fading channels,” *IEEE Trans. Commun.*, vol. 49, no. 8, pp. 1375–1387, Aug. 2001.

[75] S. Kapoor, D. J. Marchok, and Y. - F. Huang, “Adaptive interference suppression in multiuser wireless OFDM systems using antenna arrays,” *IEEE Trans. Signal Processing*, vol. 47, no. 12, pp. 3381–3391, Dec. 1999.

[76] Z. Cao, U. Tureli, and Y. - D. Yao, “Deterministic multiuser carrier-frequency offset estimation for interleaved OFDMA uplink,” *IEEE Trans. Commun.*, vol. 52, no. 9, pp. 1585–1594, Sep. 2004.

[77] M. Morelli, “Timing and frequency synchronization for the uplink of an OFDMA system,” *IEEE Trans. Commun.*, vol. 52, no. 2, pp. 296–306, Feb. 2004.

[78] D. Huang and K. B. Letaief, “An interference-cancellation scheme for carrier-frequency offsets correction in OFDMA systems,” *IEEE Trans. Commun.*, vol. 53, no. 7, pp. 1155–1165, Jul. 2005.

[79] S. M. Kay, *Fundamentals of Statistical Signal Processing, Vol. 1, Estimation Theory*. Upper Saddle River, NJ: Prentice Hall, 1993.

[80] D. Bini and V. Pan, *Polynomial and Matrix Computations*. Boston: Birkhäuser, 1994, vol. I.

[81] J. Choi and R. W. Heath Jr., "Interpolation based unitary precoding for spatial multiplexing MIMO-OFDM with limited feedback," in *Proc. IEEE Globecom'04*, vol. 1, Dallas, Tx, Nov. 2004, pp. 214–218.

[82] D. J. Love and R. W. Heath Jr., "Interpolation based transmitter beamforming for MIMO-OFDM with limited feedback," *IEEE Trans. Signal Processing*, vol. 53, no. 11, pp. 4125–4135, Nov. 2005.

[83] H. Bölcakei, D. Gesbert, and A. J. Paulraj, "On the capacity of OFDM-based spatial multiplexing systems," *IEEE Trans. Commun.*, vol. 50, no. 2, pp. 225–234, Feb. 2002.

[84] A. T. James, "Distribution of matrix variates and latent roots derived from normal samples," *Ann. Math. Statist.*, vol. 35, pp. 457–501, 1964.

[85] G. L Stüber, *Principles of Mobile Communication*, 2nd ed. Boston: Kluwer Academic Publishers, 2001.

[86] T. L. Martetta and B. M. Hockwald, "Capacity of a mobile multiple-antenna communication link in Rayleigh flat fading," *IEEE Trans. Inform. Theory*, vol. 45, no. 1, pp. 139–157, Jan. 1999.

[87] H. Bölcskei, M. Borgmann, and A. J. Paulraj, "Impact of the propagation environment on the performance of space-frequency coded MIMO-OFDM," *IEEE J. Select. Areas Commun.*, vol. 21, no. 3, pp. 427–439, Mar. 2003.

[88] J. Akhtar and D. Gesbert, “A closed-form precoder for spatial multiplexing over correlated MIMO channels,” in *Proc. IEEE Globecom’03*, vol. 4, San Francisco, CA, Dec. 2003, pp. 1847–1851.

[89] H. Sampath and A. J. Paulraj, “Linear precoding for sapce-time coded systems with known fading correlations,” *IEEE Commun. Lett.*, vol. 6, no. 6, pp. 239–241, Jun. 2002.

[90] Y. Zhao, R. Adve, and T. J. Lim, “Precoding of orthogonal STBC with channel covariance feedback for minimum error probability,” in *Proc. IEEE PIMRC’04*, vol. 1, Barcelona, Spain, Sep. 2004, pp. 503–507.

[91] E. Yoon, J. Hansen, and A. J. Paulraj, “Space-frequency precoding with space-tap correlation information at teh transmitter,” *IEEE Trans. Commun.*, vol. 55, no. 9, pp. 1702–1711, Sep. 2007.

[92] R. W. Heath Jr. and A. J. Paulraj, “Switching between diversity and multiplexing in MIMO systems,” *IEEE Trans. Commun.*, vol. 53, no. 6, pp. 962–968, Jun. 2005.

[93] R. W. Heath Jr. and D. J. Love, “Multimode antenna selection for spatial multiplexing systems with linear receivers,” *IEEE Trans. Signal Processing*, vol. 53, no. 8, pp. 3042–3056, Aug. 2005.

[94] D. J. Love and R. W. Heath Jr., “Multimode precoding for MIMO wireless systems,” *IEEE Trans. Signal Processing*, vol. 53, no. 10, pp. 3674–3687, Oct. 2005.

[95] A. Forenza, M. R. McKay, I. B. Collings, and R. W. Heath Jr., “Switching between OSTBC and spatial multiplexing with linear receiver in spatially correlated MIMO channels,” in *Proc. IEEE VTC’06-Spring*, vol. 3, Melbourne, Australia, May 2006, pp. 1387 – 1391.

[96] M. Brookes, *The Matrix Reference Manual*. [online] http://www.ee.ic.ac.uk/hp/staff/dmb/matrix/intro.html, 2005.

[97] Y. Ding, T. N. Davidson, Z. - Q. Luo, and K. M. Wong, "Minimum BER block precoders for zero-forcing equalization," *IEEE Trans. Signal Processing*, vol. 51, no. 9, pp. 2410–2423, Sep. 2003.

[98] İ. E. Telatar, "Capacity of multi-antenna Gaussian channels." Lucent Technol., Bell Laboratories: Tech. Rep., BL0112170-950615-07TM, 1995.

[99] G. Ganesan and P. Stoica, "Space-time block codes: a maximum SNR approach," *IEEE Trans. Inform. Theory*, vol. 47, no. 4, pp. 1650–1656, May 2001.

[100] J. Yang and S. Roy, "On joint transmitter and receiver optimization for multiple-input-multiple-output (MIMO) transmission systems," *IEEE Trans. Commun.*, vol. 42, no. 12, pp. 3221–3231, Jan. 1994.

[101] Y. Fu, W. A. Krzymień, and C. Tellambura, "Transmitter precoding for orthogonal space-time block-coded OFDM in transmit-antenna and path-correlated channels," in *Proc. IEEE VTC'06-Fall*, Montreal, QC, Canada, 2006.

[102] B. Zerlin, M. Joham, W. Utschick, and J. A. Nossek, "Covariance-based linear precoding," *IEEE J. Select. Areas Commun.*, vol. 24, no. 1, pp. 190–199, Jan. 2006.

[103] A. Pascual-Iserte, D. P. Palomar, A. I. Pérez-Neira, and M. A. Lagunas, "A robust maximin approach for MIMO communications with imperfect channel state information based on convex optimization," *IEEE Trans. Signal Processing*, vol. 54, no. 1, pp. 346–360, Jan. 2006.

[104] G. Barriac and U. Madhow, "Space-time precoding for mean and covariance feedback: application for wideband OFDM," *IEEE Trans. Commun.*, vol. 54, no. 1, pp. 96–107, Jan. 2006.

[105] Y. Fu, C. Tellambura, and W. A. Krzymień, "Precoding for multiuser orthogonal space-time block-coded OFDM downlink over transmit-antenna-correlated channels," in *Proc. IEEE WCNC'07*, Hong Kong, China, 2007.

[106] F. Rey, M. Lamarca, and G. Vazquez, "Robust power allocation algorithm for MIMO OFDM systems with imperfect CSI," *IEEE Trans. Signal Processing*, vol. 53, no. 3, pp. 1070–1085, Mar. 2005.

[107] Y. Fu, W. A. Krzymień, and C. Tellambura, "Non-linear precoding for OFDM systems in spatially-correlated frequency-selective fading MIMO channels," in *Proc. IEEE Globecom'06*, San Francisco, CA, 2006.

[108] I. S. Gradshteyn and I. M. Ryzhik, *Table of Integrals, Series, and Products*, 6th ed. San Diego: Academic Press, 2002.